CATHODOLUMINESCENCE AND DEGRADATION OF OXIDE THIN FILM AND POWDER PHOSPHORS

By

LIZANDRA CLARISSA WILLIAMS

A DISSERTATION PRESENTED TO THE GRADUATE SCHOOL
OF THE UNIVERSITY OF FLORIDA IN PARTIAL FULFILLMENT
OF THE REQUIREMENTS FOR THE DEGREE OF
DOCTOR OF PHILOSOPHY

UNIVERSITY OF FLORIDA

2004

This dissertation is dedicated to the Trilogen and the memory of my loving grandfather, Andrew Guy, Sr.

ACKNOWLEDGMENTS

I would like to first thank God for his blessings and unending presence in my life. He is the reason I have been so successful thus far in life. I must then acknowledge and thank my mother for my life and all the sacrifices she has made for me. Her help and endless support is another reason I have made it to this point in life. Of course, the rest of my family and friends are next on the list.

I would like to thank my advisor, Dr. Holloway, and committee (Dr. Abernathy, Dr. Norton, Dr. Hummel, and Dr. Tanner) for their interest and support in my academic endeavors. I would like to acknowledge the Major Analytical and Instrumentation Center (MAIC) staff for their assistance with characterization as well as training on the instruments. I would like to like to acknowledge the assistance received from the staff of Oak Ridge National Laboratory, Dr. Kumar and his staff at North Carolina A&T State University, and Mr. Kang and Dr. Summers at Georgia Institute of Technology for their assistance with this work.

I truly appreciate Ludie's attention to all the details that made working in this research group even better. I am grateful for all her help and talks. A big thanks goes to all of the members of Dr. Holloway's group, past and present for their assistance.

TABLE OF CONTENTS

page

ACKNOWLEDGMENTS iv

LIST OF TABLES viii

LIST OF FIGURES ix

ABSTRACT xiii

CHAPTER

1 INTRODUCTION 1

2 LITERATURE REVIEW 3

2.1 Introduction 3
2.2 Development of Cathodoluminescent Phosphors 4
2.3 Evolution of the Field Emission Display 7
2.4 Cathodoluminescent Phosphor Materials 9
2.4.1 Host Material 9
2.4.2 Activator-Luminescent Center 10
2.5 Materials Development 11
2.5.1 Sulfide Phosphors 11
2.5.2 Oxide Phosphors 13
2.5.2.1 Zinc silicate phosphors (Zn_2SiO_4: Mn) 13
2.5.2.2 Zinc germanate phophors (Zn_2GeO_4: Mn) 15
2.6 Processing of Phosphors 17
2.6.1 Powder Phosphors 17
2.6.2 Thin Film Phosphors 17
2.6.2.1 Pulsed laser deposition 18
2.6.2.2 Sputter deposition 22
2.7 Evaluation of Phosphor 24
2.7.1 Chromaticity 25
2.7.2 Spectral Distribution 25
2.7.3 Degradation Characteristics 27

3 CATHODOLUMINESCENCE FROM THIN FILM ZINC GERMANATE DOPED WITH MANGANESE PHOSPHORS....33

3.1 Introduction....33
3.2 Experimental Procedures....33
3.2.1 Substrates and their Preparation....33
3.2.2 Phosphor Processing....34
3.2.3 Thin Film Phosphor Characterization....37
3.2.3.1 X- ray diffraction....37
3.2.3.2 Relative composition analysis: EDX....38
3.2.3.3 Cathodoluminescence characterization....40
3.2.3.4 Photoluminescence characterization....41
3.3 Results....42
3.3.1 X- Ray Diffraction Results....42
3.3.2 Cathodoluminescent Properties....45
3.3.3 Zinc to Germanium Ratio in the Films....48
3.3.4 Photoluminescence Excitation and Emission....49
3.4 Discussion....50

4 DEVELOPMENT OF ZINC SILICATE DOPED WITH MANGANESE THIN FILM PHOSPHORS....54

4.1 Introduction....54
4.2 Experimental Procedures....54
4.2.1 Substrates and their Preparation....54
4.2.2 Phosphor Processing....55
4.2.2.1 Sputter deposition....55
4.2.2.2 Pulsed laser deposition....56
4.2.2.3 Combustion chemical vapor deposition....57
4.2.3 Thin Film Phosphor Characterization....57
4.2.3.1 X- ray diffraction....57
4.2.3.2 Scanning electron microscopy....58
4.2.3.3 Wavelength dispersive X- ray spectrometry....58
4.2.3.4 X- ray photoelectron spectroscopy....59
4.2.3.5 Cathodoluminescence characterization....60
4.3 Results from Pulsed Laser Deposited Phosphors....60
4.3.1 Structural Characterization....60
4.3.2 Morphological Characterization....63
4.3.3 Cathodoluminescence Results....65
4.3.4 Composition of Films....67
4.4 Results from Sputter Deposited Phosphors....68
4.4.1 Target 1....68
4.4.1.1 Structural characterization....69
4.4.1.2 Cathodoluminescence results....70
4.4.2 Target 2....74
4.4.2.1 Structural characterization....75
4.4.2.2 Cathodoluminescence results....75

4.5 Results from Combustion Chemical Vapor Deposition Phosphors....77
4.5.1 Cathodoluminescence Results....77
4.6 Discussion....78

5 DEGRADATION OF ZINC SILICATE DOPED WITH MANGANESE POWDER AND THIN FILM PHOSPHORS....81

5.1 Introduction....81
5.2 Experimental Procedures....81
5.3 Results....83
5.3.1 Thin Film Zn_2SiO_4: Mn Phosphor....83
5.3.1.1 24 hour CL degradation....83
5.3.1.2 Cathodoluminescence recovery....89
5.3.2 Powder Zn_2SiO_4: Mn Phosphor....93
5.3.2.1 24 hour CL degradation....93
5.3.2.2 Cathodoluminescence recovery....101
5.4 Discussion....105
5.4.1 Thin Film Zn_2SiO_4: Mn phosphor Degradation....105
5.4.2 Powder Zn_2SiO_4: Mn phosphor Degradation....108

6 CONCLUSIONS....111

6.1 Cathodoluminescence of Zn_2GeO_4: Mn Thin Films....111
6.2 Development of Zn_2SiO_4: Mn Thin Films....112
6.3 Degradation of Zn_2SiO_4: Mn Phosphors....112

LIST OF REFERENCES....115

BIOGRAPHICAL SKETCH....121

LIST OF TABLES

Table page

2-1 Color and wavelength emission for common dopants in ZnS host 12

2-2 Common oxide phosphors and their luminescent properties 13

2-3 Summary of Zn_2SiO_4: Mn properties 15

2-4 Summary of Zn_2GeO_4: Mn properties. 16

2-5 Typical excimer lasers and their operating wavelengths 19

3-1 Raw materials used to make target. 36

3-2 Zn/Ge Atomic Ratio in Deposited Zn_2GeO_4: Mn Film vs. Deposition Temperature on Various Substrates 49

4-1 Rapid thermal anneal recipe for heat treatment of thin film samples 56

4-2 Processing conditions for sputter deposition of Zn_2SiO_4: Mn thin films using Target 1 69

4-3 Processing conditions for sputter deposition of Zn_2SiO_4: Mn thin films using Target 2. 75

5-1 Species monitored during AES analysis 82

LIST OF FIGURES

Figure page

2-1 Cathode Ray Tube 5

2-2 Generation of electron beams in a CRT display 6

2-3 Pixel view beyond shadow mask where A → red, green, blue posphors; B → shadow mask; C →glass of display screen 7

2-4 Illustration of how the red, green, and blue hues combine to give a full spectrum of colors for full color displays 7

2.5 Pixel view of field emission display. 8

2-6 Cross section view of phosphor screen for a CRT 9

2-7 Energy excitation (absorption) leads to photon emission. 11

2-8 PL spectra for as deposited and annealed $Zn_2Si_{0.5}Ge_{0.5}O_4$: Mn thin films. 17

2-9 Sketch of basic pulsed laser deposition system 18

2-10 Picture of plume developed during PLD. 21

2-11 Schematic diagram of a typical set up for a sputter system 23

2-12 Planar magnetron sputter source 25

2-13 CIE chromaticity chart. 26

2-14 Visible light spectrum and corresponding wavelengths 26

2-15 Semi logarithmic plot of CL intensity vs. electron dose for a ZnS: Ag phosphor 31

2-16 Linear and logarithmic plot of S Auger peak to peak height (APPH) vs. electron dose for ZnS: Ag phosphor 31

2-17 Plot of CL intensity of Y_2O_3: Eu phosphor and selected Auger peak to peak heights vs. electron dose 32

3-1 Flow chart outlining substrate preparation and phosphor processing method. 35

3-2 Representative sketch of mosaic target where 75% area = Zn_2GeO_4: Mn and 25% area = ZnO. 36

3-3 Interaction of incident and diffracted X- rays in an XRD specimen. 38

3-4 Interaction volume in sample where electron beam penetrates and the resulting signals are generated 40

3-5 Picture of cathodoluminescence vacuum system. 42

3-6 XRD pattern for Zn_2GeO_4: Mn films grown on MgO substrate at different deposition temperatures: (a) 750 °C, (b) 700 °C, (c)650 °C, (d)600 °C where * denotes GeO_2 impurity phase. 43

3-7 XRD pattern for films grown on Si substrate at different deposition temperatures: (a) 750 °C, (b) 700 °C, (c)650 °C, (d)600 °C. 44

3-8 XRD pattern for films grown on YSZ substrate at different deposition temperatures: (a) 750 °C, (b) 700 °C, (c)650 °C, (d)600 °C. 45

3-9 CL emission spectrum of Zn_2GeO_4: Mn on MgO substrate at various deposition temperatures. 46

3-10 CL emission spectrum of Zn_2GeO_4: Mn on a Si substrate for various deposition temperatures. 47

3-11 CL emission spectrum of Zn_2GeO_4: Mn on YSZ substrate at various deposition temperatures. 48

3-12 Green emission spectrum of Zn_2GeO_4: Mn excited with 325 nm radiation at 540 nm and excitation spectrum monitored at 540 nm. 50

3-13 Red emission spectrum of Zn_2GeO_4: Mn excited with 325 nm radiation at 625 nm and excitation spectrum monitored at 625 nm. 51

4-1 Powder XRD pattern for Zn_2SiO_4: Mn. This is consistent with the rhombohedral crystal structure reported in JCPDS 37- 1485. 61

4-2 XRD pattern of Zn_2SiO_4: Mn thin film phosphor (0.85 μm thick) before and after annealing. * designates peaks from SiO_2. 62

4-3 XRD pattern of Zn_2SiO_4: Mn thin film phosphor (1.40 μm thick) before and after annealing. * designates peaks from SiO_2. 63

4-4 SEM pictures of the surface of the phosphor films after annealing at 1100 °C for the A) 0.85 μm sample and for B) 1.4 μm thick sample. 64

4-5 Cathodoluminescent emission spectra from Zn_2SiO_4: Mn at V= 5keV, i= 8.0 μA, with inset of CL spectrum for 1.4 μm thick sample. 66

4-6 CL brightness versus primary beam voltage for PLD Zn_2SiO_4: Mn thin films. 66

4-7 Comparison of composition in the PLD thin film samples. 68

4-8 XRD pattern of 1100 ºC annealed sputtered films at two different sputter conditions. 70

4.9 Cathodoluminescent spectra from sputtered deposited thin film samples. 71

4-10 Maximum CL brightness for sputter deposited and annealed Zn_2SiO_4: Mn thin films from 1000 to 5000 eV. 72

4-11 Maximum CL intensity at V= 5keV for i= 2.5 to 7 μA. 73

4-12 Maximum CL brightness for PLD vs. sputter deposited Zn_2SiO_4: Mn thin films from 500 to 5000 eV. 74

4-13 X- ray diffraction pattern from Zn_2SiO_4: Mn thin film sputter deposited with target 2. 76

4-14 Cathodoluminescent emission from sputter deposited Zn_2SiO_4: Mn at electron beam V= 5keV, i= 15μA for sputter powers of 40- 70W. 76

4-15 CL spectra from CCVD Zn_2SiO_4: Mn phosphor films at beam V= 5keV, i= 7.0 μA. 78

5-1 Cathodoluminescent degradation of thin film phosphor at V= 2 keV, i= 3.0 μA (95.49 μA/ cm^2). 84

5-2 Degradation within the first 20 minutes for the thin film phosphor at i= 3.0 μA. ...85

5-3 Cathodoluminescent spectrum of thin film phosphor before and after degradation at low current excitation density. 86

5-4 Auger electron spectrum before and after degradation on thin film, i= 3.0 μA.....87

5-5 Cathodoluminescent degradation of thin film phosphor at V= 2 keV, i= 13 μA.....87

5-6 Cathodoluminescent spectrum of thin film phosphor before and after degradation at high excitation current density. 88

5-7 Auger spectrum before and after degradation on thin film, i= 13.0 μA.....88

5-8 CL spectra of thin film Zn_2SiO_4:Mn at V= 2keV, i= 3.0 μA for 10 minutes of continuous beam exposure and recovery over 3.67 hours indicating permanent degradation of phosphor. 90

5-9 AES spectra from Zn_2SiO_4: Mn thin film phosphor during and after beam exposure (i= 3.0 μA). 91

5-10 CL spectra of thin film Zn_2SiO_4:Mn at V= 2keV, i= 13.0 μA for 10 minutes of continuous beam exposure and recovery over 60 minutes indicating permanent degradation of phosphor. 92

5-11 AES spectra from Zn_2SiO_4: Mn thin film phosphor during and after beam exposure (i= 13.0 μA). 93

5-12 Cathodoluminescent degradation of powder phosphor at V= 2 keV, i= 3.0 μA. 94

5-13 Degradation within the first 20 minutes for the powder phosphor at i= 3.0- 6.0 μA. 95

5-14 Cathodoluminescent spectrum of powder phosphor before and after 24 hours of degradation at low excitation current density. 97

5-15 Auger spectrum before and after 24 hours degradation on powder phosphor, i= 3.0 μA. 98

5-16 Cathodoluminescent degradation of powder phosphor at V= 2 keV, i= 13μA. 99

5-17 Cathodoluminescent spectrum of powder phosphor before and after degradation at high excitation current density. 100

5-18 Auger spectrum before and after degradation on powder phosphor, i= 13.0 μA. ..101

5-19 CL spectra of powder Zn_2SiO_4:Mn at V= 2keV, i= 3.0 μA for 10 minutes of continuous beam exposure and recovery over 15 hours indicating permanent degradation of phosphor. 102

5-20 AES spectra from Zn_2SiO_4: Mn powder phosphor during and after beam exposure (i= 3.0 μA). 103

5-21 CL spectra of powder Zn_2SiO_4:Mn at V= 2keV, i= 13.0 μA for 10 minutes of continuous beam exposure and recovery over 12 hours indicating permanent degradation of phosphor. 104

5-22 AES spectra from Zn_2SiO_4: Mn powder phosphor during and after beam exposure (i= 13.0 μA). 105

Abstract of Dissertation Presented to the Graduate School
of the University of Florida in Partial Fulfillment of the
Requirements for the Degree of Doctor of Philosophy

CATHODOLUMINESCENCE AND DEGRADATION OF
OXIDE THIN FILM AND POWDER PHOSPHORS

By

Lizandra Clarissa Williams

December 2004

Chair: Paul H. Holloway
Major Department: Materials Science and Engineering

The low voltage cathodoluminescent characteristics of Zn_2GeO_4: Mn thin film phosphors grown by pulsed laser deposition were investigated. The effects of substrate heating (600-750ºC) and substrate type (MgO, Si, and yttria-stabilized zirconia) on cathodoluminescent properties were studied. A characteristic green emission peak at 540 nm was observed at substrate temperatures of 650, 700, or 750°C. However, the emission was red shifted to 650 nm for a substrate temperature of 600°C. The red shift in emission wavelength from 540 to 650 nm was attributed to a change in ionic state of the activator from Mn^{2+} to Mn^{4+}. While the spectral position was independent of substrate type, the relative intensities of the cathodoluminescent emission peak varied with both substrate type and substrate temperature. At a substrate temperature of 600°C, the crystal structure of the film was mixed polycrystalline and amorphous. However, at substrate temperatures ranging from 650-750°C, the films were only polycrystalline, with varying degrees of crystallinity that correlated with the cathodoluminescence intensity.

Zn_2SiO_4: Mn thin film phosphors were developed by pulsed laser deposition, sputter deposition, and combustion chemical vapor deposition. Films were grown by pulsed laser deposition at an oxygen pressure of 300 mTorr onto (100) Si substrates heated to 700ºC. The films were polycrystalline after a rapid thermal anneal (RTA) for five minutes at 1100ºC in N_2 atmosphere. The cathodoluminescence of the films depended upon the Zn/ Si atomic ratio, which was less than stoichiometric. The film with the higher zinc content exhibited the brightest cathodoluminescence although the film was also the thinnest. An increase in the deposition time was correlated with a reduction in zinc content.

Sputter deposition of Zn_2SiO_4: Mn thin films were completed on room temperature quartz substrates in O_2/ Ar atmosphere. The films were polycrystalline and green cathodoluminescence was observed from the samples after a RTA for five minutes at 1100ºC in N_2 atmosphere. The cathodoluminescence from the films was compared for a sputter power range, 40- 70W. The cathodoluminescence was brightest for films deposited at 60- 70W and dimmest for films deposited at 40- 50 W. The increased brightness from the films deposited at the higher power was attributed to an increase in the film thickness. The films created by sputter and pulsed laser deposition were compared. The sputter deposited film was at least 30% brighter than the films made by pulsed laser deposition. The lower response was attributed to the Zn deficiency present in the films made by pulsed laser deposition.

The brightest films were made by combustion chemical vapor deposition. The Zn_2SiO_4: Mn phosphor films were deposited onto quartz substrates heated to 1200ºC at atmospheric pressure with ambient room environment supplying the oxygen needed for

this reaction. The cathodoluminescence was compared at two dopant levels: 2 and 4 mol% Mn, with the higher intensity coming from the 4 mol% Mn film.

The degradation behavior was examined for Zn_2SiO_4: Mn thin film and powder phosphors. The degradation was less for both thin film and powder phosphors at a low current excitation density. The CL intensity decreased to 86 and 44% of the CL intensity at time = 0 min. after continuous beam electron beam exposure for 24 hours for the thin film and powder phosphor, respectively. As the beam current density increased, an increase in degradation was also noted. The degradation for the film phosphor was 74% and 24% of initial intensity for the powder after exposure to a continuous electron beam for 24 hours. The increased degradation with increased beam current was correlated to the presence of more severe charging from the phosphor, as observed from the Auger data. At both current levels, the thin film phosphor degraded less than the powder phosphor. No changes in the surface composition, other than the removal of adventitious carbon, were observed through Auger electron spectroscopy during the periods of electron beam exposure. The degradation of the phosphors is attributed to development of internal electric fields and charging of phosphor surface.

CHAPTER 1
INTRODUCTION

Cathodoluminescent phosphors may have applications in many emissive technologies, such as field emission flat panel displays, where the phosphor is responsible for production of the screen image. There is a need by consumers for portable displays that are more durable and have better resolution. Developing an adequate display that meets these requirements depends on development of the screen material as a critical component.

Performance of potential phosphors must be studied to determine which materials would be most adequate. Performance parameters, such as brightness and chemical stability of the phosphor, which affect the reliability and lifetime of the device must be investigated and understood for successful advancements to be made toward identifying potential phosphors for display technologies.

Chapter 2 will provide a survey of recent research developments for cathodoluminescent phosphors, with emphasis on oxide phosphors. A discussion of the experimental parameters and characterization methods will be presented in Chapter 3 for Zn_2GeO_4:Mn thin films grown by pulsed laser deposition. The results from the development of thin film Zn_2SiO_4: Mn by sputter deposition, pulsed laser deposition, and combustion chemical vapor deposition are given in Chapter 4. Insight is given into the critical processing parameters needed to successfully grow Zn_2SiO_4: Mn. Chapter 5 provides an analysis of cathodoluminescent degradation of both powder and thin film Zn_2SiO_4: Mn phosphors at high and low beam current densitites, with an aim of

determining the mechanism for oxide degradation. Chapter 6 provides a summary of the conclusions from the experimental results for these oxide phosphors.

CHAPTER 2
LITERATURE REVIEW

2.1 Introduction

Cathode ray tube (CRT) monitors and televisions are the conventional display for image and visible information transfer. The CRT television is still the most popular type, [1] although there is competition from other display technologies. Flat panel display technologies such as the active matrix liquid crystal display and the plasma display panel are the newest options in the television market [1]. The CRT display has several advantages over its competitors. It offers the best contrast, best resolution, widest viewing angle, and lowest cost [1]. With a lower price tag than its competitors, the CRT display offers the best value for your money. However, a major disadvantage of the CRT monitor is the size and bulk associated with this type of display. These CRTs are the heaviest of all types of televisions [1]. Many competitive technologies have been developed to respond to this inconvenience. Demand is growing for displays that are lighter and thinner, offering the convenience of easy portability.

One technology that meets the demand for a more compact and portable display is liquid crystal display (LCD). The LCD technology was developed in the 1970s.[1] These LCDs are used in front projectors, rear-projection TVs, and flat panel displays. The main advantage of LCDs is that they are very marketable to consumers who need a compact and portable display. An LCD offers a thinner, lighter, and sleeker alternative to the CRT. However, the customer can expect to pay more for this convenience. Disadvantages of using an LCD include limited viewing angle and contrast ratio,

resulting in displays with a lower resolution than the conventional choice.[1] There are markets where small displays would be desirable, but an LCD is not the optimal choice. Developing displays that are brighter and more rugged; and that have an extended operating temperature range, and less sensitivity to constant movement would be beneficial to applications involving military, medicine, and transportation displays.[2]

2.2 Development of Cathodoluminescent Phosphors

Cathodoluminescent phosphors have been researched for over 100 years. Improvements are still being made in this area, as new applications for cathodoluminescent phosphors have emerged. Braun invented the cathode ray tube oscilloscope in 1897 [3,4], which is noted as the first practical application of displaying an image by bombardment of electrons. This led to more investigations on the behavior of phosphors. Phosphors are materials that emit light when stimulated by an incident energy source [5]. In this example of cathodoluminescence (CL), the electrons emitted from the cathode were the source of energy. An example of a cathode ray tube is shown in Figure 2.1. The cathode ray tube is a glass tube sealed to maintain a vacuum, where most of the air has been removed. Inside the vacuum tube, a piece of metal coated with a phosphor is placed horizontally between the cathode and anode. This coating on the metal allows the observer to visibly observe the path of the electrons. The electrons originate from the cathode, which is the negative electrode. The electrode is connected to a power source by the alligator clip. The anode directs the path of the electrons due to the attraction of the electrons to the positive electrode. The result is a visible luminescent line between the negative and positive electrodes indicating the path of the electrons. In 1907, Boris Rosing made a significant development with the cathode ray tube when he demonstrated that it was possible to transmit an image. Since then, many inventions and

discoveries have been made. Presently, cathode ray tubes are used in many commercial display devices such as televisions, computer monitors, modern oscilloscopes, and electron microscopes.

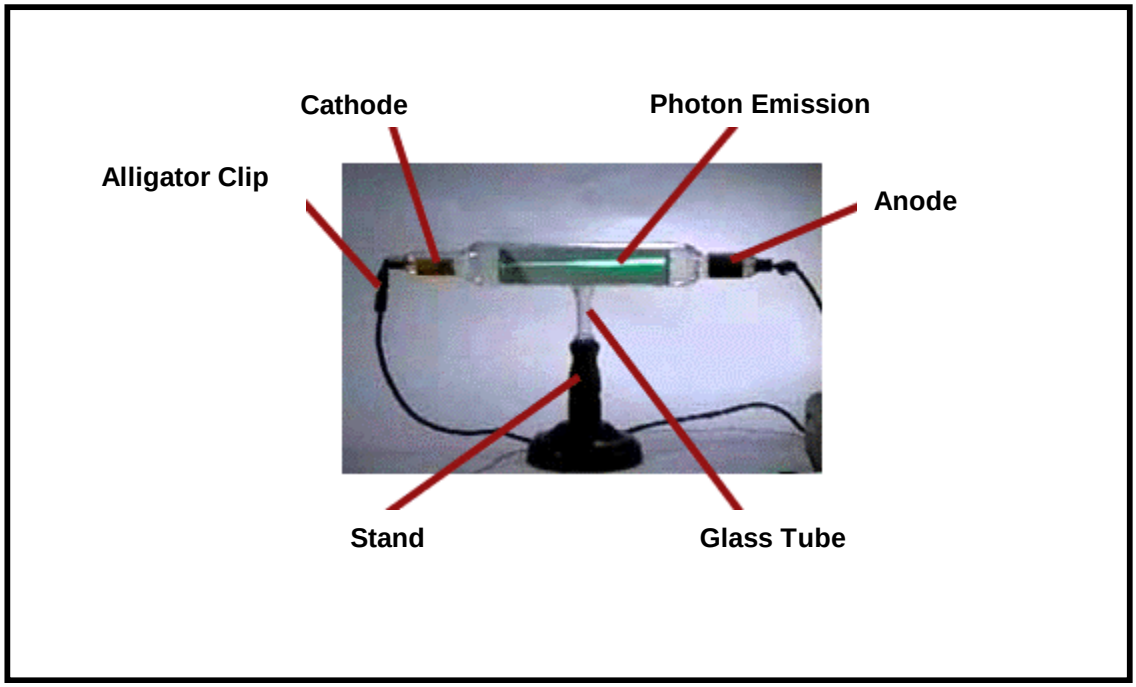

Figure 2-1. Cathode Ray Tube [6].

Initially, black and white televisions relied on only two phosphors for its display image. The phosphors combined to produce a bluish- white emission color [7]. The best phosphors for this application were ZnS:Ag and $Zn_{0.5}Cd_{0.5}S$:Ag or $Zn_{0.9}Cd_{0.1}S$:Cu, Al [7]. With the development of full color displays, the number of electron guns increased to three. Each electron beam emitted from the gun is directed to one of three phosphors emitting red, green, or blue. An example of a full color CRT with an illustration on the operation of the electron beams is shown in Figure 2.2. The display screen is divided into subdivisions called pixels. Each pixel has a red, green, and blue phosphor in its sub-pixel matrix. The number of pixels on a display screen determines the resolution that is

available for the display. As the number of pixels increase, the color detail for the images also increase. The pixel matrix is depicted in Figure 2.3. Additive mixing of red, green, and blue (RGB) colors result in all of the colors needed for a full color display [7-9]. The illustration in Figure2.4 shows the range of colors produced by the RGB phosphors as they are mixed together. The best phosphors for full color CRT displays are ZnS: Ag (blue); ZnS: Cu, Al (green); and Y_2O_2S: Eu (red) [7]. The choice of phosphors will change as the thick CRT evolves into a thinner model.

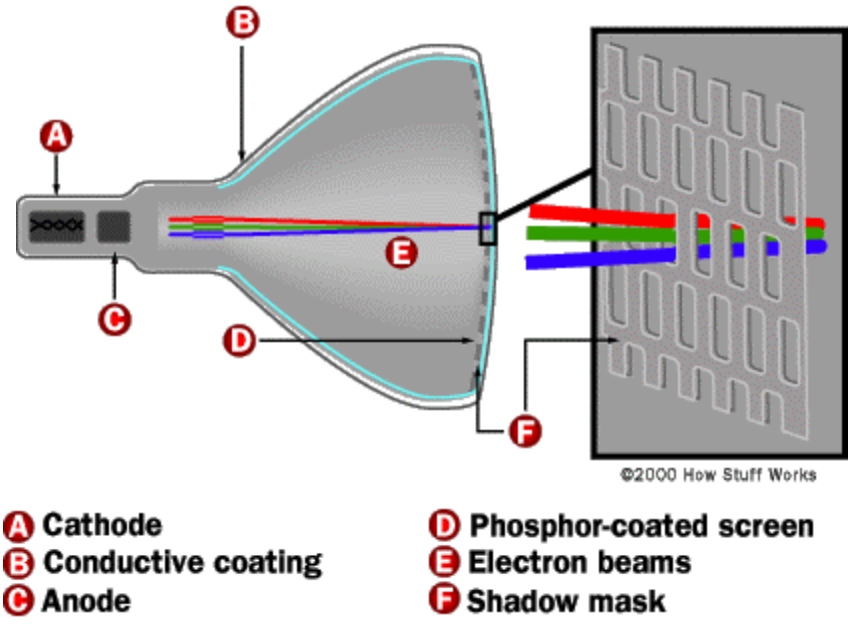

Figure 2-2. Generation of electron beams in a CRT display [10].

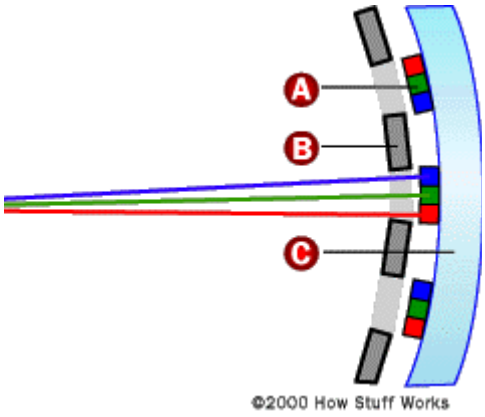

Figure 2-3. Pixel view beyond shadow mask where A → red, green, blue posphors; B → shadow mask; C →glass of display screen [10]

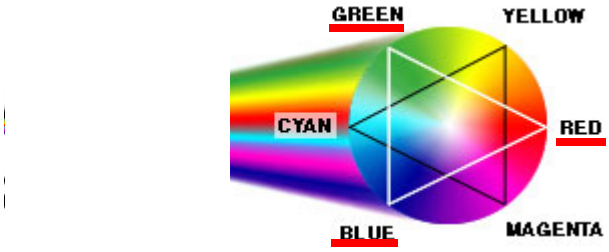

Figure 2-4. Illustration of how the red, green, and blue hues combine to give a full spectrum of colors for full color displays [9].

2.3 Evolution of the Field Emission Display

Field emission displays (FEDs) are flat panel displays that are similar to the conventional cathode ray tube (CRT) displays [11]. Both technologies produce an image on the display screen by using an electron source. The main components of the FED that have been the attention of many researchers are the phosphor and emitter. The emitter is the component that produces the electrons. The phosphor has the responsibility of producing the image on the device screen.

The filed-emitters for an FED are analogous to the electron guns found in CRTs. A CRT uses only three electron guns, whose focused beam of electrons are scanned across the screen to produce an image; whereas, FEDs use an array of thousands of micron scale

cold cathode emitters to direct electrons at each pixel as shown in Figure 2.5. These small emitters allow FEDs to be scaled to millimeters in width, allowing for the feasibility of a thin display. However, the narrow thickness requires device operation at lower voltages to prevent vacuum breakdown [12]. In order to obtain an acceptable brightness at low voltages, the current density requirement must be increased.

A thermionic cathode using high accelerating voltages produces electrons in CRT. The voltages may range from 20- 30 kV for a CRT [13,14]. In FED, the electrons are produced via a cold cathode by electron tunneling at high fields. The target operating voltage for an FED ranges from 1- 8 kV [13]. The lower voltage results in a higher current to maintain necessary power to yield adequate brightness from the phosphor. The amount of light that is emitted from the phosphor depends upon beam power, i.e. primary beam voltage times current [13]. The phosphors used for CRTs are usually coated by a thin aluminum layer (0.2- 0.5 μm), as shown in Figure 2.6 [13]. [13]. The phosphors used for CRTs are usually coated by a thin aluminum layer (0.2- 0.5 μm), as shown in

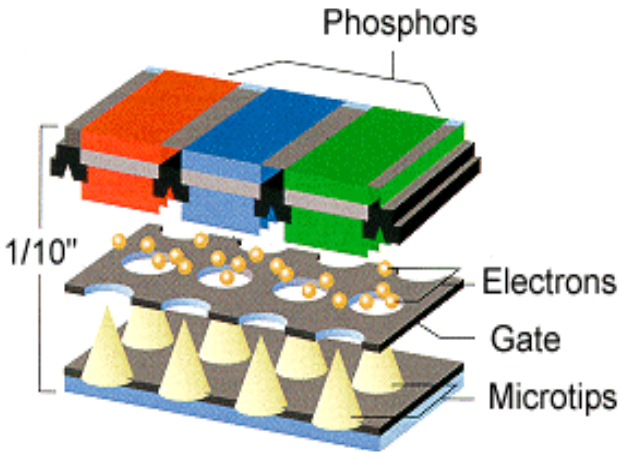

Figure 2.5. Pixel view of field emission display.

Figure 2.6 [13]. The cross section shows that the aluminum layer may protect the phosphor from the reaction with residual vacuum gases. However, for the FED, the aluminum layer is not always applied. This leaves the phosphor exposed to the vacuum environment. Consequently, the effect of the residual vacuum gases on the phosphor are a critical reliability concern for the device. Thus, conditions such as charging and outgassing are huge concerns for this application [2,13]. Therefore, it is important to understand what happens to the phosphor during electron beam exposure in different ambients. Anticipated advantages of FEDs over LCDs include: better viewing angle, better response time, wider operating temperature range, better price & power consumption [13].

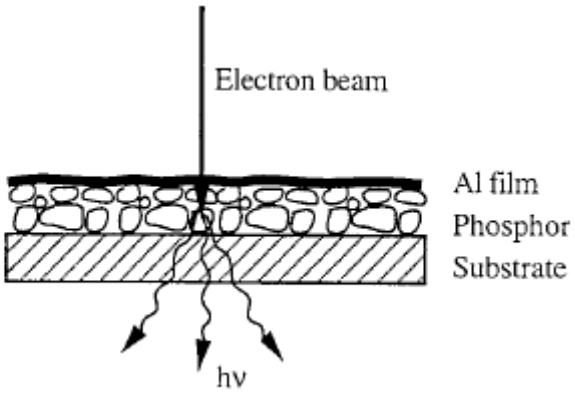

Figure 2-6. Cross section view of phosphor screen for a CRT [13].

2.4 Cathodoluminescent Phosphor Materials

2.4.1 Host Material

The host material is responsible for the electrical and optical properties of the phosphor. The inert host lattice is transparent to the excitation radiation [13]. Nevertheless, the surroundings of the activator in the host material dictate the optical behavior of the activator.

2.4.2 Activator-Luminescent Center

The activators control the emission spectra of luminescent materials [15]. An activator, or luminescent center, is an impurity added to the host material in small quantities. It is known as the light-emitting center of a phosphor and is responsible for the optical properties of a phosphor. Activators provide distinct energy levels in the energy gap between the conduction and valence bands of the host material [15]. The interaction of the incident energy source with a luminescent material is critical for the production of light.

In the case of electron- hole pair excitation by the primary electrons for CL, the energy levels associated with the activators determines the energy of the photon emission. A phosphor absorbs the incident energy, which leads to electron excitation from the valence band to the conduction band. It is the behavior of these electrons, which determines the luminescence of a phosphor. The electrons are excited either to the conduction band or to a trap as shown in the first step illustrated in Figure 2.7. The traps are the distinct energy levels formed by the activator. These energy levels are referred to as traps since electrons and/ or holes may become held in them for long times at the temperature of operation. In the second step, shown in Figure 2.7, the electrons may be excited from one trap to another or into the conduction band. The elemctrons can then be captured by upper empty activator levels, and subsequently emit photons when they drop further down to lower excited state or ground state activator levels, as shown in step 3 of Figure 2.7. The energy of the photon emitted, E, is associated with a specific wavelength of light, λ, as given by [16]:

$$\lambda = \frac{h\nu}{E} \qquad (2\text{-}1)$$

and with substitution of the appropriate phosphors, results in:

$$\lambda(\mu m) \cong \frac{1.2398}{E(eV)} \qquad (2\text{-}2)$$

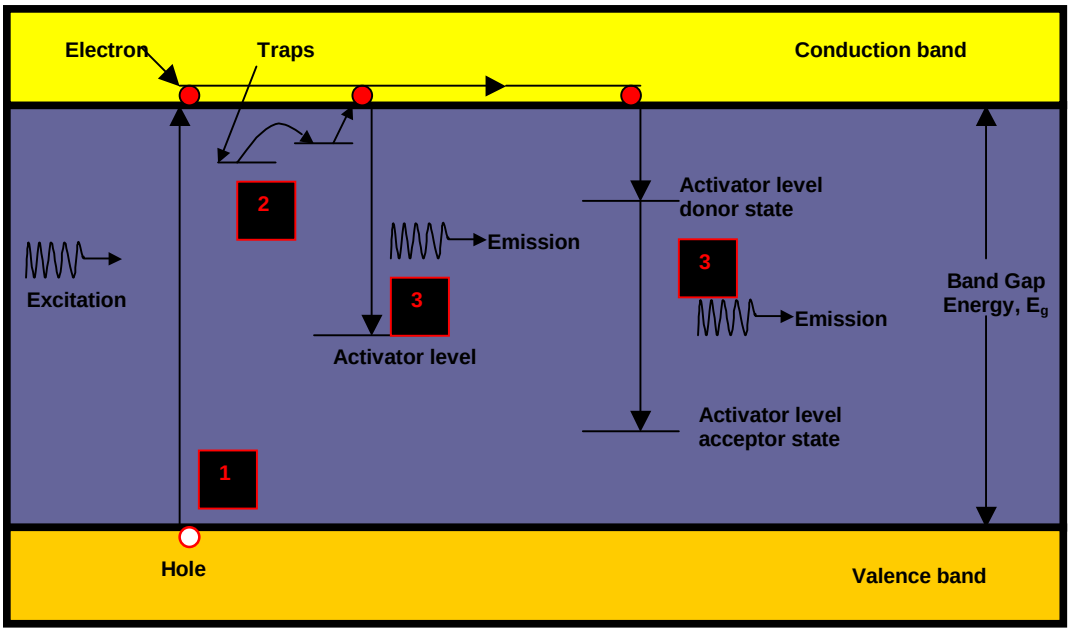

Figure 2-7. Energy excitation (absorption) leads to photon emission.

2.5 Materials Development

Phosphors are often characterized as either a sulfide or oxide phosphor. Conventional cathodoluminescent phosphors are sulfide based, where sulfur is an element present in the composition.

2.5.1 Sulfide Phosphors

A lot of research has been devoted to sulfide phosphors since they are used in many display applications. Zinc sulfide, ZnS, is a common host material for cathodoluminescent and electroluminescent phosphors. It has been noted for its excellent electrical properties. The most efficient materials for host lattice excitation have relatively small values for the band gap energy, E_g. The band gap energy of ZnS = 3.75

eV. Thus, zinc sulfide has been noted for its excellent cathodoluminescent efficiency of 20- 25% [3]. Depending upon the dopant, this phosphor can exhibit a specific color luminescence. Many elements have been incorporated in the ZnS host lattice. Table 2.1 shows some of the dopants and colors that may be emitted from the ZnS phosphor.

Table 2-1 Color and wavelength emission for common dopants in ZnS host [2,3,7].

DOPANT	COLOR
Mn	Yellow
Mn (filtered)	Red
Cl	Blue
Ag, Cl	Blue
Cu, Cl (or Al)	Green
Tb or TbOF	Green
Tm	Blue
Sm, Cl	Red

Sulfide phosphors have also been considered for use in FEDs [17]. However, these phosphors are not very efficient at low voltages. In addition, conventional sulfide phosphors such as ZnS:Cu,Al degrade significantly and decompose under electron beam bombardment at the operating conditions required for field emission displays [18-20]. The products of degradation may potentially contaminate the cathode components, reducing the performance of the emitters [20,21].

2.5.2 Oxide Phosphors

Oxide phosphors have also received attention as potential phosphors in low voltage display applications, such as the FED. Oxide materials are generally more chemically and thermodynamically stable than sulfide phosphors [22,23], so they are now investigated as the potential phosphor type for low voltage applications. There are a host of oxides that have been investigated and a summary of these phosphors are given in the following table.

Table 2-2 Common oxide phosphors and their luminescent properties [24].

PHOSPHOR	COLOR
Zn_2SiO_4: Mn	Green
ZnO: Zn	Green
$ZnGa_2O_4$: Mn	Green
$Y_3Al_5O_{12}$: Ce	Green
ZrO_2: Mn, Cl [25]	Red
Y_2O_3: Eu	Red
YVO_4: Eu	Red
Y_2SiO_5: Ce	Blue
$ZnGa_2O_4$	Blue
$CaWO_4$	Blue

2.5.2.1 Zinc silicate phosphors (Zn_2SiO_4: Mn)

Zinc silicate is already known as a phosphor for CRT and plasma display applications. Several research groups have investigated its luminescent properties in powder and thin film form [26-33]. Its feasibility as a phosphor for field emission

displays, electroluminescent devices, medical imaging detectors for low- voltage radiography and fluoroscopy is also being studied.

Sun et al. observed a correlation between the film crystallinity and morphology for as deposited and annealed films. The films were grown on heated 300 °C substrates by pulsed laser deposition and were annealed at 1000 °C, before Zn_2SiO_4 crystallized [30] indicating that a high temperature treatment is needed for a polycrystalline material. The morphology, observed by scanning electron microscopy, indicated that the finer grains and rougher surface correlates with an increase in the photoluminescence intensity due to disruption of light guiding in high index thin films [30,34].

The high crystallization temperature of Zn_2SiO_4 is a definite disadvantage. Cho et al. demonstrated that temperatures as high as 1400 °C may be necessary to fully crystallize Zn_2SiO_4 when the powder is processed in a solid state reaction. The authors also developed a novel solution reaction method to lower the processing temperature. However, the temperature was reduced by only 200 °C [29]. One group has tried to overcome the temperature hurdle, by processing zinc silicate by combustion synthesis. Nonetheless, after initial processing at 500 °C, the powder still required heating to 900 °C for 1 hour in a reducing atmosphere, where the powder then gained the characteristic white appearance [28]. The authors also indicated that the second thermal treatment improved the luminescence of the Zn_2SiO_4: Mn phosphor.

Zinc silicate is a promising phosphor for CL applications. A brief summary of the relevant properties for zinc silicate is shown in Table 2.3. Cathodoluminescent emission has been observed with peak emission exhibited around 525 nm [33]. Its high efficiency makes it a possible phosphor in low voltage applications. However, the need for a high

processing temperature is a definite disadvantage. Another approach for getting beyond the temperature hurdle has been to alter the composition of the material as will be discussed in the next section.

Table 2-3 Summary of Zn_2SiO_4: Mn properties [30].

Property	Value
Bandgap	5.5 eV
Index of Refraction	1.69
Crystal structure	Rhombohedral

2.5.2.2 Zinc germanate phophors (Zn_2GeO_4: Mn)

Zinc germanate has been evaluated as a potential phosphor in alternating current thin film electroluminescent displays (ACTFEL) [22,35-37]. In this phosphor, Ge atoms substitute for the Si atoms from Zn_2SiO_4. The resulting composition, Zn_2GeO_4, leads to a lower crystallization temperature and a smaller bandgap. Crystallization temperatures as low as 650 °C have been reported. Some researchers found that a slight raise in processing temperature to 810 °C improved the luminance of the electroluminescent phosphor. A survey of the literature indicates that Zn_2GeO_4: Mn thin films have been fabricated mostly by sputter deposition [22,35-37].

A brief summary of known zinc germanate properties are shown in Table 2.4. The electroluminescent emission peak of Zn_2GeO_4: Mn has been observed to be between 535-540 nm [22,35,38]. Zn_2GeO_4: Mn has been characterized as having a short decay time (100 microseconds), resulting from the formation of a perfect structure and the low coordination number (4) of manganese in host lattice [38]. The cathodoluminescent

efficiency of Zn_2GeO_4: Mn at 2 keV has been reported as 2.4 lm/W for the thin film phosphor [23].

Table 2-4 Summary of Zn_2GeO_4: Mn properties.

Property	Value
Bandgap	4.68 eV [35]
Index of Refraction	1.80 [22]
Dielectric constant	6 [22]
Crystal structure	Rhombohedral

Zinc silicate- germanate ($Zn_2Si_{0.5}Ge_{0.5}O_4$: Mn) thin film phosphors have also been created by sputter deposition [39,40]. This phosphor was developed from incorporating Ge into the silicate (SiO_4) lattice of Zn_2 SiO_4. The Ge substitutes for the Si resulting in a lower annealing temperature. Temperatures as low as 700 °C have been reported for annealing conditions, resulting in a polycrystalline film [39,40]. The photoluminescent and electroluminescent emission peak of annealed $Zn_2Si_{0.5}Ge_{0.5}O_4$: Mn is at ~ 530 nm [39,40], a slightly shorter wavelength than pure Zn_2GeO_4: Mn. It is interesting, however, that the as- deposited amorphous phosphor film show PL emission at two separate wavelengths, which is not near the emission at 531nm, observed only in the annealed case [40]. This PL emission behavior is shown in Figure 2.8. No further explanation of the emission results was given by the authors.

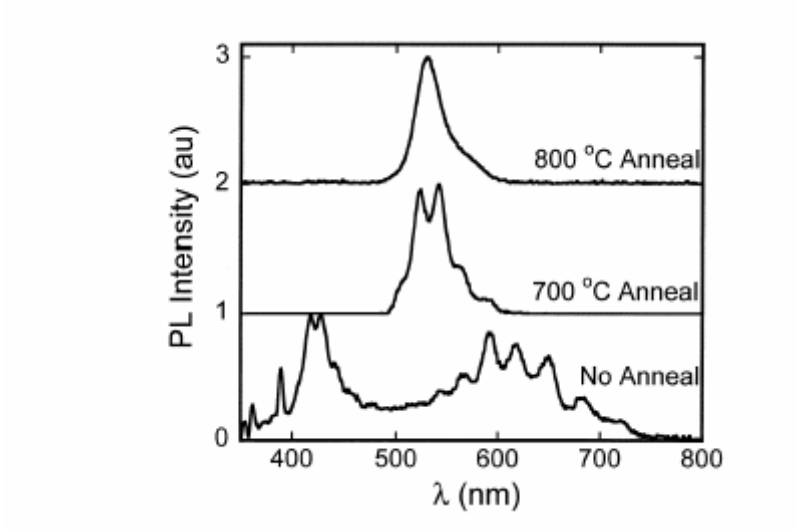

Figure 2-8. PL spectra for as deposited and annealed $Zn_2Si_{0.5}Ge_{0.5}O_4$: Mn thin films [40].

2.6 Processing of Phosphors

2.6.1 Powder Phosphors

Powder phosphors are usually made by a solid state reaction, although there are various other methods that are employed as well. In this process, the raw materials are first combined through chosen synthesis method. The powder is then fired with a flux and the activator [7]. After the product is sieved, the flux is removed. The powder is then milled with care to obtain the desired particle size [7].

2.6.2 Thin Film Phosphors

Thin film cathodoluminescent phosphors have been grown by a variety of growth techniques. Pulsed laser deposition, sputter deposition, electron beam evaporation, and metal- organic chemical vapor deposition are some of the common processes used to develop thin film phosphors [30,32,41-44]. In this work, pulsed laser deposition and rf magnetron sputter deposition were used to create the thin film phosphors. Accordingly, further details of these methods are given below.

2.6.2.1 Pulsed laser deposition

Pulsed laser deposition is one of the most simplistic methods to deposit thin films. It allows for the precise arrival rates of atoms for compound films. This has been shown to be favorable for obtaining stoichiometric films of multi-component materials with a high energy of dissociation [45]. This method has received considerable attention for its ability to deposit the complex oxides needed to produce superconducting thin films [45-49]. It also has the ability to operate in high pressure reactive gases, unlike other deposition methods [45].

A deposition system usually consists of an excimer laser and optical elements to maneuver and focus the laser beam. Some of the optical elements that are used in the set up are focusing lens, apertures, mirrors, beam splitters and laser windows. A schematic of a basic deposition system that uses oxygen as its reactive gas is shown in Figure 2.9.

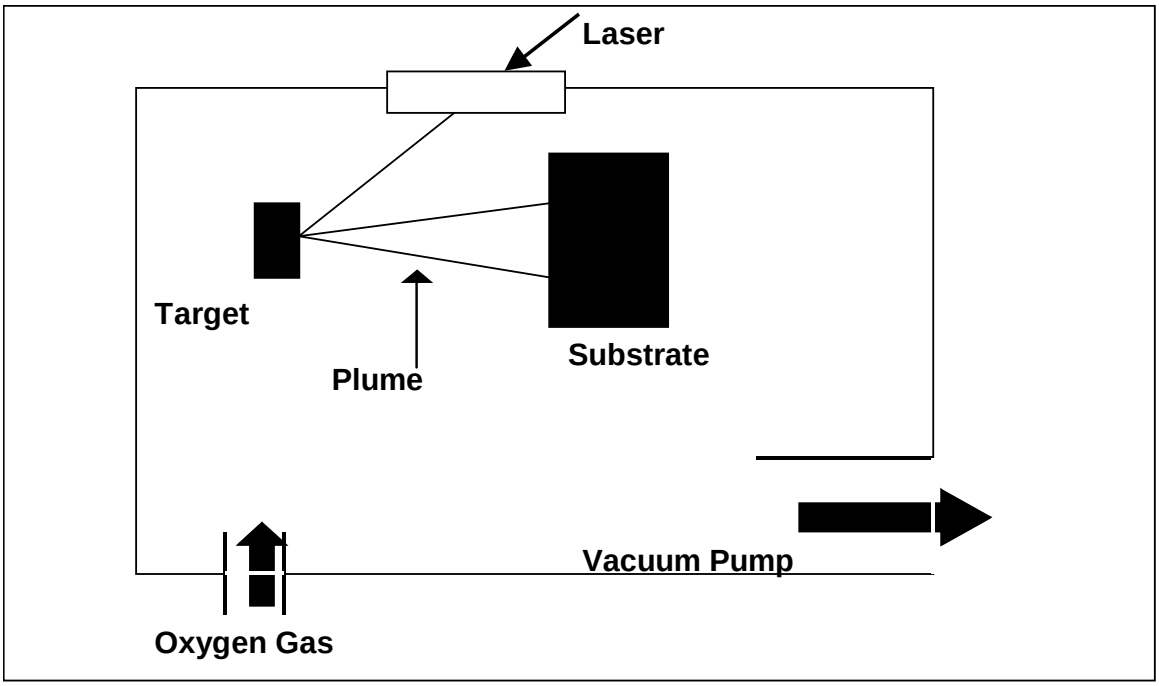

Figure 2-9. Sketch of basic pulsed laser deposition system [45].

Excimer lasers with wavelengths between 200 and 400nm are most often used for pulsed laser deposition [45]. A list of common excimer lasers and their operating wavelengths are given in Table 2.3. Excimer lasers below 200nm are not typically used for PLD due to the possibility of absorption by the Schumann- Runge bands of molecular oxygen. As shown in Figure 2.9, the laser source is located external to the vacuum chamber. The external energy source allows the film growth process to take place in a reactive environment with any type and amount of gas. The external source gives the added advantage of the laser being available for more than one deposition system.

Table 2-5 Typical excimer lasers and their operating wavelengths [45].

Excimer	Wavelength (nm)
F_2	157
ArF	193
KrCl	222
KrF	248
XeCl	308
XeF	351

Once the laser is focused into the chamber, the target absorbs the energy from the laser. The ultra- violet (UV) radiation is converted to electronic excitation. This is converted into thermal, chemical, and mechanical energy, leading to ablation and evaporation of the target. The evaporants form a mixture of energetic species including atoms, molecules, electrons, ions, and micron sized particulates. This mixture is the often referred to as a plume. An example what a plume looks like during the film growth process is shown in Figure 2.10. The plume quickly expands in the vacuum from the

target to form a “nozzle jet” [45]. As the plume reaches the substrate (which may be heated), film nucleation commences.

The quality of the thin films produced by pulsed laser deposition is dependent on several variables. Laser power and spot size have a significant effect on particulate size and density. As the laser fluence is increased beyond a threshold, the number of particulates that are formed also increases [45]. Laser fluence is defined as the laser energy per unit area and thus, may be adjusted by varying the laser power or laser spot size. Background gases may change growth parameters such as the deposition rate and the kinetic energy distribution of the depositing species [45]. For instance, an oxidizing environment can help oxides to form and stabilize the desired crystal phase at the deposition temperature [45]. Substrate temperature has an effect on the stoichiometry of the film as well as the film structure [45]. Film structure has also been influenced by the deposition rate. Wu et al. found that an increase in the deposition rate led to a decrease in the crystallinity of $YBa_2Cu_3O_{7-\delta}$ thin films. At the higher deposition rates, the arrival rate exceeds the diffusion rate. Equilibrium conditions are not maintained and structural defects are formed [47].

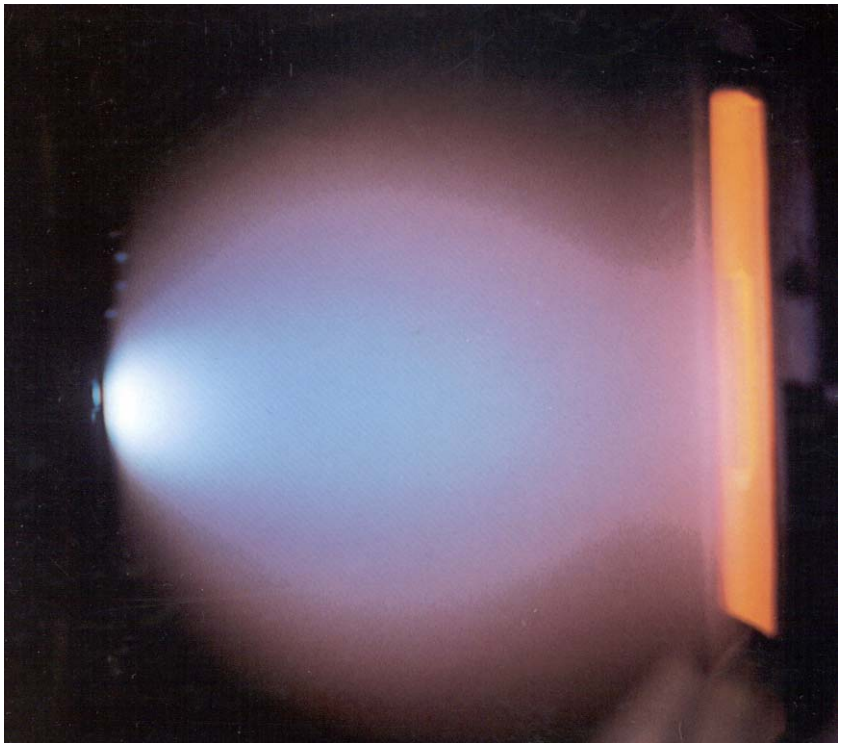

Figure 2-10. Picture of plume developed during PLD [45].

In summary, the advantages of this growth method include [45]:

- Flexibility to use energy source with more than deposition chamber
- Easy process control
- Ability to use high reactive gas pressures
- Decreased contamination from outside sources
- Control of film stoichiometry.

The short laser pulses result in congruent evaporants. Congruent evaporation aids in stoichiometry control of the thin films during mass transfer from target to substrate. One obvious disadvantage is the presence of micron sized particulates. Also, scale up to large area deposition is not easily completed.

Pulsed laser deposition has been shown as an appropriate method for growing phosphor films, specifically oxide phosphors. Yttria and silicate phosphors are some of the oxide materials that have been grown by this method [30,34].

2.6.2.2 Sputter deposition

Sputter deposition is another thin film growth method that allows the use of a solid target based on the same composition that is expected in the resulting film [50,51]. Sputter deposition is performed by extracting ions (usually Ar) from a plasma that strike a target consisting of the material to be deposited. The plasma is formed by partially ionizing an inert background gas that is flow- controlled into the system. The energetic Ar ions produce a continuous flux of sputtered atoms that deposit on a nearby substrate. The plasma is sustained by a DC voltage, radio frequency (rf) power, or a magnetron operating at milliTorr pressures. A typical sputtering system is composed of a stainless steel vacuum chamber, pumping system, internal sputter source, and a biased substrate holder. A schematic of a typical sputter deposition chamber is given in Figure 2.11.

Radio frequency (rf) magnetron sputtering is often used for dielectric thin film growth [52-54]. The higher degree of ionization associated with this sputtering method makes it a popular choice for those materials which would otherwise be affected by charging [51,54,55]. With this method, the target material self biases to a negative potential and is charged as the cathode [53]. In this case, the background gas is first ionized by primary electrons. These positive ions may be accelerated to energies adequate for sputtering the negatively powered cathode, and upon bombardment, emit secondary electrons and atoms from target surface. Magnetron sputter sources have a magnetic field of 50- 500 gauss parallel to the target surface [52]. The placement of the magnets relative to the target is shown in Figure 2.12. In combination with an electric field, the magnetic field causes the secondary electrons to drift in a closed circuit in front of the target surface. Consequently, the magnetic field controls the motion of the

electrons since a magnetic field can exert a force on a charged particle in motion as dictated by Lorentz's law [56]. Lorentz's law is given by:

$$F = q\vec{v} \times \vec{B} \qquad (2\text{-}3)$$

where F is the force exerted on a particle with charge, q, and velocity, v, from an incident magnetic field B.

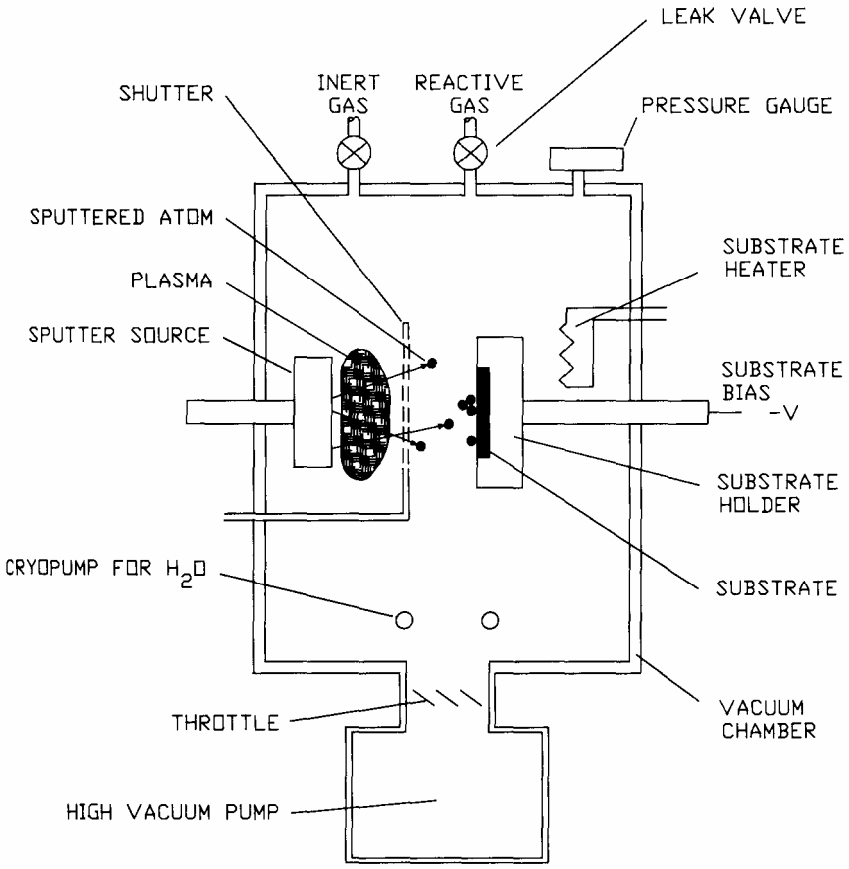

Figure 2-11. Schematic diagram of a typical set up for a sputter system [52].

The magnetic field also dictates that the particles move in a helical path with a radius, r, determined by [56]:

$$r = \frac{mv_{\perp}}{qB} \qquad (2\text{-}4)$$

where m is the mass of the charged particle, q is the charge of the particle, and $v_{\perp}$ is the component of the particle's velocity normal to the applied magnetic field. Due to electrostatic attraction, the Ar ions move with the electrons keeping the plasma neutral. Under the best conditions, the plasma discharge is kept close to the cathode surface, and bombardment of the growing film by electrons and ions is minimized. However, it is possible to get "negative ion resputtering", resulting in sputtering of film as well [57]. Ion resputtering is characterized by damage to film, resulting in amorphous structure [57]. Condensation of the atoms from the target onto the substrate initiates film nucleation [54].

Sputter deposition is used in many commercial applications. Compact discs, integrated circuits, magneto optical storage media, window coatings, and wear- resistant coatings are some of the industries that have found sputter deposition applicable to their respective processing methods [52,53]. Some of the advantages of sputter deposition that have been realized are [52]:

- Control of thickness
- Good film adhesion
- High deposition rates
- Good film uniformity over large area.

The disadvantages of sputter deposition include the inevitable waste of target material. Only about 20- 30% of the target material is used in magnetron sputtering [52].

2.7 Evaluation of Phosphor

There are several experiments that are completed to evaluate the overall performance of phosphors. This includes chromaticity, spectral distribution, and lifetime of luminescence.

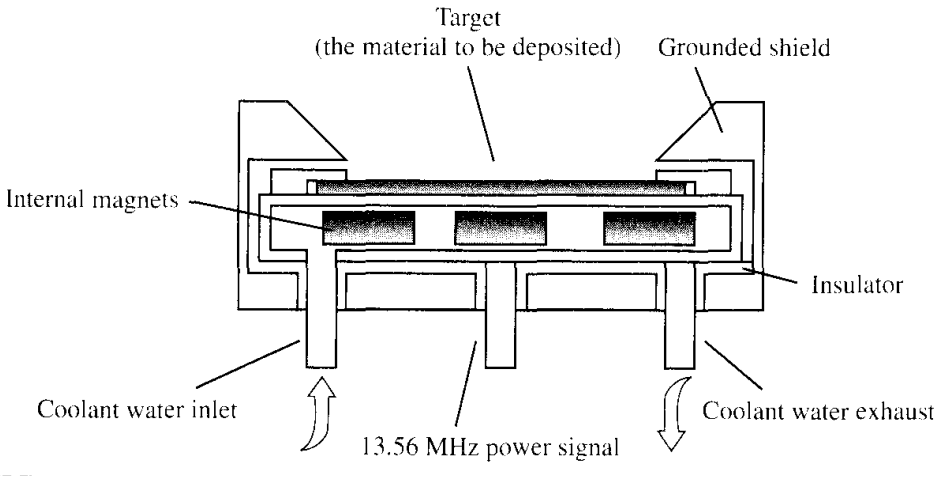

Figure 2-12. Planar magnetron sputter source [56].

2.7.1 Chromaticity

A quantitative method has been established that relates the color produced on display screens to a standard value. The 1931 Commission Internationale de l'Eclairage (CIE) established a standard that defines chromaticity by x,y, and z coordinates. The chromaticity values are plotted on a two- dimensional graph, shown in Figure 2.13, using the x and y coordinates. The third value, z, is found by knowing $x+y+z=1$. Thus, when mentioning the chromaticity of a phosphor, usually the x and y coordinates are only given. The CIE diagram also shows how red, green, and blue blend to give all hues needed for image production on a display screen.

2.7.2 Spectral Distribution

The spectral distribution gives information about the characteristic emission of a phosphor. The visible light emission of phosphors is within 400- 700 nm. This range of wavelengths is divided into six major divisions for the following colors: red, orange, yellow, green, blue, and violet. An example of this range with its corresponding colors is

shown in Figure 2.14. The color that each phosphor emits corresponds to a wavelength within the visible light spectrum.

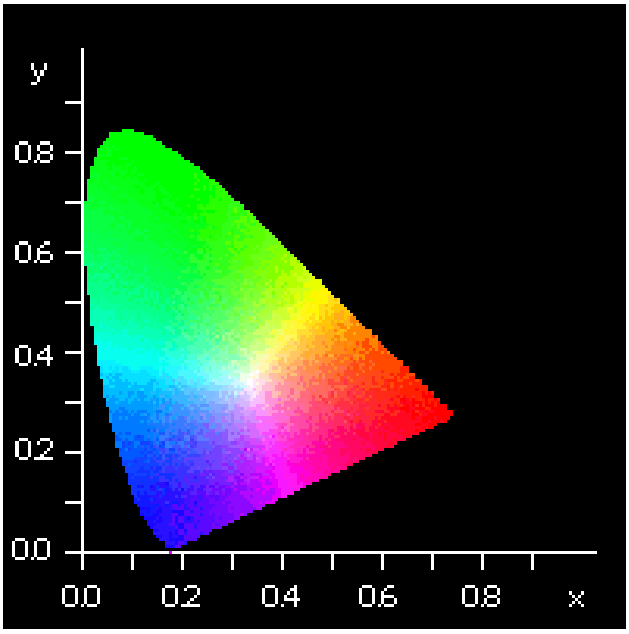

Figure 2-13. CIE chromaticity chart.

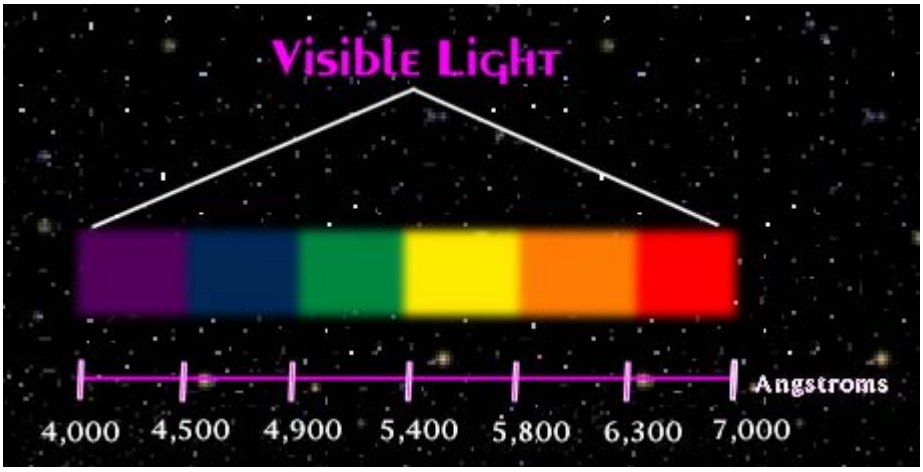

Figure 2-14. Visible light spectrum and corresponding wavelengths [58].

2.7.3 Degradation Characteristics

In this section, vacuum ambient effects on phosphor performance and electron stimulated surface chemical reactions will be discussed. A phosphor is said to experience degradation when there is a loss in the CL intensity over time during exposure to an electron beam. Several research groups have studied degradation of sulfide phosphors extensively [18,19,59-61].

Several theories have been developed to explain the degradation of a phosphor. Pfahnl has studied the rate of degradation of several phosphors. (This will be expanded-need to get book)

Surface chemical reactions have also been investigated as a culprit for the observed degradation in cathodoluminescent phosphors. The electron stimulated surface chemical reaction model was developed to explain the loss of cathodoluminescence for these phosphors through the development of a "dead layer". The dead layer is the surface layer that inhibits or reduces the CL intensity. A mathematical model for describing electron stimulated surface chemical reactions (ESSCR) has been developed by Holloway et al. This model explains that the degradation is dependent upon the type and concentration of gases present in the vacuum, energy of electron beam, as well the beam current and time of exposure to electron beam. A description of this mathematical model follows.

This model focuses on the surface interactions, since the low beam energy would involve the surface of the phosphor rather than the bulk [18]. Additionally, the model uses the ZnS phosphor for its description of the material system. In terms of cathodoluminescent degradation for the ZnS system, the loss in sulfur (*S*) has been correlated with a loss in CL intensity. This concentration of *S* on the surface was modeled by the following standard chemical reaction rate equation:

$$\frac{dC_s}{dt} = -kC_sC_{as}^n \qquad (2\text{-}5)$$

where C_s is the concentration of *S* on the surface, *k* is the chemical rate constant, C_{as} is the concentration of the adsorbed atomic species that will react with ZnS, and *n=1* where a first order reaction is assumed [18]. The model also assumes that the chemical reaction takes place on the surface, not in the gas phase, such that C_{as} can be expressed as:

$$C_{as} = Z\Phi_{ma}C_mJ\tau_{as} \qquad (2\text{-}6)$$

where *Z* is the number of reactive atomic species produced from the parent molecule, Φ_{ma} is the dissociation cross section of the molecule to atoms, C_m is the surface concentration of the molecular species, *J* is the current density of the electron beam causing the dissociation, and τ_{as} is the lifetime of the reactive species lifetime [18]. It should be noted that the dissociation cross-section is a function of the electron beam energy. This expression dictates that the reaction rate is limited by the rate of production of the adsorbed species. In other words, the rate of production of the adsorbed atomic species that will react with ZnS is controlled by the surface concentration of the molecular species. This adsorbed molecule concentration, C_m, may be expressed by Henry's isotherm as:

$$C_m = \sigma\left(\tau_o \exp\left[\frac{Q}{kT}\right]\right)\left(\frac{P_m}{\left[2\Pi mkT\right]^{1/2}}\right) \qquad (2\text{-}7)$$

where σ is the molecular sticking coefficient (assumed to be independent of coverage), τ_o is the mean time between attempts by the physisorbed molecule to escape from the surface, *Q* is the energy required to desorb from the surface, *k* is Boltzman's constant, *T* is the absolute temperature, and P_m is the partial pressure of the molecular gas in the vacuum. The first term in brackets in the preceding equation collectively describes the

molecular mean stay time on the surface, where the second term is an expression for the molecular flux onto the surface. Inserting equation 2-7 into 2-6 and then equation 2-6 into 2-5 results in the following rate expression:

$$\frac{dC_s}{dt} = -k\sigma C_s Z\phi_{ma} J\tau_{as}\left(\tau_o \exp\left[\frac{Q}{kT}\right]\right)\left(\frac{P_m}{\left[2\Pi mkT\right]^{1/2}}\right) \qquad (2\text{-}8)$$

This equation may be adjusted to

$$\frac{dC_s}{C_s} = -K' JP_m dt \qquad (2\text{-}9)$$

where

$$K' = k\sigma Z\phi_{ma}\tau_{as}\left(\frac{\left(\tau_o \exp\left[\frac{Q}{kT}\right]\right)}{\left[2\Pi mkT\right]^{1/2}}\right). \qquad (2\text{-}10)$$

Integrating equation 2-7 with respect to time and using the boundary condition, $C_s = C_o$ for t = 0, results in:

$$C_s = C_s^o \exp\left[-K' P_m Jt\right] \qquad (2\text{-}11)$$

where *Jt* is the coulombic dose [Coulombs/ Area]. The resulting model predicts that the concentration of sulfur will decrease exponentially with the coulombic dose and the cathodoluminescence loss rate increases with a higher pressure of the molecular gas in the system.

These predictions have been observed experimentally [18] and are shown in Figures 2.15 and 2.16. Figure 2.15 shows the loss in CL intensity for a ZnS: Ag phosphor irradiated by a 2 keV electron beam at varying vacuum pressures. This graph shows experimentally that the CL degradation rate is dependent upon the gas pressure in

the vacuum system as predicted by the mathematical model. The rate of degradation is higher at higher gas pressures. Figure 2.16 shows that the prediction from the model for an exponential loss in sulfur surface concentration with electron dose can be observed experimentally.

The degradation of one oxide phosphor, Y_2O_3: Eu, has been investigated [62]. The degradation behavior of this powder phosphor was evaluated as function of the oxygen pressure in the vacuum. Y_2O_3: Eu was exposed to electron beam energy of 2 keV and a high current density of 88.5 mA/ cm^2 in a vacuum atmosphere of 1x 10^{-7} Torr oxygen. After an electron dosage of 3500 C/ cm^2, the CL intensity was reduced to 45% of its original intensity as shown in Figure 2.17 [62]. The yttrium, carbon, and oxygen peaks were also monitored by Auger electron spectroscopy (Figure 2.17) during electron beam exposure. However, no change in the signal from these elements was detected. Therefore, even though it was clear that the presence of oxygen affects the rate of degradation, the mechanism that resulted in the reduced CL intensity could not be determined [62].

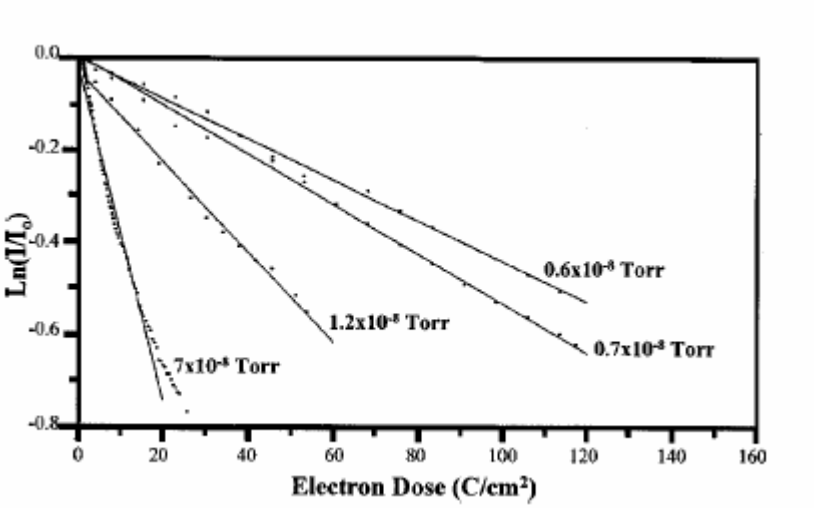

Figure 2-15. Semi logarithmic plot of CL intensity vs. electron dose for a ZnS: Ag phosphor [18].

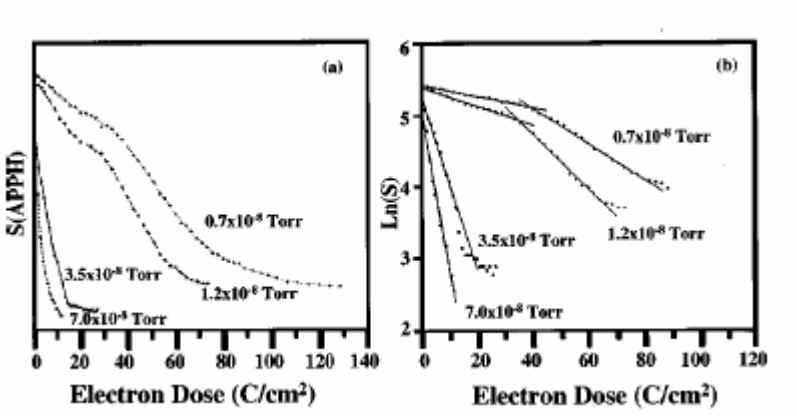

Figure 2-16. Linear and logarithmic plot of S Auger peak to peak height (APPH) vs. electron dose for ZnS: Ag phosphor [18].

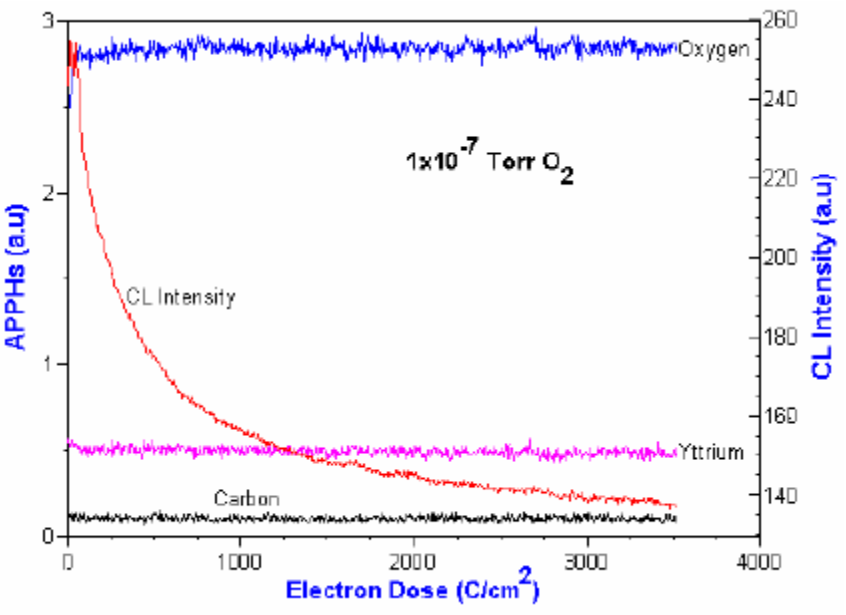

Figure 2-17. Plot of CL intensity of Y_2O_3: Eu phosphor and selected Auger peak to peak heights vs. electron dose [62].

CHAPTER 3
CATHODOLUMINESCENCE FROM THIN FILM ZINC GERMANATE DOPED WITH MANGANESE PHOSPHORS

3.1 Introduction

In this study, the low voltage cathodoluminescent properties of thin film zinc germanate doped with manganese (Zn_2GeO_4: Mn) are examined. Pulsed laser deposition was used to grow Zn_2GeO_4: Mn on magnesium oxide (MgO), yttria stabilized zirconia (YSZ), or silicon (Si) substrates. The structural properties as well as the cathodoluminescence (CL) and photoluminescence (PL) spectra of the films are reported. The variation of the CL emission spectra with film deposition temperature and crystalline quality of film is also studied.

The first section in this chapter outlines the experimental procedures used to develop and characterize the thin film samples. The second section reports on the results from the characterization and experiments. Finally, the last section will provide insight into the influence of deposition temperature and type of substrate on the luminescent qualities of the Zn_2GeO_4: Mn phosphor.

3.2 Experimental Procedures

The preparation of the substrates and the processing steps for the film development in outlined in Figure 3.1. The details of each step are described in this section.

3.2.1 Substrates and their Preparation

Single crystal (100) MgO, (100) yttria stabilized zirconia (YSZ), and (100) Si substrates were chosen as the substates for this experiment. The substrates were cleaned

by a solvent wash in a sonicator prior to deposition. The solvents that were used were trichloroethylene, acetone and methanol. The substrates were cleaned in 3 sequential solvent washes, with each wash lasting five minutes. The substrates were dried by air.

3.2.2 Phosphor Processing

A Zn_2GeO_4 ablation target doped with 1.5 at% Mn was prepared by mixing and then ball milling ZnO, GeO_2, and MnO_2 powders for 60 minutes. The mass of each powder used for the mixture is given in Table 3.1. The mixture was then calcined in air at 1000 °C for 8 hr in covered alumina crucibles that were placed in a conventional furnace. The powder mixture was milled again for 60 minutes and was then checked for photoluminescence. A hand held ultra- violet (UV) lamp was used for the check. Visible green luminescence from the powder was observed with human eye. Next, the powder mixture was pressed into 2.5 cm diameter targets. The targets were sintered in air at 1250 °C for 36 hours in a conventional furnace. In addition, ZnO powder was milled, pressed into targets, and sintered. A Zn_2GeO_4: Mn/ ZnO mosaic target was formed to control the cation ratio of Zn/Ge in the films. The area ratio of the target was 75 % Zn_2GeO_4: Mn and 25 % ZnO. Previous research has shown that a zinc rich target can compensate for Zn loss at elevated temperatures during deposition, which is due to the high vapor pressure of zinc [63,64]. The target was rotated during the deposition cycles to ensure that the laser ablated the Zn_2GeO_4: Mn and ZnO portions of the target.

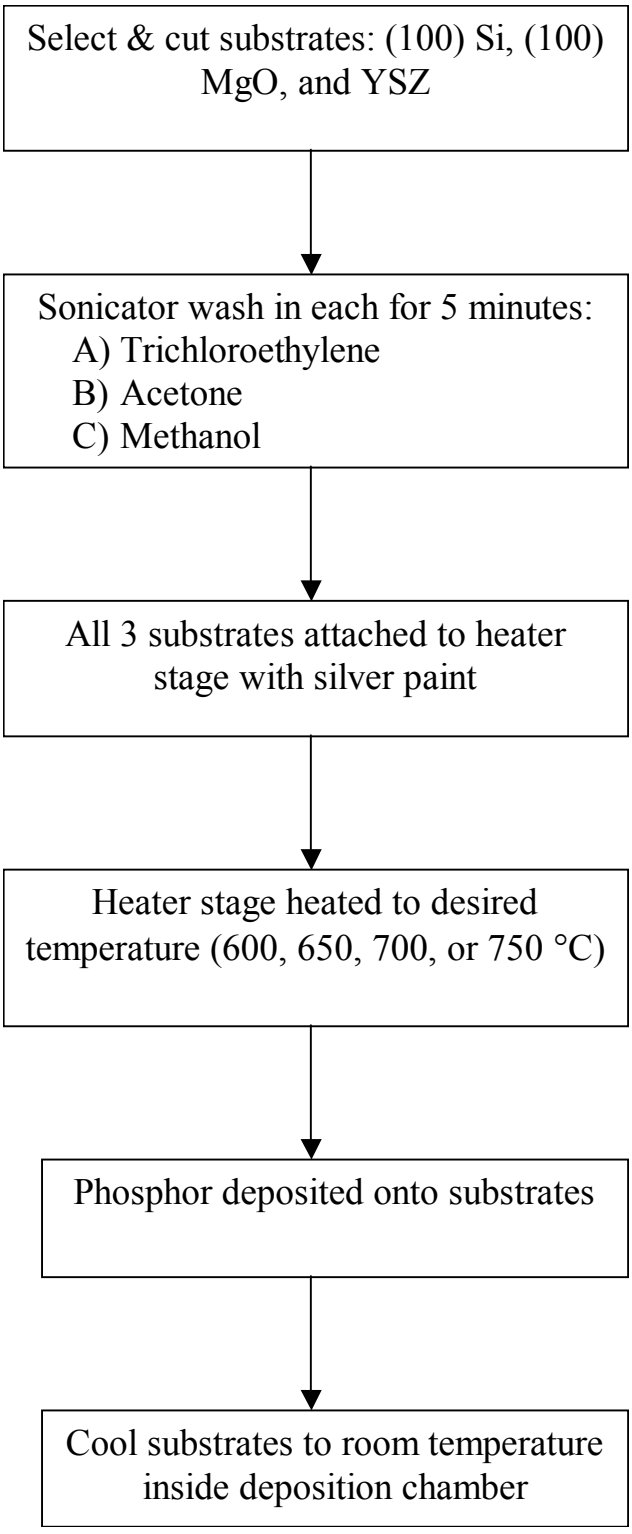

Figure 3-1. Flow chart outlining substrate preparation and phosphor processing method.

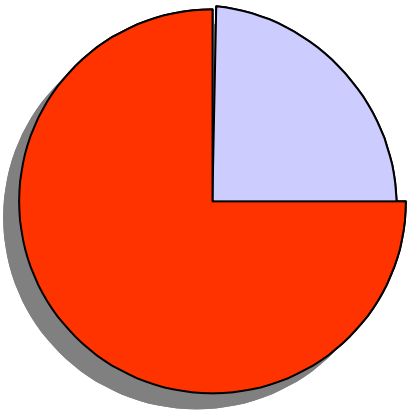

Figure 3-2 Representative sketch of mosaic target where 75% area = Zn_2GeO_4: Mn and 25% area = ZnO.

Table 3-1 Raw materials used to make target.

Material	Mass (g)
ZnO	12.1758
GeO_2	7.8242
MnO_2	0.0975

The films were grown using an excimer KrF laser with a wavelength of 248 nm. The energy of the laser was 130 mJ/pulse. The target was pre- ablated before each deposition cycle. Four different deposition temperatures (600, 650, 700, and 750 °C) were maintained by a substrate heater and a thermocouple attached to the substrate stage. The substrates were allowed to reach the desired temperature before film growth commenced. The number of pulses and pulse frequency during deposition was 10,000 pulses at 10 Hz, immediately followed by a second cycle of 20,000 pulses at 20 Hz. The oxygen partial pressure in the system was maintained at 100 mTorr during all film growth.

3.2.3 Thin Film Phosphor Characterization

3.2.3.1 X- ray diffraction

X- ray diffraction (XRD) is a useful method for identifying the crystalline phases present in a sample, as well as for measuring the structural properties of these phases. For instance, it can also be used to determine the preferred orientation of the phases present in a crystalline material [65]. X- ray diffraction results from incident X- rays that are scattered by the atomic planes present in a crystal. When there is constructive interference from these X- rays, a diffraction peak is observed [65]. The condition for constructive interference is dictated by Bragg's law such that

$$\lambda = 2d_{hkl} \sin \theta_{hkl} \qquad (3\text{-}1)$$

where λ is the wavelength of the incident X- ray, d_{hkl} is the d- spacing between (hkl) planes, and θ_{hkl} is the angle between the atomic planes and the incident X- ray beam. These terms are illustrated in Figure 3.3 which shows the interaction of the X- ray with the specimen.

The diffraction angle, 2θ, is the angle between the incident and diffracted X- rays (Figure 3.3). The XRD experiment yields data for the diffracted intensity vs. diffraction angle. For polycrystalline thin films, diffraction occurs from any crystallite or small crystalline region that satisfies the diffraction conditions [65]. If the distribution of orientations is random, diffraction peaks will result from more than one plane, similar to a powder diffraction pattern. As a result, multiple peaks will be present in the pattern representing the different orientations of the crystallites. A textured film will possess a preferred orientation of the crystallites, where most of the crystallites have parallel planes.

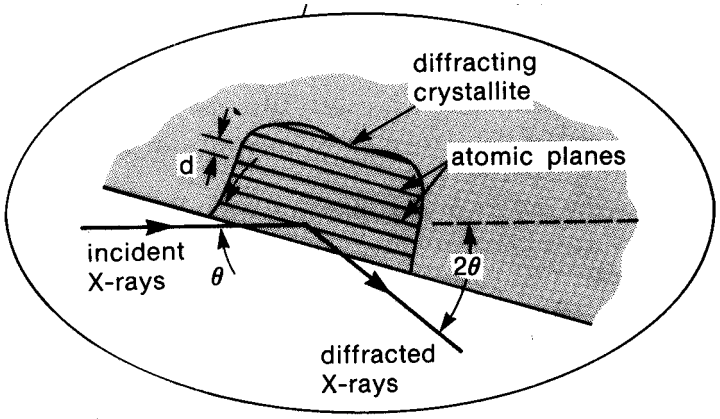

Figure 3-3 Interaction of incident and diffracted X- rays in an XRD specimen [65].

For this study, the crystalline quality of the films was investigated using a Philips APD 3720 X- ray diffractometer. X- ray diffraction (XRD) was completed with Cu Kα radiation (0.15406 nm wavelength) generated by a 40 keV and 20 mA electron beam. The scan range for the samples was from 10 to 80 2theta degrees, while the scan rate was 0.080 ° 2θ / sec in continuous scan mode. The resulting X- ray diffraction patterns were then indexed with a collection of patterns from the Joint Committee on Powder Diffraction Standards (JCPDS) catalog.

3.2.3.2 Relative composition analysis: EDX

Electrons may interact with the sample to produce multiple signals. These signals include X-rays, UV and visible emission, and auger electrons, as depicted in Figure 3.4. The signals result from the electron interactions within the sample volume. Electron probe microanalysis (EPMA) is a compositional analysis method that uses the characteristic X- ray emission generated by an electron beam to provide a quantitative analysis of the elements present in a specimen. This method relies on an electron probe,

thus resulting in fine spatial resolution as low as 100 nm [65]. The accuracy of the quantitative analysis is dependent upon the standards used for the analysis. To reduce error, the sample and standards must be measured under identical conditions of beam energy and spectrometer parameters and should be normalized to the same electron dose. Failure to replicate conditions will increase the error in the measurements.

Energy dispersive X- ray (EDX) spectroscopy is one type of EPMA that detects elements with an atomic number higher than beryllium, Z= 4. For EDX, the incident electron beam ionizes and ejects inner shell electrons from the atoms within the sample. The atoms are returned to ground state when an electron from a higher energy shell moves to fill the inner shell vacancy. During the transition, the electron releases the amount of energy equal to energy difference between the two shells. This excess energy, unique for each atomic transition, may be released in the form of an X- ray photon [65]. This X-ray is referred to as the characteristic X- ray for that atom and is detected by the spectrometer. The minimum detection limit for an EDX spectrometer attached to a scanning electron microscope is about 0.1 wt % [65].

Energy dispersive X- ray fluorescence (EDX) with a JEOL JSM 6400 scanning electron microscope (SEM) at a primary beam energy of 5 keV was used to measure the relative concentrations of the elements in the film. The absolute values of the atomic content for these films are considered to be subject to large errors because the sensitivity factors for the Zn and Ge Lα signals used were from look- up tables using different transitions and higher primary beam energies. Neither factor could be accurately corrected for by the quantitative calculation program.

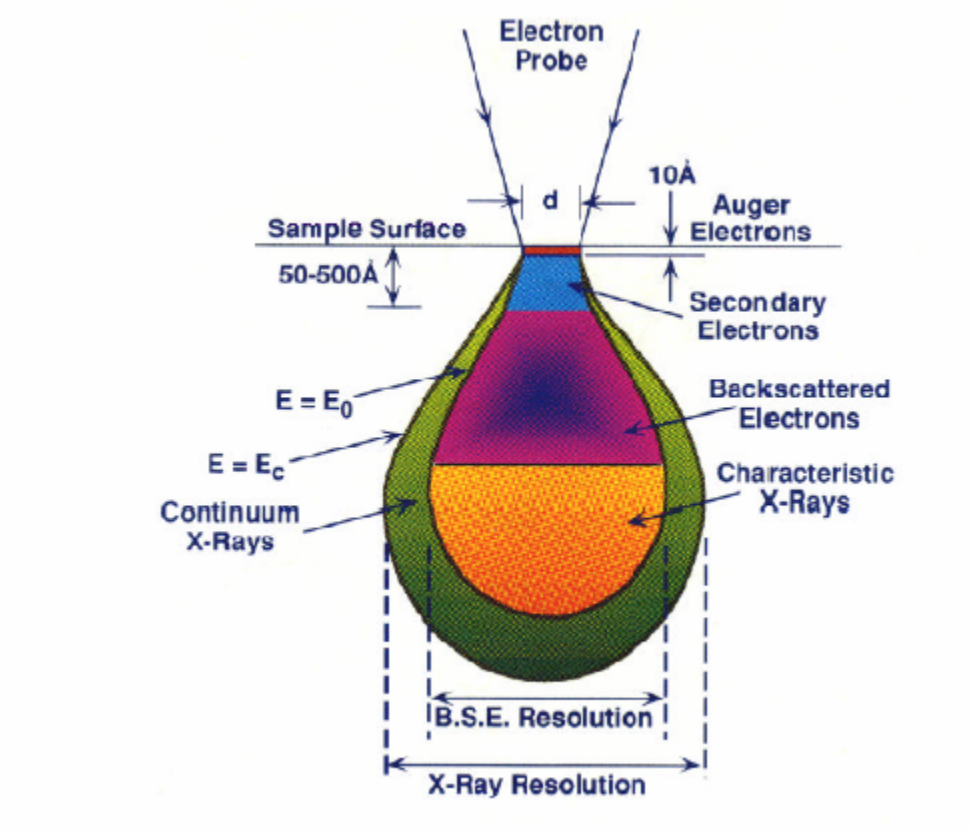

Figure 3-4. Interaction volume in sample where electron beam penetrates and the resulting signals are generated [66].

3.2.3.3 Cathodoluminescence characterization

The theory of cathodoluminescence was introduced in Chapter 2. Cathodoluminescence (CL) from the phosphors was measured in an ultra high vacuum stainless steel chamber depicted in Figure 3.5. The ultra high vacuum was maintained by a Perkin Elmer Ultek D- I ion pump, which maintained a system pressure of approximately 1 X 10^{-8} Torr. An Edwards RV3 turbo molecular pump was used for initial pumping of the system to about 1 X 10^{-6} Torr, after which the system was crossed over to the ion pump. The system also has a load-lock chamber. The chamber allows introduction of new samples into the vacuum system without disturbing the vacuum. The CL system recovers to its normal pressure within thirty minutes. Cathodoluminescence

was stimulated by an electron beam generated by a Kimball Physics EFG- 7 electron gun operated at 4 keV and 8.5 μA. An optical fiber connected to an Ocean Optics S2000 optical spectrometer was used to detect photoemission from the samples. The detected spectral range was from 200 to 850 nm.

3.2.3.4 Photoluminescence characterization

Photoluminescence (PL) is the excitation of photons by absorption of light. It can be used to provide a qualitative analysis of a sample. The wavelength of the emitted light is longer than the incident light [65]. The spectral properties can be analyzed to provide information such as the optical, electrical, and structural properties of the material [65]. A photoluminescence excitation (PLE) spectrum can be used to find out information about the excitation process that leads to the photon being emitted. The intensity and spectral properties of a PLE spectrum is dependent upon the absorption of the incident light and the initial and relaxed excited states that take part in emission [65]. For PLE, a set emission wavelength is monitored and the wavelength of the incident light is scanned through a desired range.

The photoluminescence measurements were taken in a dark room at room temperature. A xenon lamp (Oriel Instruments, model 66902) was selected as the excitation energy source for photoluminescence. The excitation wavelength could be tuned to the desired level with a monochromator (Oriel Instruments, Cornerstone 74100 spectrometer) placed in between the lamp and sample. Any wavelength between 200 and 1200 nm could be selected with the excitation monochromator. The emitted light was focused to a monochromator (Oriel Instruments, MS257) and photo- multiplier tube

(Oriel Instruments, 77265) that has the ability to detect photoemission from 300 to 800 nm.

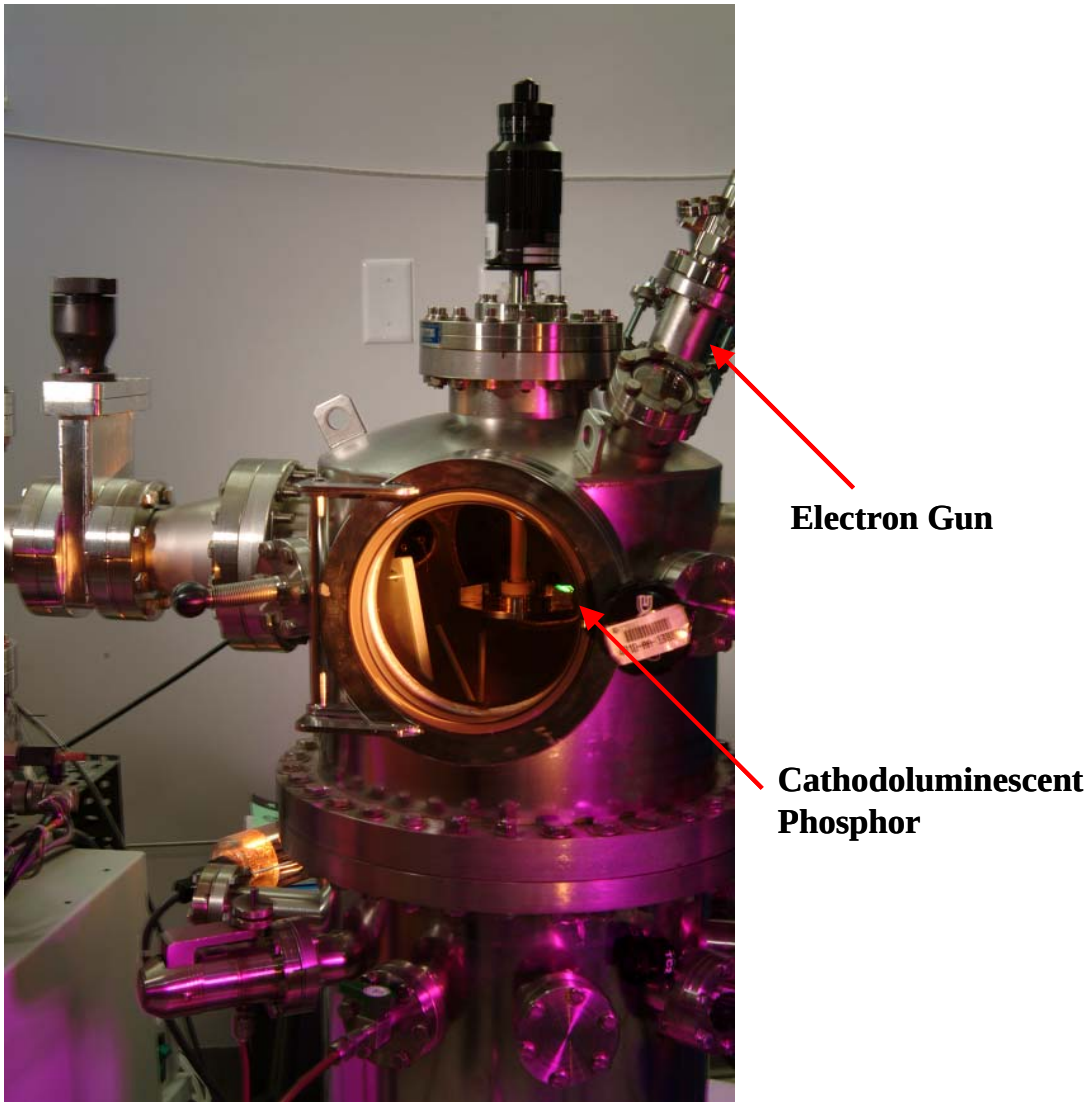

Figure 3-5 Picture of cathodoluminescence vacuum system.

3.3 Results

3.3.1 X- Ray Diffraction Results

The X- ray diffraction (XRD) data in Figure 3.5 show the effect of the deposition temperature on the structural properties for film grown on MgO substrates. At 600 °C

(Fig. 3.5d), (223) and (550) weak diffraction peaks for Zn_2GeO_4 are evident indicating that some structural order exists. However, the weak peak intensity and the broad maximum at 2θ of ~ 18° suggest that the majority of the film was amorphous with respect to X- ray diffraction. The presence of additional Zn_2GeO_4 diffraction peaks in the XRD pattern shown in Figure 3.5 (a- c) indicate that the films grown at 650, 700, and 750 °C are polycrystalline and exhibit better long-range order. Additional diffraction peaks at 2θ of ~ 28° and 36° for films grown at 750 and 700 °C are attributed to an impurity GeO_2 phase. The shoulder diffraction peak at 2θ of ~ 41°, detectable only in film grown at 750 and 700 °C, also results from the GeO_2 impurity phase.

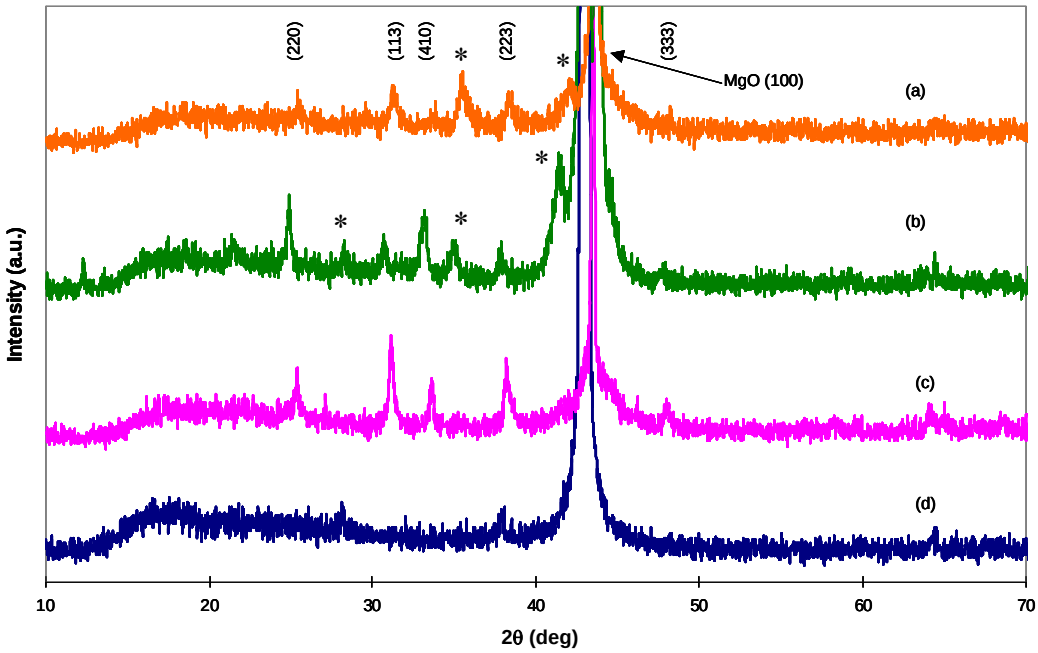

Figure 3-6 XRD pattern for Zn_2GeO_4: Mn films grown on MgO substrate at different deposition temperatures: (a) 750 °C, (b) 700 °C, (c)650 °C, (d)600 °C where * denotes GeO_2 impurity phase.

XRD patterns from films grown on Si are shown in Figure 3.6, which are comparable to the results for films grown on MgO. At 600 °C, the presence of weak (223) and (550) Zn_2GeO_4 peaks and a broad peak at 2θ of ~ 18° in the diffraction pattern indicate that the film structure is mixed amorphous and polycrystalline. Again, the XRD patterns shown in Figure 3.6 (a- c) indicate that the films grown at temperatures from 650- 750 °C are polycrystalline with better long range order.

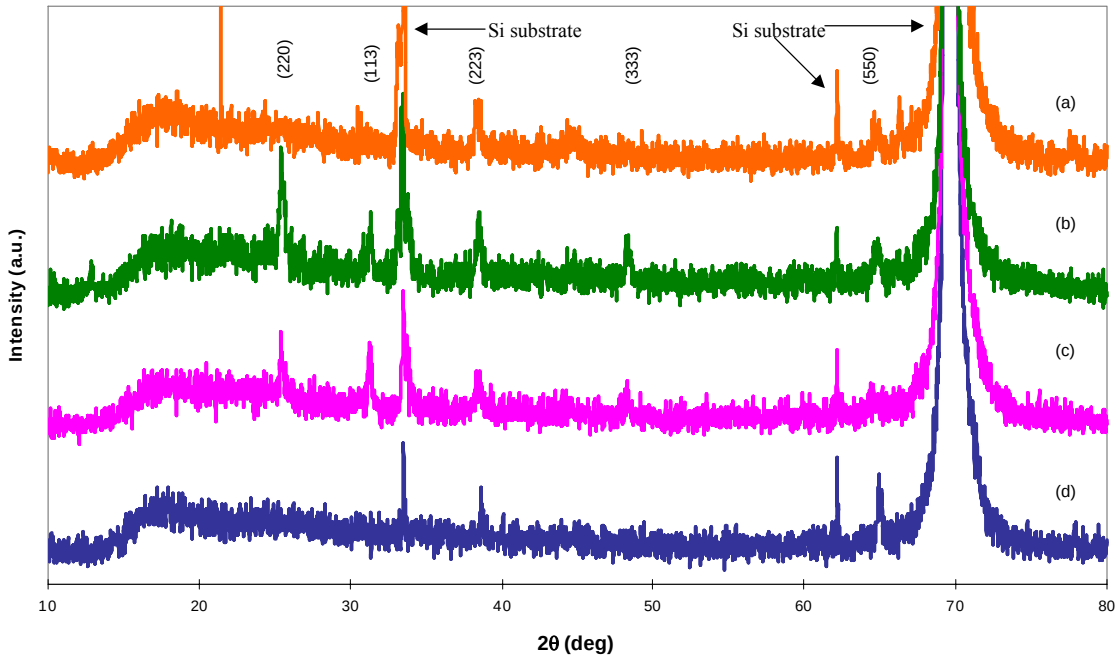

Figure 3-7. XRD pattern for films grown on Si substrate at different deposition temperatures: (a) 750 °C, (b) 700 °C, (c)650 °C, (d)600 °C.

Figure 3.7 presents the XRD pattern for films deposited on the third substrate, YSZ, at different deposition temperatures. For films deposited at 600 °C (Fig. 3.7d), only a weak (550) diffraction peak is present, which indicates that Zn_2GeO_4 is again mixed amorphous and polycrystalline. Additional diffraction peaks from Zn_2GeO_4 were

observed from films deposited at higher temperatures. Polycrystalline Zn_2GeO_4 films were formed at 650 and 700 °C. The diffraction pattern for the film grown at 750 °C (Fig. 3.7a) reveals a strongly preferred (110) texture.

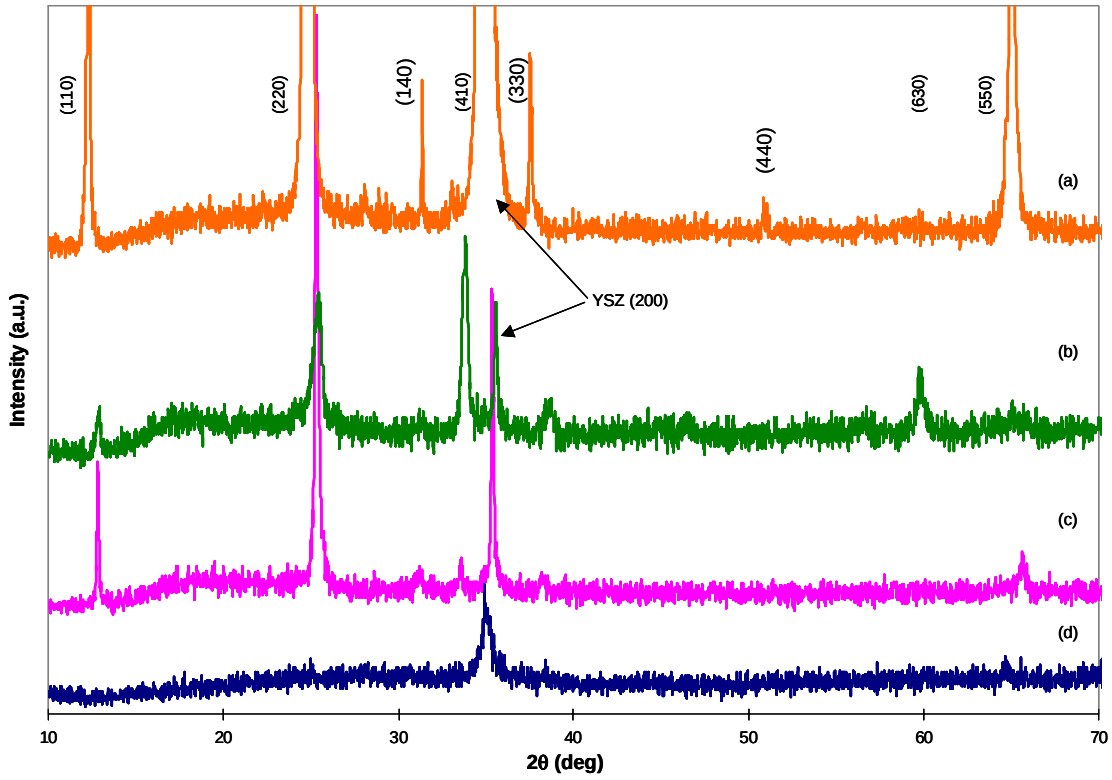

Figure 3-8. XRD pattern for films grown on YSZ substrate at different deposition temperatures: (a) 750 °C, (b) 700 °C, (c)650 °C, (d)600 °C.

3.3.2 Cathodoluminescent Properties

With respect to luminescent properties, the characteristic PL and EL emission wavelength of Zn_2GeO_4: Mn is a broad peak with a maximum at 540 nm [22,35,37] as discussed in Chapter 2. The CL emission spectra for Zn_2GeO_4: Mn on MgO deposited at various temperatures are shown in Figure 3.8. The CL emission peak intensity was observed to be at 540 nm, as well. The highest 540 nm CL intensity came from films that

were grown at 650 and 700 °C. For 600 °C sample, no CL emission at 540 nm is noted. Rather, the emission peak has shifted to 650 nm.

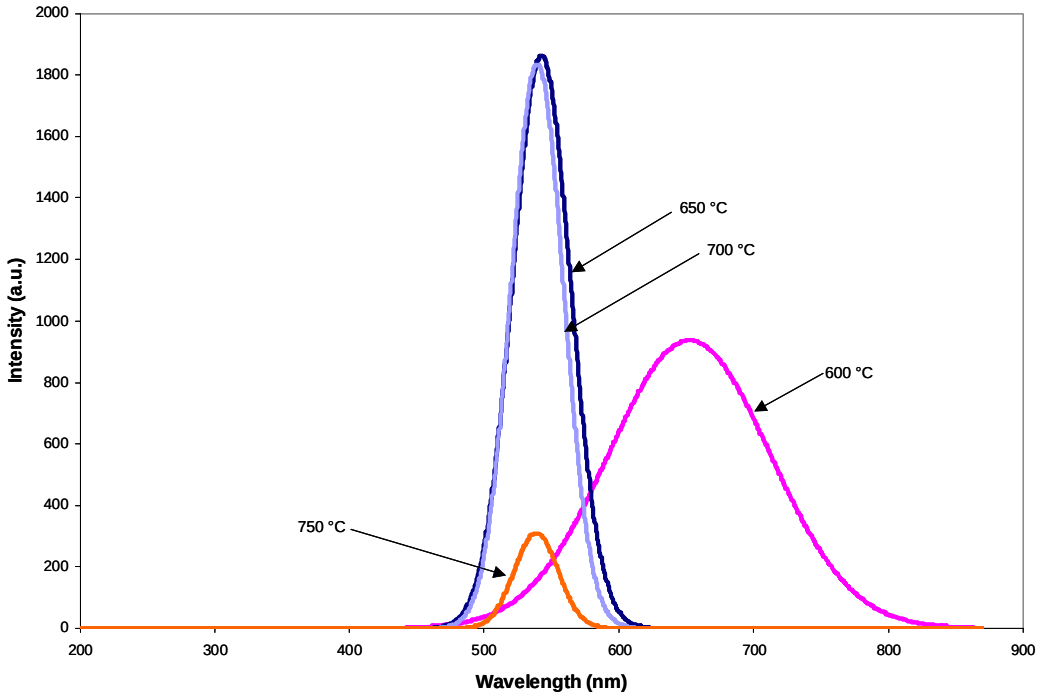

Figure 3-9. CL emission spectrum of Zn_2GeO_4: Mn on MgO substrate at various deposition temperatures.

The CL emission spectra from film deposited onto Si substrates are shown in Figure 3.9. CL emission at 540 nm resulted only from the film grown at 750 and 700 °C. Films grown at temperatures of 600 and 650 °C did not show any detectable CL emission at 540 nm, but did show emission at 650 nm.

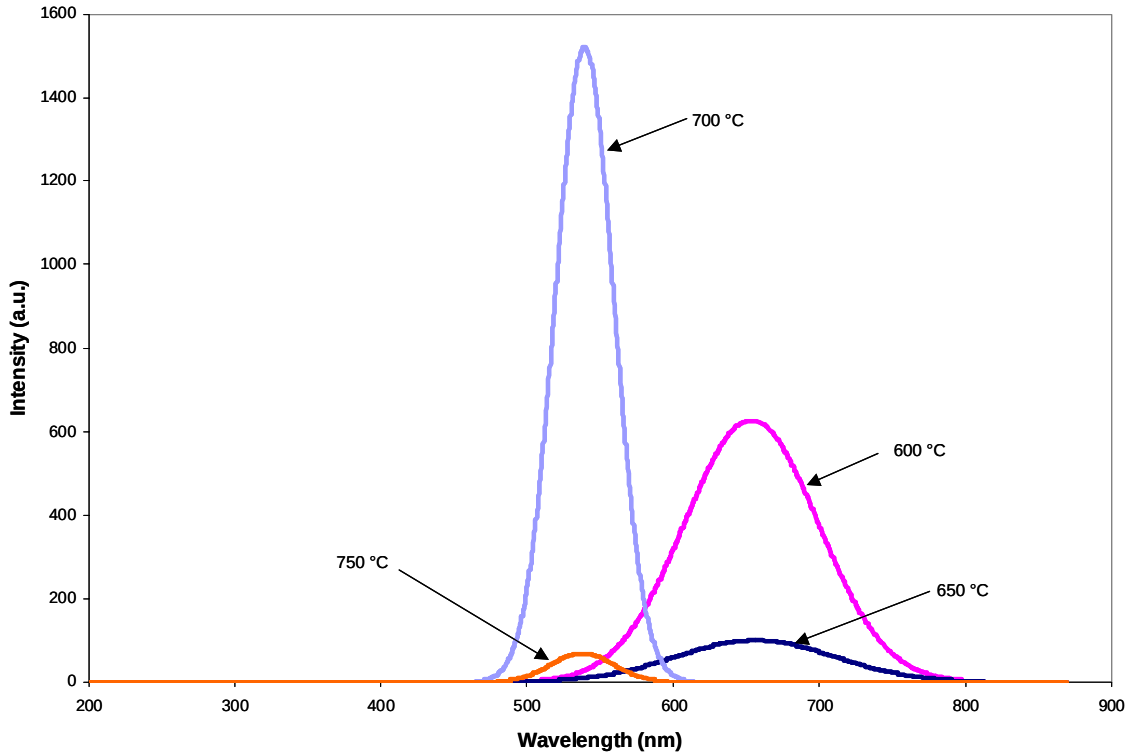

Figure 3-10. CL emission spectrum of Zn_2GeO_4: Mn on a Si substrate for various deposition temperatures.

The CL emission spectra from film deposited onto YSZ are presented in Figure 3.10. The highest CL intensity, in this case, results from the film grown at 750 °C. In contrast to the results for films grown on MgO and Si, the intensities for CL emission from the films deposited at 700 and 650 °C on YSZ are less than that from the film grown at 750 °C. There was no CL response at 540 nm from the film grown at 600 °C, but again the emission peak was shifted and broadened to 650 nm.

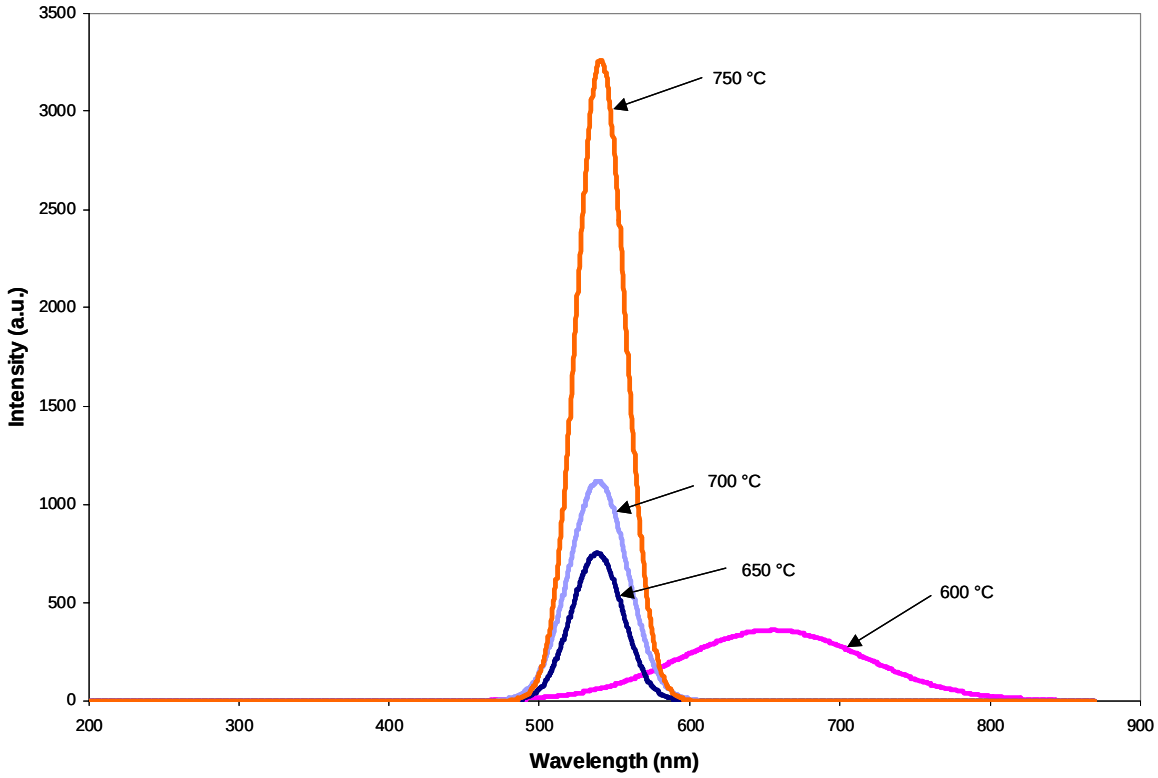

Figure 3-11. CL emission spectrum of Zn_2GeO_4: Mn on YSZ substrate at various deposition temperatures.

3.3.3 Zinc to Germanium Ratio in the Films

The Zn to Ge atomic percent ratio was measured using energy dispersive X- ray fluorescence (EDX). These ratios, given in Table 3.2, were measured for films deposited at $T \geq 650$ °C. All of the deposited films exhibited a low Zn/Ge ratio, ranging from 0.31 to 0.89, suggesting a Zn deficiency. As discussed earlier, the absolute values of these ratios are subject to error. Nonetheless, the relative changes in the ratios correlate well with the changes in crystalline quality and CL intensities, suggesting that the ratios present valid trends. The fact that the XRD patterns indicate that Zn_2GeO_4 with varying degrees of crystallinities was present is consistent with these ratios having large absolute errors, but accurate trends. As shown in Table 3.2, films deposited on MgO and Si

substrates at 650 and 700 °C have a higher Zn/Ge ratio than films deposited at 750 °C. Because of the low Zn/Ge ratio for films deposited at 750 °C on MgO or Si substrates, the crystalline quality decreases. The Zn/Ge ratio is highest (0.89) for the (110) textured film deposited at 750 °C on YSZ, and this film has the best diffraction pattern, indicating the highest crystalline quality.

Table 3-2 Zn/Ge Atomic Ratio in Deposited Zn_2GeO_4: Mn Film vs. Deposition Temperature on Various Substrates

	750 ºC	**700 ºC**	**650 ºC**
MgO	0.31	0.60	0.36
Si	0.42	0.47	0.57
YSZ	0.89	0.65	0.44

3.3.4 Photoluminescence Excitation and Emission

The photoluminescence (PL) emission and the excitation (PLE) spectra for a Zn_2GeO_4 sample that emits green light are shown in Figure 3.11. The emission excited with 325 nm radiation showed a peak at 540 nm. The excitation spectrum, monitored at 540 nm, exhibited an excitation peak at 310 nm with a small shoulder at 265 nm. The results are similar to what has been noted for green emission from Zn_2GeO_4: Mn [35]. The PL emission and excitation spectra for Zn_2GeO_4 samples that have longer wavelength emission are shown in Figure 3.12. The PL emission for these samples, when excited with 325 nm radiation, results in a broad peak at 625 nm with a smaller peak showing at 535 nm. The excitation spectrum, monitored at 625 nm, exhibited a peak at 270 nm with a small shoulder at 330 nm.

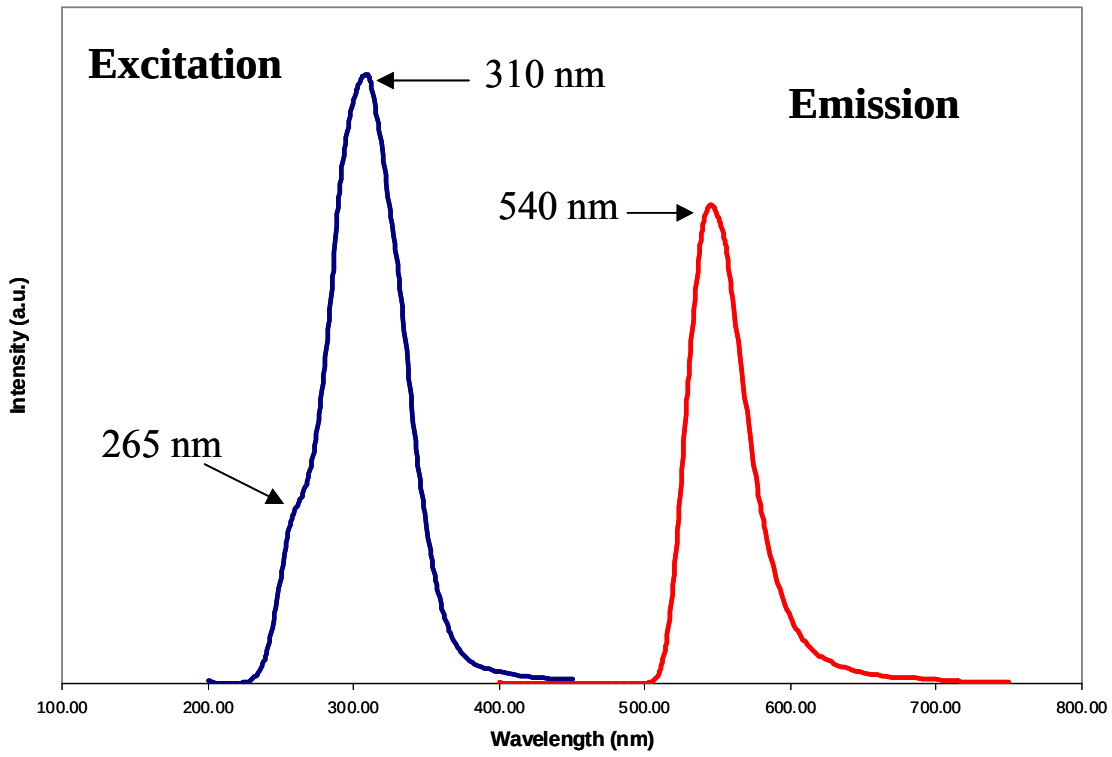

Figure 3-12. Green emission spectrum of Zn_2GeO_4: Mn excited with 325 nm radiation at 540 nm and excitation spectrum monitored at 540 nm.

3.4 Discussion

In summary, Zn_2GeO_4: Mn was successfully pulsed laser deposited onto MgO, Si, and YSZ substrates. The X- ray diffraction data show improved crystallinity in films deposited at T ≥ 650 °C. For the films deposited at 600 °C, on all substrates, the structure of films was mixed amorphous and polycrystalline. The quality of the diffraction peaks was good for films deposited at 650 and 700 °C on MgO and Si substrates. The best diffraction pattern was for the textured film deposited at 750 °C on YSZ substrate.

A relationship between the CL emission maximum intensity and the film crystal quality and stoichiometry is obvious. The film with the best CL emission intensity at 540

nm was the (110) textured film grown on the YSZ substrate at 750 °C. The Zn/Ge ratio is highest (0.89) for this film and this film has the best diffraction pattern, indicating the highest crystalline quality.

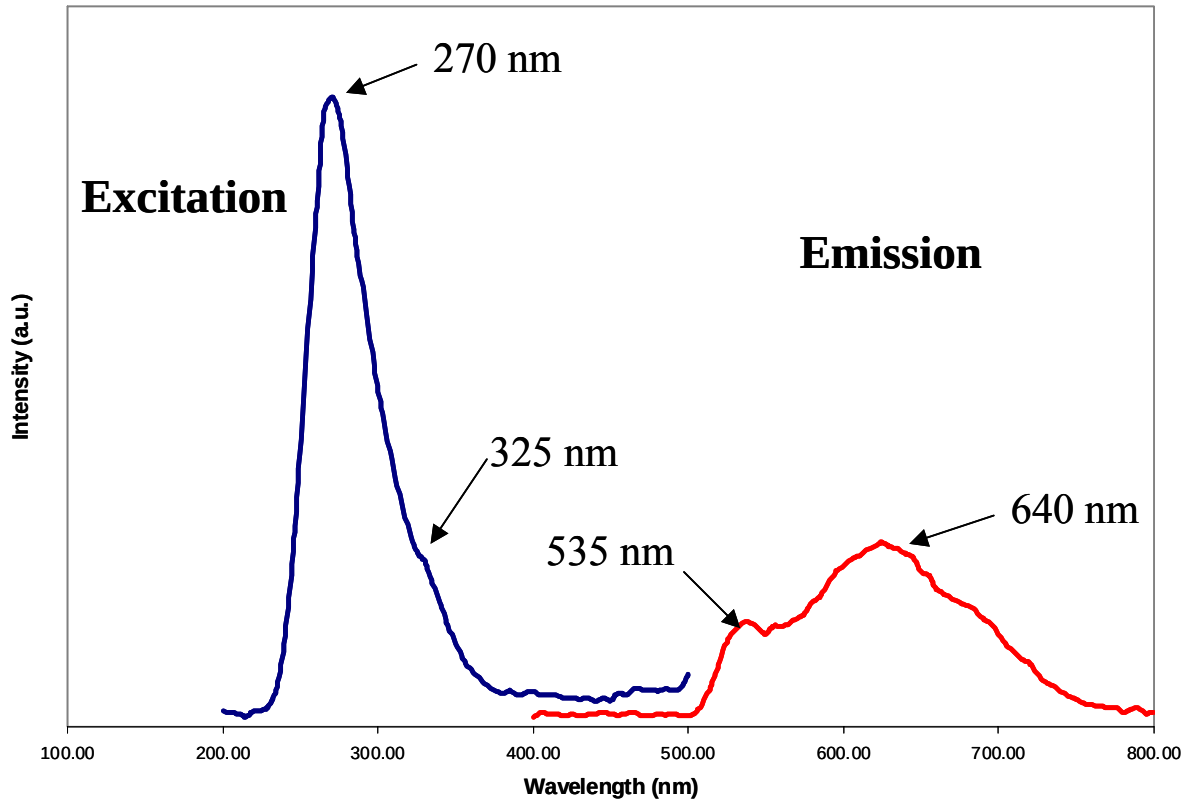

Figure 3-13. Red emission spectrum of Zn_2GeO_4: Mn excited with 325 nm radiation at 625 nm and excitation spectrum monitored at 625 nm.

The films deposited at 700 and 650 °C on MgO, which were determined to have good crystal quality and Zn/Ge ratios ~0.5 also exhibited the highest CL emission intensities at 540 nm for films deposited on this substrate. For films deposited on a Si substrate, the CL emission was also highest for the films with the best crystal quality, which again correlated with higher Zn/Ge ratios. The fact that higher Zn/Ge ratios lead to brighter CL emission is consistent with observation of better crystallinity for the Zn_2GeO_4 crystal structure.

The highly textured film grown on the YSZ substrate at 750 °C had the highest crystallinity, highest Zn/Ge ratio, and the best CL properties. It has been suggested that grain boundaries may limit the luminescent performance of a phosphor [63], which is consistent with emission from more randomly oriented polycrystalline film being lower when compared to the textured film on YSZ.

A red shift in wavelength of emission from green to red has also been noted in Mn-doped $ZnGa_2O_4$ phosphors [67]. It was reported that Mn^{4+} ions in the octahedral sites led to red emission, while Mn^{2+} ions that occupied the tetrahedral sites in the spinel structure resulted in green emission [67]. At 600 °C, where the Zn_2GeO_4: Mn films exhibit mixed short and long range order, the dominant CL emission was at 650 nm. It is postulated that the Mn^{4+} ions are responsible for red emission at 650 nm. The rhombohedral crystal structure of Zn_2GeO_4 has only tetrahedral sites [68]. Therefore, a change in substitution site must occur to accommodate the change in valency of Mn in Zn_2GeO_4: Mn. The Mn^{4+} ions may substitute for Ge^{4+} at the lower temperature. This substitution is possible since the ionic radii of both ions are 0.39 Å [69]. At higher deposition temperatures (650, 700, & 750 °C), the films develop a polycrystalline structure and the Mn^{2+} ion gains enough energy to move into the expected tetrahedral site and substitute for Zn^{2+}. This is again possible since the ionic radii of these atoms are close, 0.60 Å versus 0.66 Å for Zn^{2+} and Mn^{2+}, respectively [69]. The Mn^{2+} activator ions resulted in emission at 540 nm, as expected.

The difference in photoluminescence excitation spectra for green (540 nm) and red (650 nm) luminescence indicates that excitation of different states are responsible for each type of emission. This correlation between the excitation of different ionic states

and the PL excitation spectra has also been observed in for the$ZnGa_2O_4$ host [67]. The excitation spectra are consistent with the Mn ion exhibiting different valence states and substituting for either Zn or Ge, depending upon the temperature during deposition.

CHAPTER 4
DEVELOPMENT OF ZINC SILICATE DOPED WITH MANGANESE THIN FILM PHOSPHORS

4.1 Introduction

This chapter describes the development of zinc silicate doped with manganese (Zn_2SiO_4: Mn) thin film phosphors. The overall effects of the processing conditions on the resulting films will be evaluated. In the first section, the experimental procedures that were used to grow the films will be described. The films were produced by sputter deposition, pulsed laser deposition, or combustion chemical vapor deposition. The luminescent and structural properties of these films have been evaluated and are discussed in the results section. The resulting composition of the films will be discussed as it relates to the film growth method and post- processing conditions. These growth methods are excellent choices for growing thin film phosphors, however it was found that the zinc loss must be controlled to obtain the best performance from the phosphor film. The thin film phosphors were also studied for cathodoluminescence degradation, as will be discussed in Chapter 5.

4.2 Experimental Procedures

4.2.1 Substrates and their Preparation

Clear fused quartz and (100) Si were chosen as the substrates for film growth. These substrates were chosen since they could withstand the high annealing temperatures required to crystallize zinc silicate. The substrates were cleaned by a solvent wash in trichloroethylene, acetone, and then in methanol. The substrates were placed in a beaker

with each solvent for fifteen minutes inside a sonicator and then removed. The substrates were then placed in the next solvent, and the wash was repeated. The substrates were then blown dry by compressed air.

4.2.2 Phosphor Processing

4.2.2.1 Sputter deposition

The Zn_2SiO_4: Mn sputter targets were made from raw material produced at Shanghai Yuelong New Materials Co. Ltd. in Shanghai, China, and sold primarily for plasma display panel applications. The 2" sputter target was made by Plasmaterials, Inc. by hot pressing and sintering. The target was also bonded to a 0.125" thick Cu backing plate using metallic bonding by Plasmaterials, Inc. The density of the resulting target was estimated to be ~90% of theoretical.

The sputter deposition was completed with two different targets, however the starting material was the same in both cases. The initial target was changed after cracks propagated through the target, and films deposited from it had an uncharacteristic brown tint, which was determined by EDX analysis to be carbon contamination. The source of the carbon contamination was the bonding material for adhering the target to the copper backing plate. The films that were carbon contaminated are not included in this study. A second target was used in a sputter gun that did not require a copper backing plate. This adjustment eliminated the bonding material as a source of carbon contamination.

The deposited thin films were treated to a post- deposition thermal anneal. The rapid thermal anneal (RTA) was completed in an AG Associates Heatpulse Model 4100 furnace with a high- purity nitrogen atmosphere. The anneal recipe used for the heat treatments is given below in Table 4-1. The annealing temperature for the samples was chosen as 1100 °C, since it was high enough to cause crystallization of Zn_2SiO_4

[26,27,29]. The duration of the anneal was limited to five minutes due to the operating capabilities of the furnace. Upon completion of the anneal, the heat source was turned off and an increase in N_2 flow helped to cool the samples before removal from the furnace.

Table 4-1 Rapid thermal anneal recipe for heat treatment of thin film samples.

Segment	Type	Time	Temp. (°C)	N_2 Flow (slpm)
1	Steady	10 sec	0	10
2	Ramp	125 °C/ sec	1100	2.5
3	Steady	300 sec	1100	2.5
4	Steady	60 sec	0	10

4.2.2.2 Pulsed laser deposition

Thin film samples were also made by pulsed laser deposition (PLD). The PLD target was made from the commercial Zn_2SiO_4: Mn phosphor powder obtained from Shanghai Yuelong New Materials Co. Ltd. This target was pressed using a 1" stainless steel die. The thin film processing was completed at North Carolina A & T State University.

The pulsed laser deposited phosphor films were all grown at the same processing conditions on (100) Si substrates. The oxygen pressure during growth was at 300 mTorr and the substrates were heated to and maintained at 700 ºC during the deposition cycles. After deposition, the thin film PLD samples were heat treated with a rapid thermal anneal in N_2 atmosphere for five minutes at 1100 °C. The same apparatus and program described in section 4.2.2.1 was used for the annealing of these samples.

4.2.2.3 Combustion chemical vapor deposition

Zn_2SiO_4: Mn thin film phosphors were deposited onto quartz substrates by combustion chemical vapor deposition (CCVD) at Georgia Institute of Technology. Combustion chemical vapor deposition is a novel growth method that produces crystallized films at high temperatures, eliminating the need for a post- deposition anneal [70]. In CCVD, the precursors are sprayed near or in a flame that causes the precursors to chemically react leading to the vapor deposition of a film onto a substrate [71]. The substrates are heated during the deposition through exposure to the open flame and the temperature is controlled by the substrate distance from the flame end. The films are grown at atmospheric pressure using ambient air for the reaction, making this method suitable for oxide materials [70].

The precursor solution consisted of zinc nitrate, tetraethyl orthosilicate (TEOS), and manganese nitrate [70].

4.2.3 Thin Film Phosphor Characterization

4.2.3.1 X- ray diffraction

The crystalline quality of the films was investigated using a Philips APD 3720 X-ray diffractometer. X- ray diffraction (see section 3.2.3.1) was completed with Cu Kα radiation (0.15406 nm wavelength) generated by a 40 keV and 20 mA electron beam. The 2θ scan range for the samples was from 10 to 80 degrees, while the scan rate was 0.080 °/ sec in a continuous scan mode. The resulting X- ray diffraction patterns were indexed using a collection of patterns from the Joint Committee on Powder Diffraction Standards (JCPDS) catalog, where the rhombohedral crystal structure was found to correlate with the Zn_2SiO_4 developed in this study.

A high resolution X- ray diffractometer was also used to measure the crystal structure and quality of the thinner films (less than 1000 Å). This method was useful for the thin films that were too thin for the powder diffraction method. The 2θ scans were taken from 20 to 40 degrees at a glancing angle of 0.7 °. A Philips MRD X' Pert X-ray diffraction system was used for the measurements.

4.2.3.2 Scanning electron microscopy

Scanning electron microscopy (SEM) is useful for characterizing the sample morphology. A scanning electron microscope provides a magnified image of the surface. The magnification for this type of microscopy may go as high as 300,000 [65].

A JEOL scanning electron microscope model 6400 was used for obtaining the micrographs. The SEM was operated at 15 keV. Because of the high accelerating voltage and the low conductivity of the samples, the samples were coated with carbon to reduce the effects of charging. The carbon layer was deposited onto the samples by electron beam evaporation.

4.2.3.3 Wavelength dispersive X- ray spectrometry

Wavelength dispersive X- ray (WDX) spectroscopy is an elemental analysis technique that is used to provide information about the composition of a sample. It can be used to detect elements from beryllium to the actinides. This method relies on the generation of characteristic X- rays by a focused electron beam, as in energy dispersive spectroscopy (EDX). However, WDX (versus EDX) relies for energy analysis by the constructive diffraction of X- rays by a crystal [65] for elemental analysis. Several crystals with various d- spacings are used to incorporate a broad energy range. Correction factors for X- ray intensity are usually applied in the quantitative analysis.

The ZAF [65] correction takes into accounts the effects related to the atomic number of an element (Z), X- ray absorption (A), and secondary fluorescence (F).

4.2.3.4 X- ray photoelectron spectroscopy

X- ray photoelectron spectroscopy (XPS) is a very beneficial analytical method for examining the surface chemistry of a sample [65,72]. Energetic X-rays, greater than 1000 eV [72], bombard a sample causing characteristic photoelectrons to be ejected. Chemical identification is made by analyzing the kinetic energies of the ejected photoelectrons. Electron binding energies are sensitive to the chemical state of the atom. With sensitivity to small changes in kinetic energy, information about the chemical state of the identified element can be determined. This method is good for detecting most elements, except for hydrogen and helium.

The kinetic energy of the photoelectron is dependent upon the impinging X- ray photon as dictated by Einstein photoelectric law:

$$KE = h\nu - BE \qquad (4\text{-}1)$$

where KE is the kinetic energy, $h\nu$ is the energy of the impinging photon, and BE is the binding energy of the electron in the atom. Since the energy of the photon is known and the kinetic energy is measured, the binding energy can be determined. An XPS spectra is usually given as the binding energy versus peak intensity. The peak intensities in an XPS plot are dependent upon the photoionization cross- section. The photoionization cross – section is dependent upon the probability for photoejection, which is different for each quantum orbital [65]. The probability depends upon the orbital of ejection for each element and on the energy of the X-ray. A quantitative analysis can be made if the photoionization cross- section is known, along with other experimental parameters.

4.2.3.5 Cathodoluminescence characterization

The cathodoluminescence was measured in the ultra- high vacuum chamber described in Chapter 3. A Kimball Physics model EFG- 7 electron gun was used as the energy source to stimulate cathodoluminescence. The accelerating voltage was varied for these experiments from 500- 5000 eV. The current level also varied from 2.5 to 8 μA typically in an area of 0.0314 cm^2, corresponding to current densities of 80 to 255 μA/ cm^2. A fiber optic inputted Ocean Optics S2000 spectrometer was used to detect the visible light emission from the samples.

4.3 Results from Pulsed Laser Deposited Phosphors

The thickness of the films was measured by secondary ion mass spectrometry (SIMS) profiling followed by profilometer measurements of the sputter crater and depth. The films were grown to two thicknesses: 0.85 and 1.4 μm. The increased thickness was a result of a longer deposition time. The deposition rate for both growth conditions was about 500 Å/ min. The samples were characterized for structure and morphology, composition, and cathodoluminescence emission spectrum and peak intensity.

4.3.1 Structural Characterization

The as- deposited samples and annealed samples were examined by X- ray diffraction. The XRD diffraction patterns for the thin film samples were compared with the Zn_2SiO_4: Mn powder that was used to make the ablation target. This pattern for the powder has been indexed with its corresponding planes, and is shown in Figure 4.1. The powder pattern matches closely to the JCPDS file for rhombohedral zinc silicate. All of the peaks from the powder sample can be attributed to Zn_2SiO_4. Figure 4.2 compares the diffraction pattern for the 0.85 μm thick sample for as- deposited at 700 ºC and annealed

at 1100 ºC for 5 minutes. The as- deposited film had no discernable diffraction peaks from Zn_2SiO_4. However, diffractions peaks for the (100) Si substrate are observed along with a peak at 44 2θ degrees. This peak has been identified as an impurity SiO_2 phase and is denoted by '*' in Figure 4.2. The XRD pattern for the annealed film indicates that Zn_2SiO_4 is present and has a polycrystalline structure. Figure 4.3 shows the improvement in structural quality for the thicker film, 1.4 μm, after the anneal and the corresponding zinc silicate diffraction peaks are denoted. The pattern for the as- deposited at 700 ºC film only shows diffraction peaks resulting from the Si substrate. Impurity SiO_2 phases are also present in this film, as indicated by the diffraction peaks at 22, 27, and 44 degrees and is denoted in the diffraction patterns by an asterisk '*'.

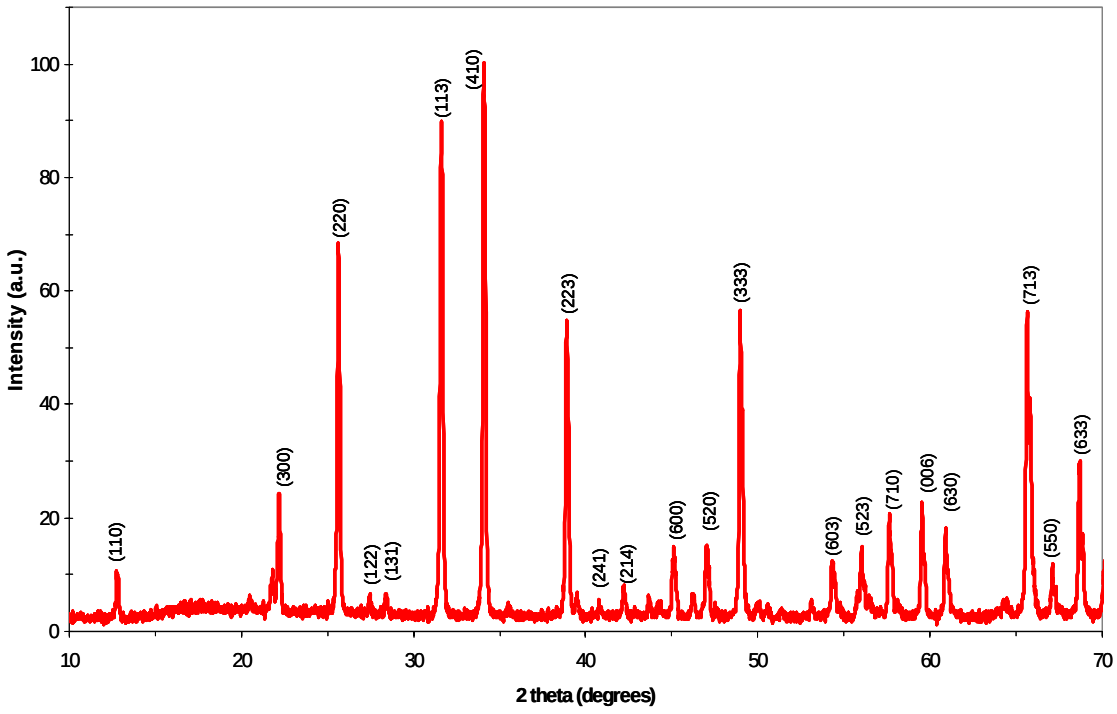

Figure 4-1. Powder XRD pattern for Zn_2SiO_4: Mn. This is consistent with the rhombohedral crystal structure reported in JCPDS 37- 1485.

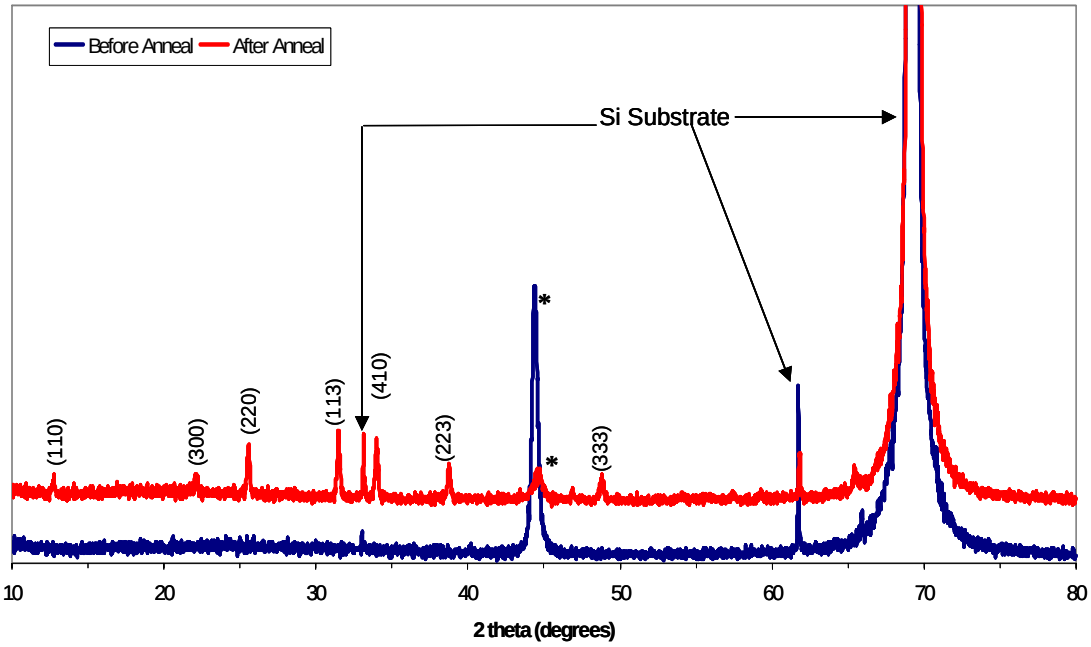

Figure 4-2 XRD pattern of Zn_2SiO_4: Mn thin film phosphor (0.85 μm thick) before and after annealing. * designates peaks from SiO_2.

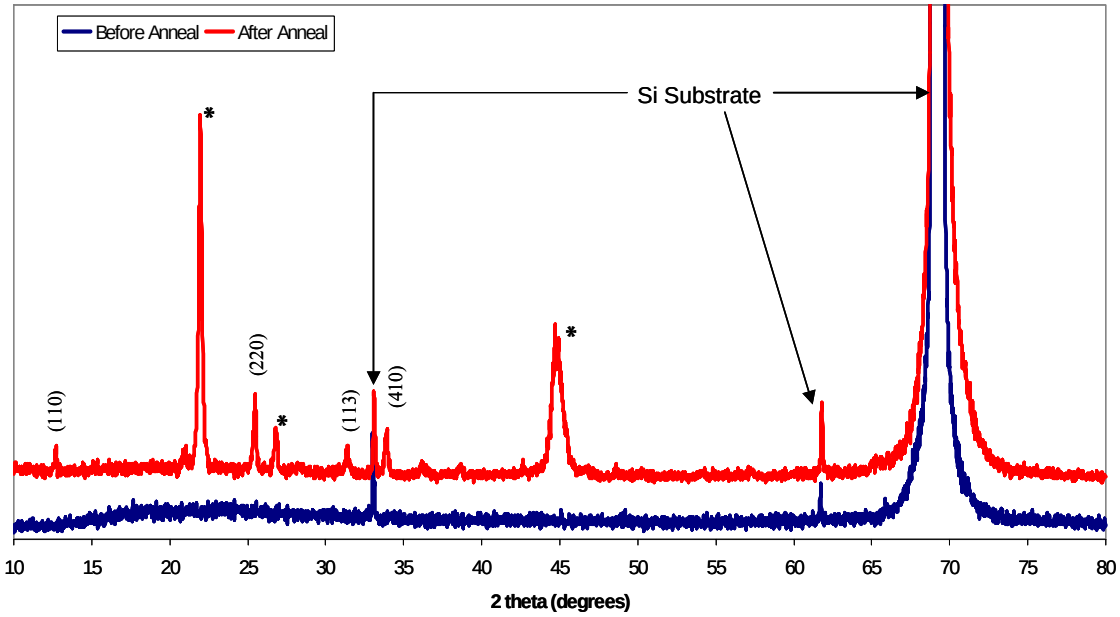

Figure 4-3. XRD pattern of Zn_2SiO_4: Mn thin film phosphor (1.40 μm thick) before and after annealing. * designates peaks from SiO_2.

4.3.2 Morphological Characterization

All films were specular reflecting before the anneal at 1100 °C. After the anneal in N_2, the thinner sample retained its reflectivity, while the thicker sample had a dull appearance. The morphologies were investigated by scanning electron microscopy (SEM) to better understand the differences in the samples, and the micrographs are shown in Figure 4.4. The micrographs indicate that different surface morphologies exist for the two different conditions. Figure 4.4 (a) shows that the thinner Zn_2SiO_4: Mn film was produced with particulates on the surface. It is

A)

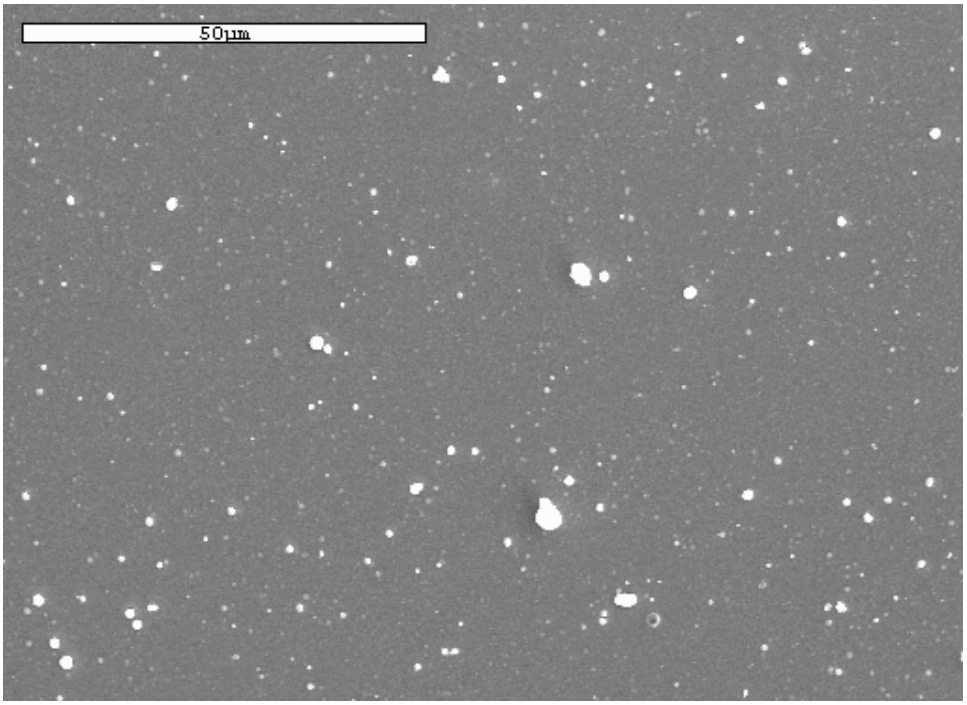

B)

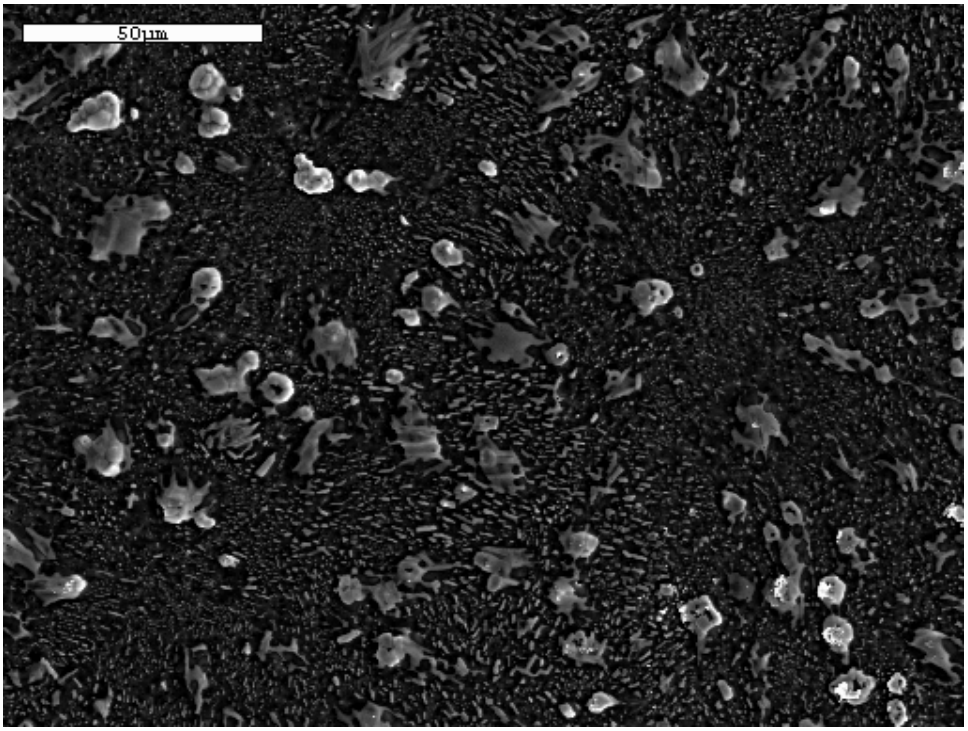

Figure 4-4. SEM pictures of the surface of the phosphor films after annealing at 1100 °C for the A) 0.85 µm sample and for B) 1.4 µm thick sample.

common for particulates to form on the surface during pulsed laser deposition [45]. The thicker film was investigated further to determine what the clusters on the surface were. It was found to compose of a silicon- oxygen rich matrix, much like the remaining surface. A small amount of zinc (1- 3 atomic%) was also present.

4.3.3 Cathodoluminescence Results

The CL emission spectra for annealed Zn_2SiO_4: Mn for each thickness are shown in Figure 4.5. The primary beam voltage and current for these spectra was 5 keV and 8.0 μA. The spectra have the characteristic Gaussian profile. The maximum peak intensity was observed at a wavelength of 530 nm. The thinner sample is significantly brighter than the thicker sample. The cathodoluminescent brightness is 9 times greater for the 0.85 μm film, compared to the 1.4 μm sample.

The maximum peak intensity was also measured for each film from 500- 5000eV as is shown in Figure 4.6. The trend indicates that the thinner film has a higher CL intensity than the thick film at all voltage levels. Previous researchers have observed the opposite trend [3,34], where the CL intensity is higher as the thickness of the films increase. CL intensity increases with an increasing accelerating voltage for the thinner sample. However, the slope of change in CL intensity for the thicker sample with beam voltage is very small.

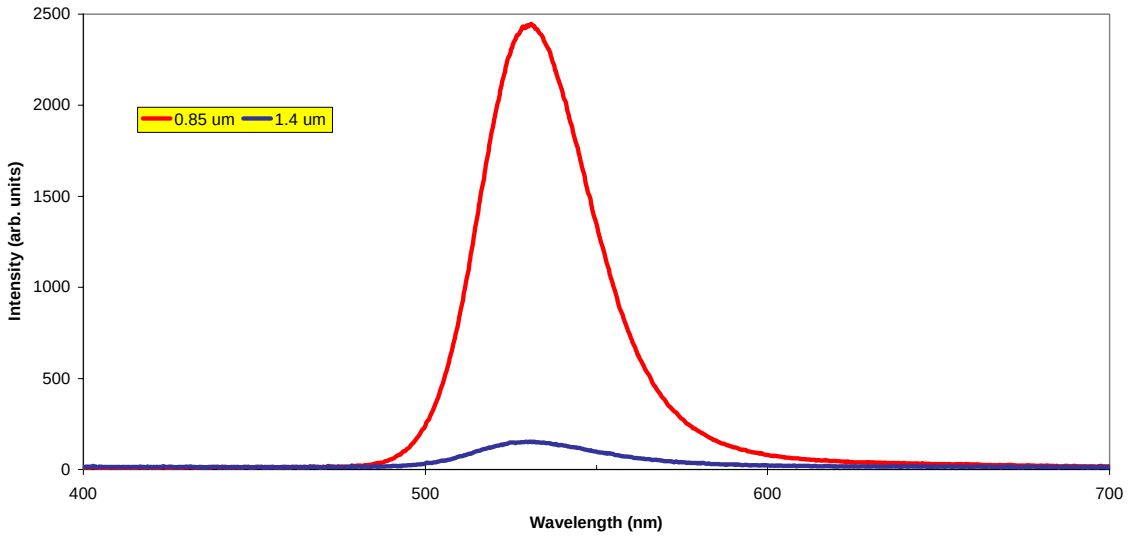

Figure 4-5. Cathodoluminescent emission spectra from Zn_2SiO_4: Mn at V= 5keV, i= 8.0 μA, with inset of CL spectrum for 1.4 μm thick sample.

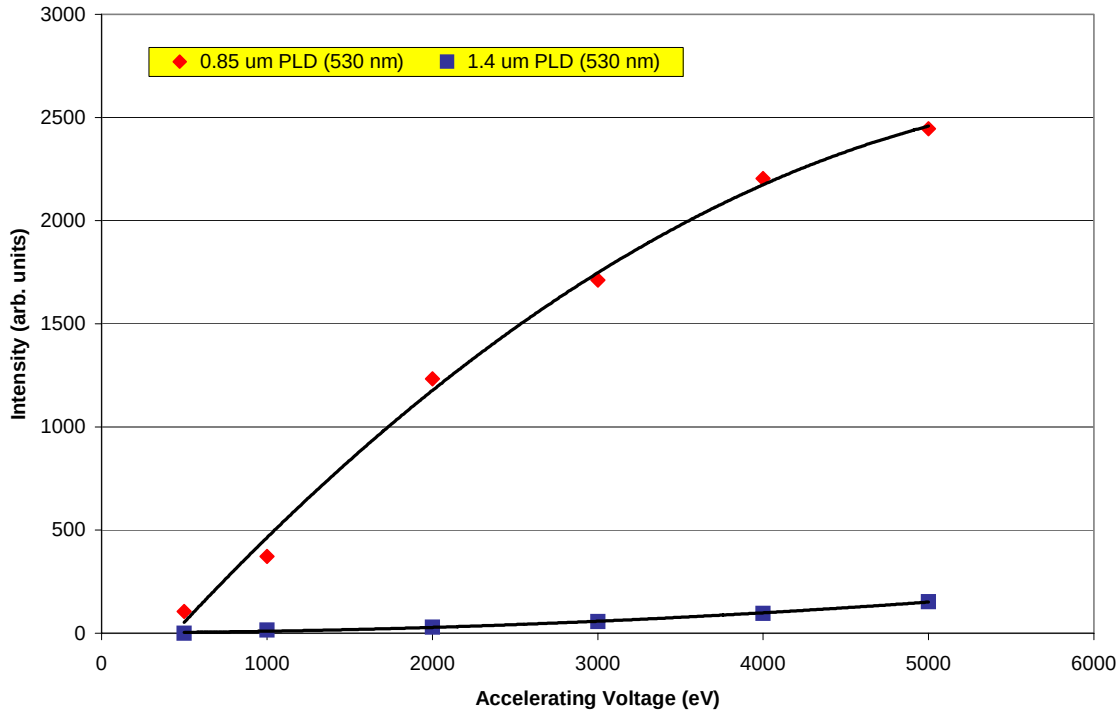

Figure 4-6 CL brightness versus primary beam voltage for PLD Zn_2SiO_4: Mn thin films.

4.3.4 Composition of Films

The composition of the films was measured by electron probe microanalysis (EPMA). The atomic % of each element for the two samples is shown in Figure 4.7. It can clearly be seen that the thin sample has a higher zinc content (12 at %) than the thicker sample (3 at %). The Zn/Si ratios were 0.58 and 0.11 for the 0.85 and 1.40 μm thick films, respectively. Both samples exhibit a lower than expected Zn/Si ratio, suggesting a Zn deficiency. The XRD diffraction patterns indicate that Zn_2SiO_4 is present, but to varying degrees. The 1.40 μm thick film had a diffraction pattern that included several peaks resulting from SiO_2 and Zn_2SiO_4. This correlates to the trend of the composition data suggesting that less Zn is present in this sample versus the 0.85 μm thick film. These data suggest that the trends from the EPMA data are correct although the absolute values may not be accurate.

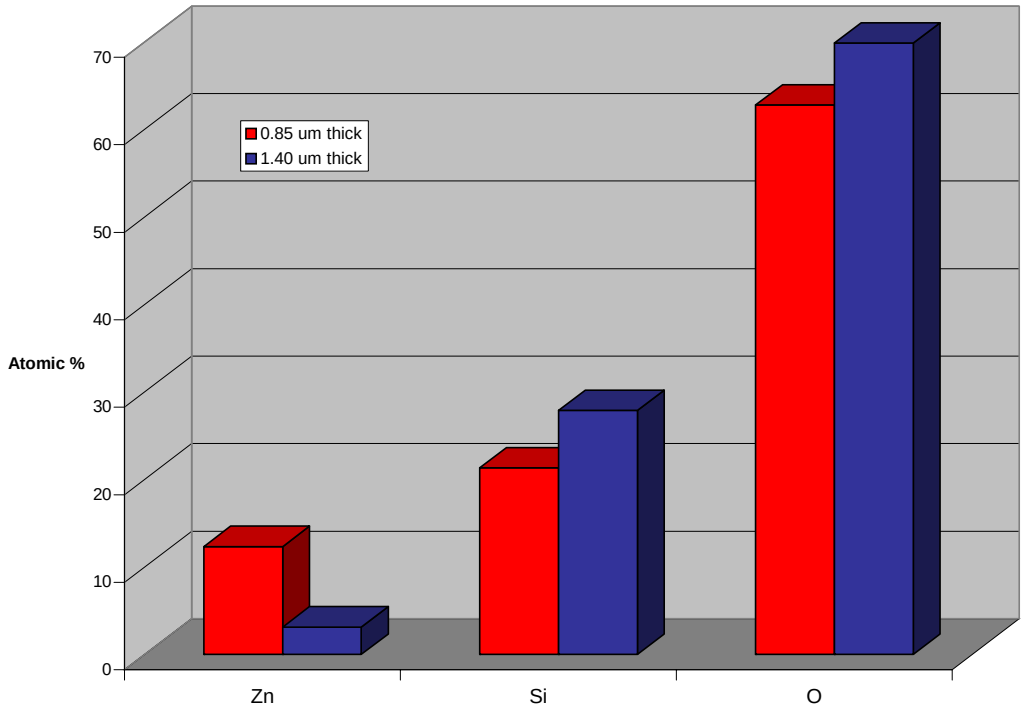

Figure 4-7 Comparison of composition in the PLD thin film samples.

4.4 Results from Sputter Deposited Phosphors

4.4.1 Target 1

Two samples were grown with Target 1under different sputter power (80 versus 100W) while all other variables remained the same. The films were deposited onto quartz substrates. The growth parameters are defined in Table 4.2. A rapid thermal anneal at 1100 ºC was necessary for detectable cathodoluminescence.

Table 4-2 Processing conditions for sputter deposition of Zn_2SiO_4: Mn thin films using Target 1.

Processing Parameter	Selected Conditions
Sputter power	80- 100 W
System pressure	18 mTorr
O_2 partial pressure	3 mTorr
Substrate temperature	room temperature- no heating
RTA temperature	1100 ºC

The thickness of a step in the thin films was measured by a profilometer. The sample that was sputtered at 80W had a deposition rate of 16 Å/ min, resulting in a thickness of 1925 Å. The sample sputtered at 100 W had a measured thickness of 2262 Å, corresponding to a deposition rate of 18.8 Å/ min.

4.4.1.1 Structural characterization

X- ray diffraction data from the films was collected before and after the 1100 ºC anneal for 5 minutes. Both as- deposited films were amorphous with no discernable diffraction peaks. The X- ray diffraction patterns for two samples that were annealed at 1100 ºC are shown in Figure 4.8. All of the diffraction peaks were indexed to zinc silicate, indicating that a polycrystalline solid exists for both growth conditions after the post- deposition anneal.

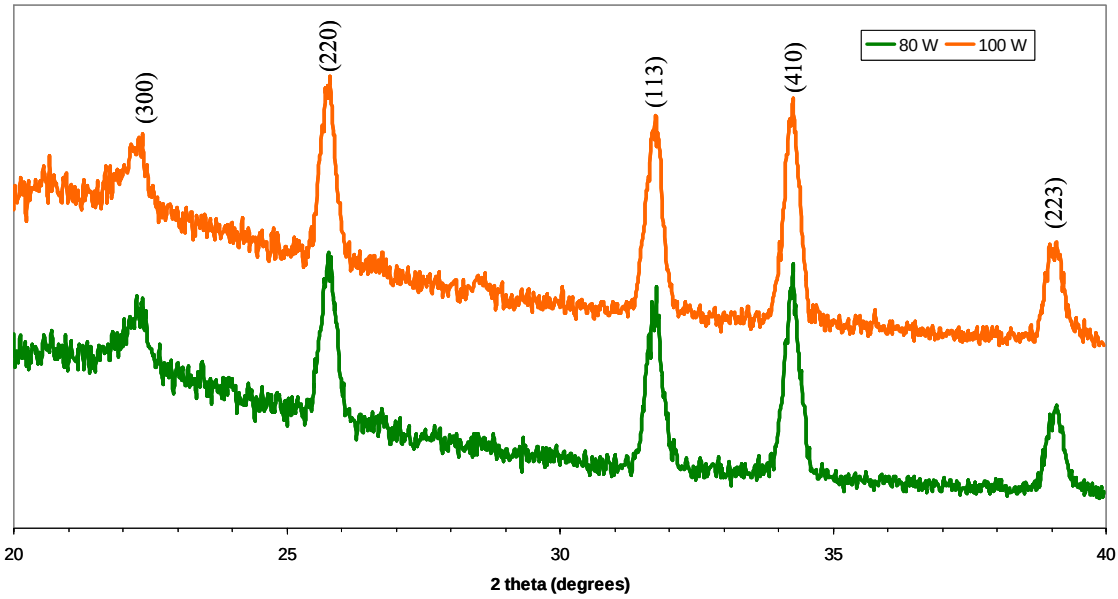

Figure 4-8. XRD pattern of 1100 ºC annealed sputtered films at two different sputter conditions.

4.4.1.2 Cathodoluminescence results

The cathodoluminescent (CL) spectra are compared in Figure 4.9 for the two different growth conditions. The emission spectra resulted from an electron beam excitation source with an energy of 5000 eV and 7.0 μA of beam current. There were no observable differences in the two spectra. The maximum emission peak for these samples was at 526 nm consistent with visible green emission. The film deposited at the higher power (100 W) was brighter than the film deposited at 80 W. In the case of sputter deposited films, the thicker film resulted in brighter luminescence. As expected, the CL brightness increased with accelerating voltage (Figure 4.10). The CL emission was evaluated for accelerating voltages from 1000- 5000 eV at a beam current of 2.5 μA. However, at the low voltages there is little difference in the maximum emission intensity for the two samples. In contrast, at 5000 eV the difference in the maximum intensity is 1.3 times as shown in Figure 4.11.

The cathodoluminescence from 500- 5000 eV and a beam current of 8.0 μA from films grown by sputter (0.1925 μm) versus pulsed laser deposition (0.85 μm) is compared in Figure 4.12. The thinner pulsed laser deposited sample was chosen since it had the best brightness for that growth method. It is compared with the less bright sample created by sputter deposition. The sputter sample is still more than 30% brighter than the thin film phosphor sample made by pulsed laser deposition, even though it is a factor of four times thinner.

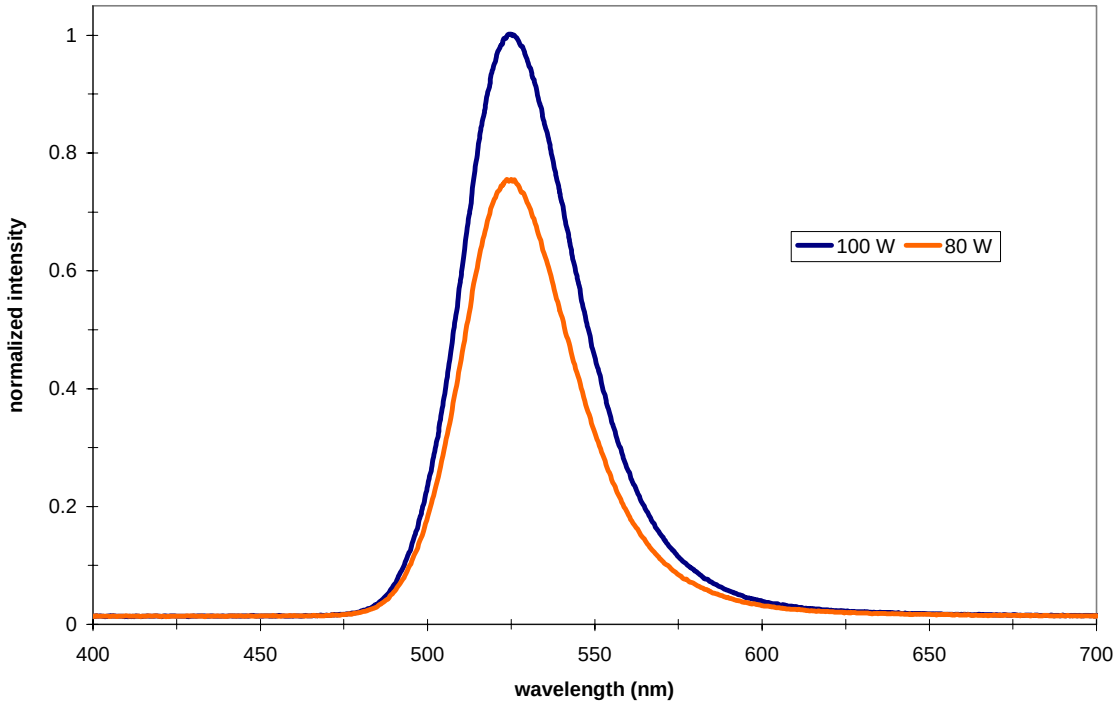

Figure 4.9. Cathodoluminescent spectra from sputtered deposited thin film samples.

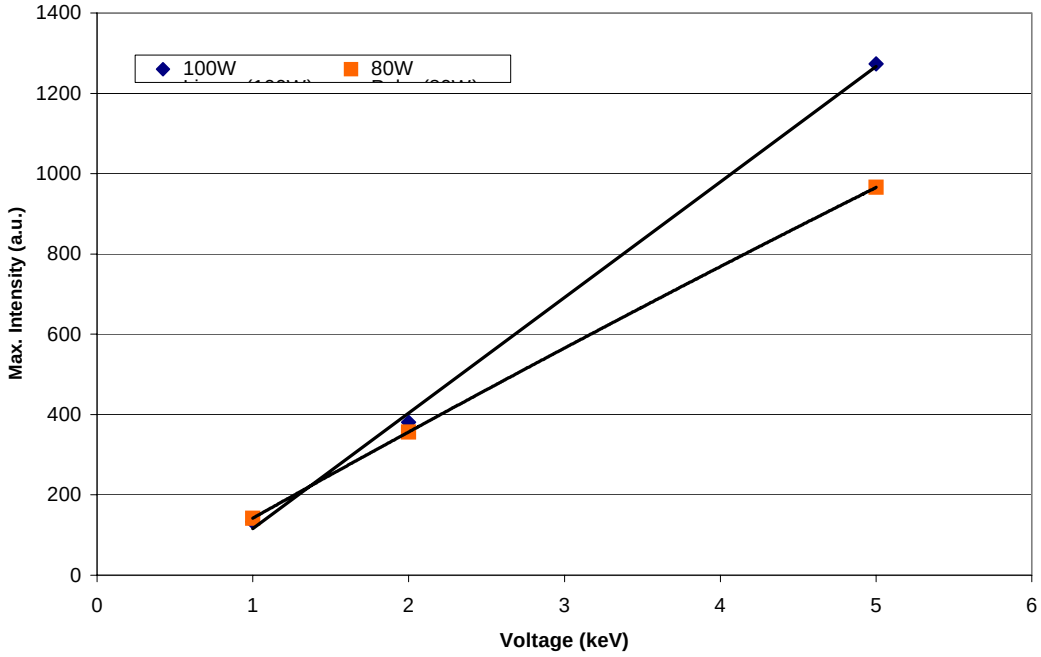

Figure 4-10. Maximum CL brightness for sputter deposited and annealed Zn_2SiO_4: Mn thin films from 1000 to 5000 eV.

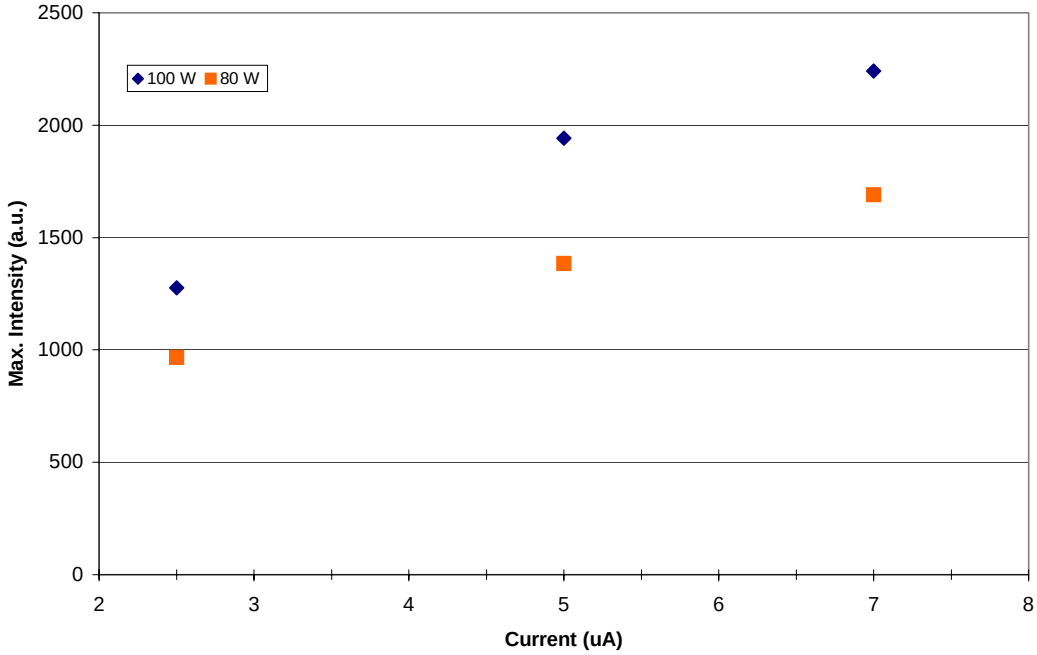

Figure 4-11. Maximum CL intensity at V= 5keV for i= 2.5 to 7 μA.

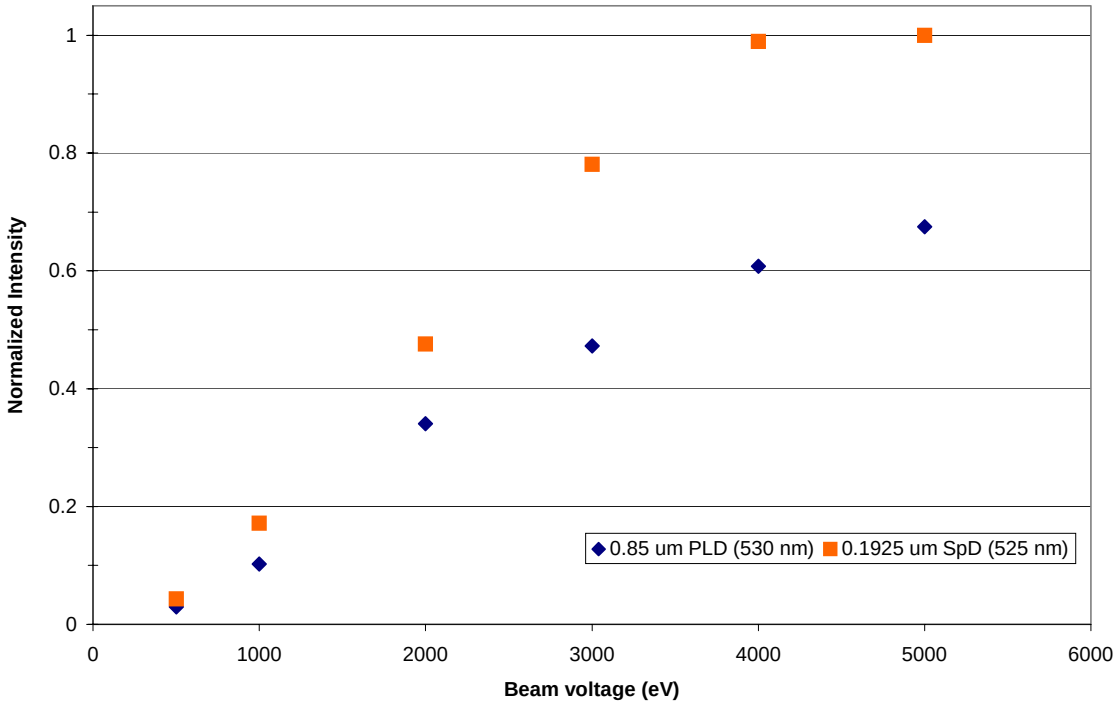

Figure 4-12. Maximum CL brightness for PLD vs. sputter deposited Zn_2SiO_4: Mn thin films from 500 to 5000 eV.

4.4.2 Target 2

As discussed earlier, a second target was used after it was noticed that the first target had become a source of carbon contamination due to the cracking and exposure of the carbon based bonding material. A different sputter gun was used with target 2, which eliminated the need for bonding the target to a backing plate with a carbon based material. A different deposition chamber was also used for these film growth cycles.

The growth parameters are outlined in Table 4.2. The films were deposited onto quartz substrates. Each deposition cycle lasted 60 minutes. A rapid thermal anneal at 1100 ºC for 5 minutes was necessary to detect cathodoluminescence.

Table 4-3 Processing conditions for sputter deposition of Zn_2SiO_4: Mn thin films using Target 2.

Processing Parameter	Selected Conditions
Sputter power	40- 70W
Sputter pressure	13 mTorr
O_2 partial pressure	2.5 mTorr
Substrate temperature	room temperature- no heating
RTA temperature	1100 ºC

4.4.2.1 Structural characterization

The as- deposited samples were all amorphous as indicated by their respective diffraction patterns. A representative X- ray diffraction pattern for the annealed at 1100 ºC phosphors is shown in Figure 4.13. All of the diffraction peaks are indexed to zinc silicate, indicating that a polycrystalline solid exists after the anneal.

4.4.2.2 Cathodoluminescence results

The cathodoluminescence spectra from the annealed sputter deposited films are shown in Figure 4.14. The maximum emission peak for these samples was at 526 nm consistent with visible green emission. The two brightest phosphors were from sputter conditions at the higher sputter powers, 70 and 60 W. As the sputter power decreased, a decrease in the cathodoluminescence is also observed. The composition was measured by X- ray photoelectron spectroscopy (XPS) to further investigate the drop in luminescence at the lower sputter power. However, the results did not accurately correlate to the trends for cathodoluminescence.

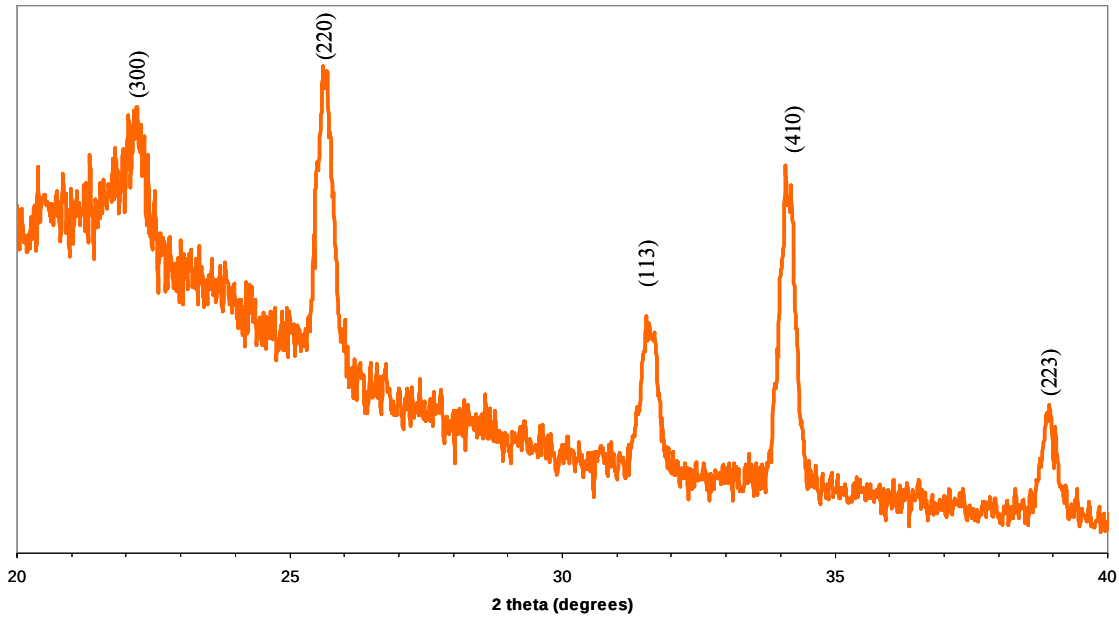

Figure 4-13 X- ray diffraction pattern from Zn_2SiO_4: Mn thin film sputter deposited with target 2.

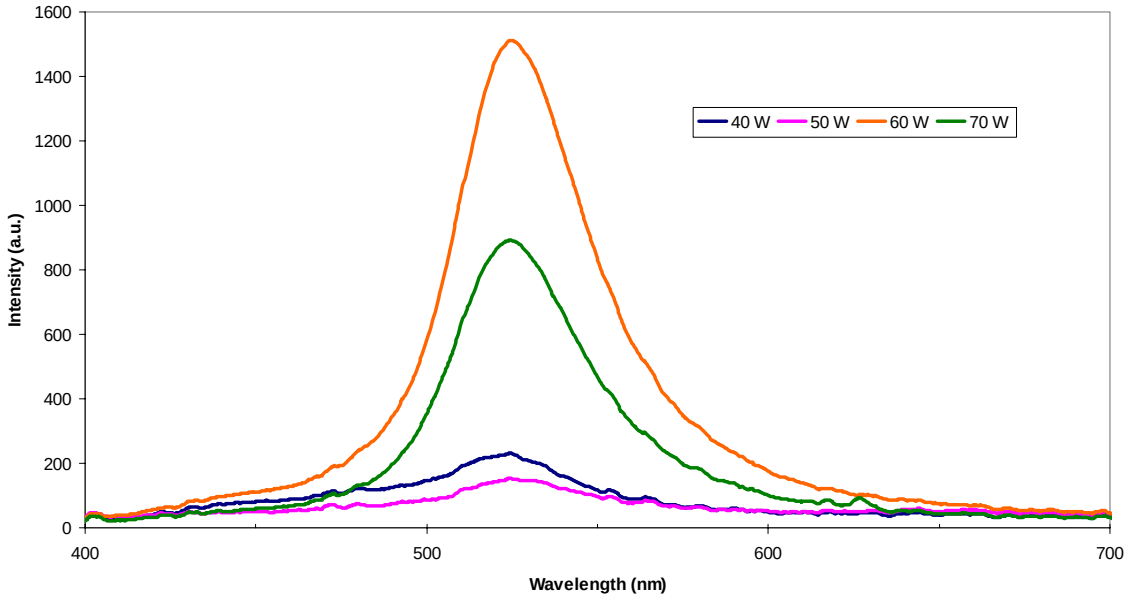

Figure 4-14 Cathodoluminescent emission from sputter deposited Zn_2SiO_4: Mn at electron beam V= 5keV, i= 15µA for sputter powers of 40- 70W.

The composition was measured by XPS which has a detection depth of about 3 nm, while the CL data result from the electron beam voltage of 5 keV penetrating more than 100 nm into the film. The XPS results indicate that a zinc deficiency exists at the surface for all films, but may not be representative of the bulk composition.

4.5 Results from Combustion Chemical Vapor Deposition Phosphors

The phosphor films grown on quartz substrates by combustion chemical vapor deposition (CCVD) contain Mn at two concentration levels, 2 and 4 mol %. The as-deposited films were investigated with X- ray diffraction, and their structure was determined to be polycrystalline Zn_2SiO_4 [70]. Therefore, no post deposition heat treatment was completed for these samples.

4.5.1 Cathodoluminescence Results

The cathodoluminescence spectra for the CCVD phosphor films are shown in Figure 4.15, and their peak maximum at 525 nm is consistent with the spectra from PLD and sputter deposited Zn_2SiO_4: Mn. The emission from the 4 mol% Mn concentration phosphor is 5% brighter than the emission from the 2 mol% Mn phosphor. Additionally, the CL intensity was compared with the brightest sputter deposited film in Figure 4.13. The films produced by CCVD were at least 40% brighter.

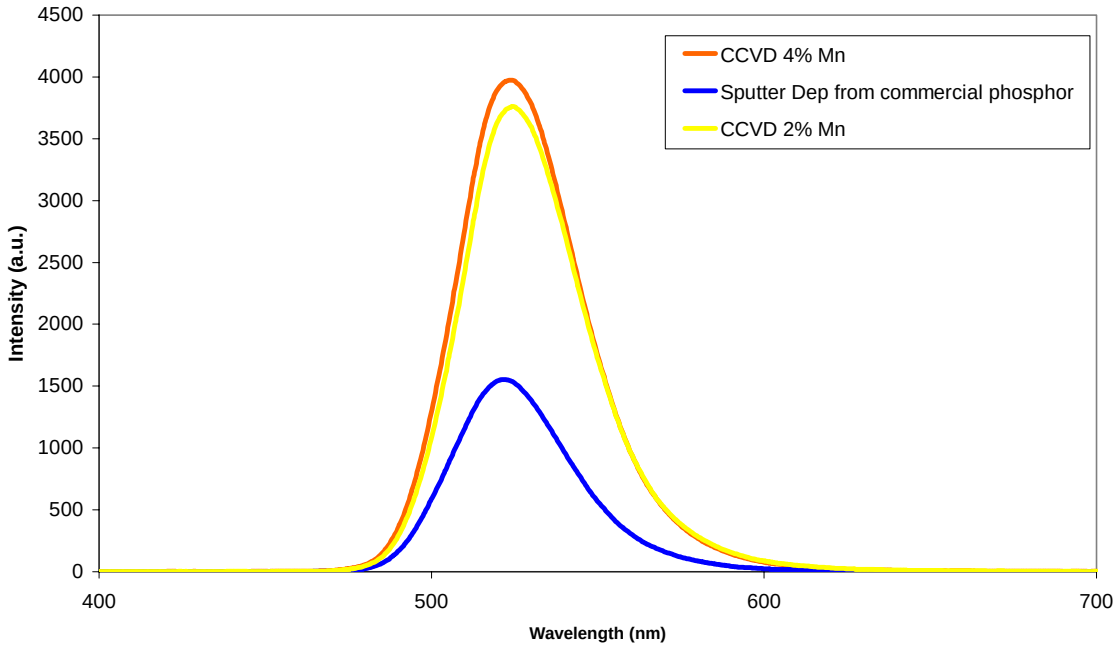

Figure 4-15 CL spectra from CCVD Zn_2SiO_4: Mn phosphor films at beam V= 5keV, i= 7.0 μA.

4.6 Discussion

Zn_2SiO_4: Mn thin film phosphors were successfully made by pulsed laser deposition, sputter deposition, and combustion chemical vapor deposition. The X- ray diffraction data indicated that the as- deposited films for PLD and sputter deposition were amorphous, even though the PLD films were deposited onto substrates at 700 ºC. The thin films were polycrystalline after a rapid thermal anneal at 1100 ºC in N_2 atmosphere.

The CL performance of the PLD films was compared for two thicknesses. The thinner film was actually 94% brighter than the thicker film. This indicates that the brightness of the films does not depend solely on the thickness, since thicker films are expected to result in brighter luminescence. The low CL performance of the thick film

was correlated to a low Zn to Si ratio, compared to the brighter film which had a higher Zn to Si ratio. Additionally, the impurity SiO_2 phase is strongly represented in the diffraction pattern for the thicker film indicating that the film is a mixture of non-luminescent SiO_2 and luminescent Zn_2SiO_4. The Mn activator is expected to substitute for the Zn atoms in the lattice structure. However, there is less Zn present in this film. The reduction in cathodoluminescence is attributed to a reduction in the luminescent center density. This is a reasonable assumption since the CL intensity changes only slightly as the excitation volume increases.

The cathodoluminescence was also characterized for films that were sputtered deposited. The results of the sputter deposited films were divided according to the sputter target and deposition chamber used for film growth. The films that used target 1 were sputter deposited at two different powers and were compared based upon growth condition and film thickness. The 20% higher sputter power resulted in a film that was 15% thicker. Green cathodoluminescence was observed from the samples after the anneal was completed, with the thicker sample being 25% brighter than the thin sample. The sputter deposited films from target 2 were grown at a slightly lower pressure and a lower sputter power range, 40- 70W. The cathodoluminescence was brightest for films deposited at 60- 70W and dimmest for those films deposited at 40- 50W sputter power. The increase brightness is due to increased thickness of the phosphor films as the sputter power is increased.

The films created by sputter and pulsed laser deposition were also compared. The cathodoluminescence was at least 30% brighter for the films made by sputter deposition

versus pulsed laser deposition. The pulsed laser deposited samples has an SiO_2 impurity phase, which limits the activator density.

The films grown by combustion chemical vapor deposition developed a polycrystalline structure during growth at 1200 ºC at atmospheric conditions. Therefore, no post- growth heat treatment was completed for these films. The films were made at two dopant levels where the 4 mol% Mn had a brighter cathodoluminescent emission than the film doped with 2 mol% Mn. The CCVD films were brighter than the films made by sputter deposition. The brightest films from this study were those made by CCVD and were chosen to study the degradation of Zn_2SiO_4: Mn thin films, as discussed in the following chapter.

CHAPTER 5
DEGRADATION OF ZINC SILICATE DOPED WITH MANGANESE POWDER AND THIN FILM PHOSPHORS

5.1 Introduction

The degradation behavior of thin film and powder Zn_2SiO_4: Mn phosphors is evaluated and discussed in this chapter. The degradation was observed under low (95 $\mu A/ cm^2$) and high (460 $\mu A/ cm^2$) current excitation densities for a period up to 24 hours. Continuous exposure to the electron source over the 24-hour period has been shown to affect the brightness of sulfide phosphors [19,73].

The first section in this chapter discusses the experimental procedures used to monitor the degradation of the phosphors. The changes in the surface chemistry of the phosphors have been observed by Auger electron spectroscopy. The decrease in cathodoluminescence observed during electron beam exposure will also be discussed. The differences between the degradation behaviors of the thin film phosphors versus the powder phosphors are discussed. It was found that the excitation density also affects the rate of degradation for both types of phosphors.

5.2 Experimental Procedures

The thin film phosphors were grown by a novel combustion chemical vapor deposition (CCVD) method [70]. The Zn_2SiO_4: Mn phosphor was introduced and evaluated for its cathodoluminescent emission in Chapter 4. It was determined to be the brightest thin film phosphor of all phosphors developed in Chapter 4, and therefore deserves further evaluation. The thin film phosphor on a quartz substrate was mounted

onto a stainless steel holder. The powder phosphor is a commercial plasma display panel (PDP) phosphor obtained from Shanghai Yuelong New Materials Co., Ltd. The powder samples were cold pressed into 4 mm deep, 6 mm diameter holes in a stainless steel holder.

The degradation experiments took place in an ultra- high vacuum stainless steel chamber with a base pressure of 3- 5 $X10^{-9}$ Torr. The phosphors were exposed continuously to an electron beam for 24 hours. The electron source was from a coaxial electron gun in a PHI model 545 scanning Auger electron spectrometer. During electron beam exposure, the cathodoluminescence was measured every minute to monitor changes in luminescence leading to degradation. An Oriel model 77400 multi- spectrometer was used to detect the emission spectra and peak intensities. Additionally, the surface chemistry was simultaneously observed through Auger electron spectroscopy (AES). A cylindrical mirror analyzer (CMA) model 15- 110 was used as the Auger electron detector. The spectra were taken every 5 minutes during the continuous beam exposure for 24 hours. The program created for AES analysis scanned the kinetic energy range of Zn, Si, O, and C for the range as specified in Table 5-1. Consecutive scans were taken for each of the species during 5- minute intervals of data collection.

Table 5-1 Species monitored during AES analysis.

SPECIES	ENERGY RANGE SCANNED (eV)
C	200- 400
O	400- 600
Si	70- 100

Table 5-1. Continued

SPECIES	ENERGY RANGE SCANNED (eV)
Zn1	900- 1050
Zn2	40- 80
Survey of All Energies	30- 1100

5.3 Results

5.3.1 Thin Film Zn_2SiO_4: Mn Phosphor

5.3.1.1 24 hour CL degradation

Thin film Zn_2SiO_4: Mn was exposed to a 2000 eV, 3.0 μA electron beam for 24 hours. Over this time period, the thin film phosphor decreased by 14% from its original cathodoluminescent intensity at the low current density of 95.5 μA/ cm^2 as shown in Figure 5.1. The spikes in CL intensity are due to system fluctuations, which have been correlated to instabilities with the Peltier cooler system that helps to reduce electrical noise. Figure 5.2 shows the CL intensity during the first 20 minutes of degradation. The phosphor actually decreased to its final intensity in less than ten minutes. The cathodoluminescent spectra before and after degradation were compared in Figure 5.3 to determine any difference in the spectral distribution. No shifts in the spectral distribution or changes in peak shape were noted. Changes in the surface chemistry were also observed during the degradation through monitoring of the Auger electron spectra. The before and after spectra are shown in Figure 5.4, indicating composition changes of the phosphor that evolved during beam exposure. A strong emission from carbon was noted initially, but decreased significantly by the end of the experiment. The carbon Auger electron signal results from adventitious surface contamination. It has been shown that

electron beam bombardment in oxidizing gases may remove this carbon during the initial beam exposure [18,19]. The zinc and oxygen signals are stronger at the end of degradation. This increase is due to the removal of the surface layer of carbon, where now the signal comes exclusively from Zn_2SiO_4. There is no evidence of a chemical reaction or change within the phosphor. Charging of the phosphor during electron beam exposure is evident from the before and after AES spectra as illustrated by the charging feature at the beginning of both spectra and the shift in the individual Auger signals.

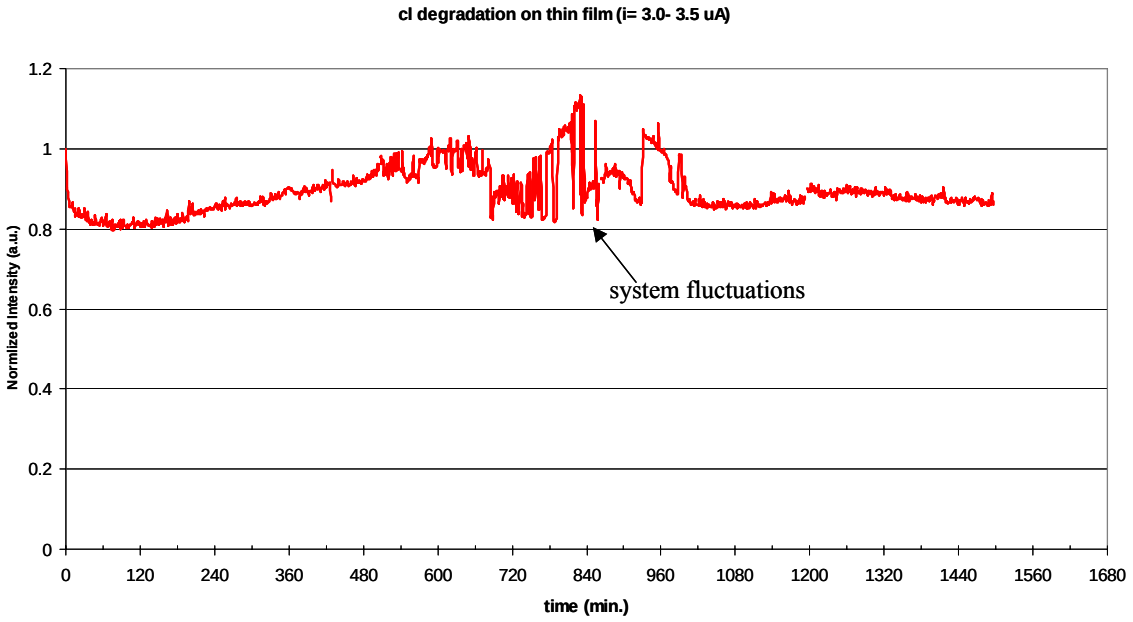

Figure 5-1. Cathodoluminescent degradation of thin film phosphor at V= 2 keV, i= 3.0 μA (95.49 μA/ cm^2).

A second CL degradation experiment was completed on the thin film phosphor at the same beam voltage (2000 eV), but with a higher current density of 461 ± 48 μA/ cm^2 (electron beam current of 14.5 ± 1.5 μA, spot size of 2 mm). The phosphor decreased to 26% of its original cathodoluminescent intensity at the higher current density as indicated in Figure 5.5. In this case, it took a longer period of time (~ 14 hours) for the phosphor

brightness to decrease to its final intensity level. The before and after cathodoluminescent spectra are shown in Figure 5.6, and no changes in the spectral distribution or peak shape is observed. The composition of the phosphor was measured by AES during exposure to the electron beam. The electron beam assisted in the removal of carbon from the surface, as indicated by the decrease in the carbon signal in the AES after spectra shown in Figure 5.7. There is no Auger signal from carbon at the end of the degradation experiment. There is a slight increase in the Auger signals from oxygen and zinc. Again, this increase is expected based on the nearly complete removal of the adventitious carbon from the surface which will reduce Auger electron scattering from Zn_2SiO_4 by C. The charging features at the low energies and the shift in the Auger signals indicate that the surface is charging during electron beam exposure.

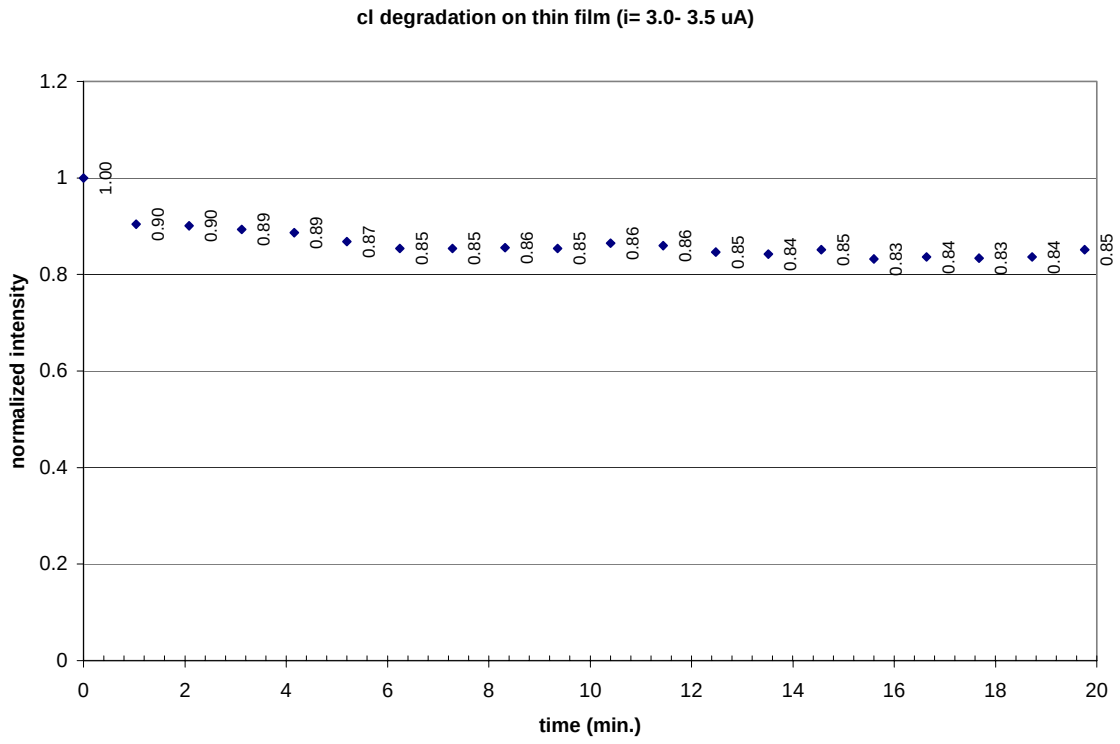

Figure 5-2. Degradation within the first 20 minutes for the thin film phosphor at i= 3.0 μA.

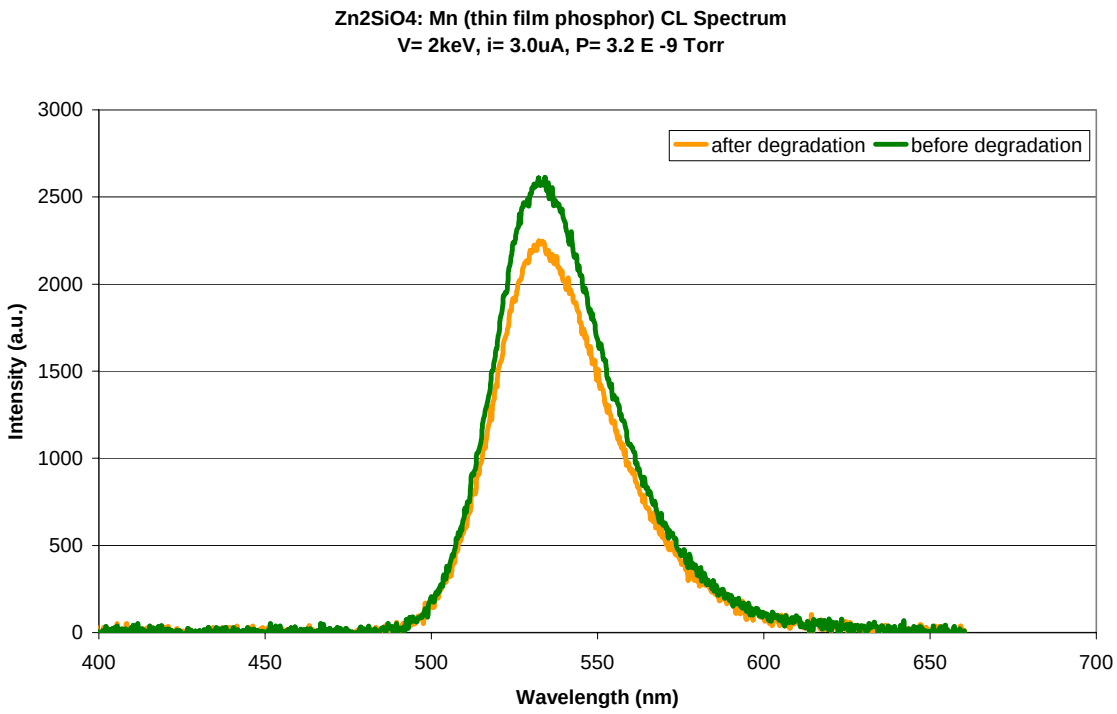

Figure 5-3. Cathodoluminescent spectrum of thin film phosphor before and after degradation at low current excitation density.

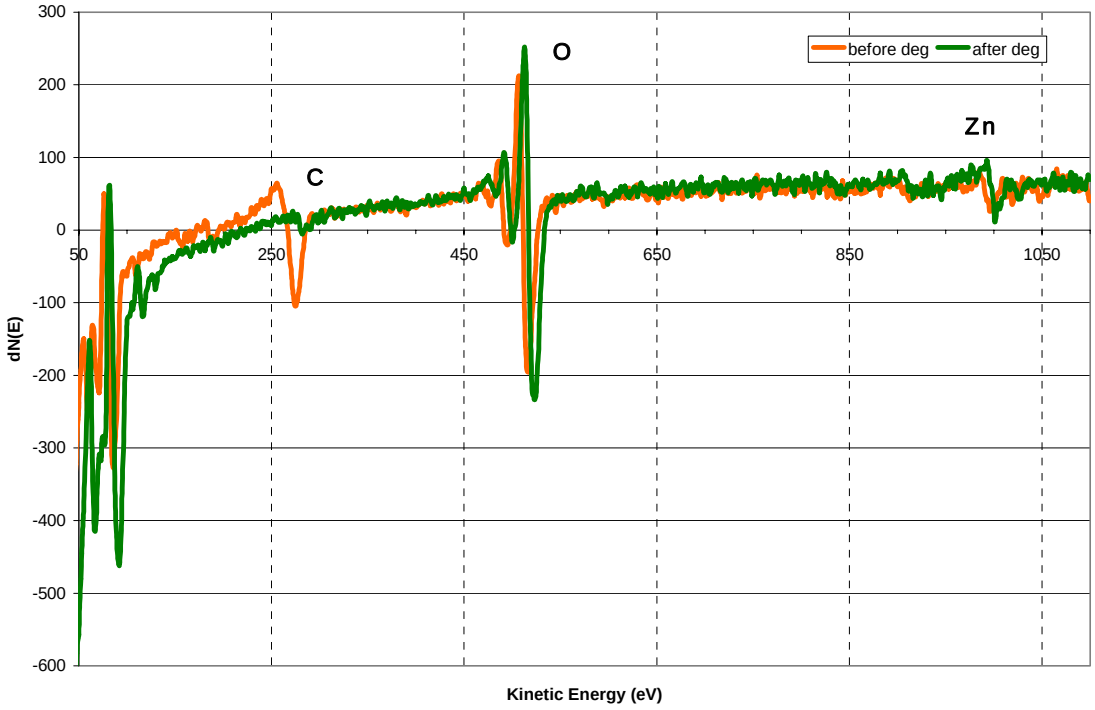

Figure 5-4. Auger electron spectrum before and after degradation on thin film, i= 3.0 μA.

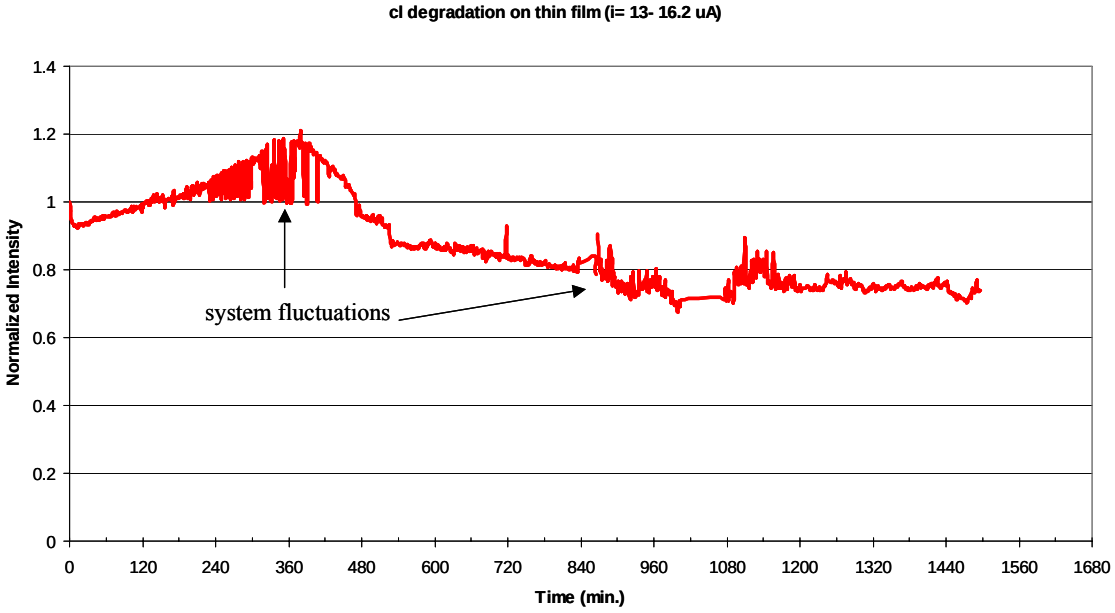

Figure 5-5. Cathodoluminescent degradation of thin film phosphor at V= 2 keV, i= 13 μA.

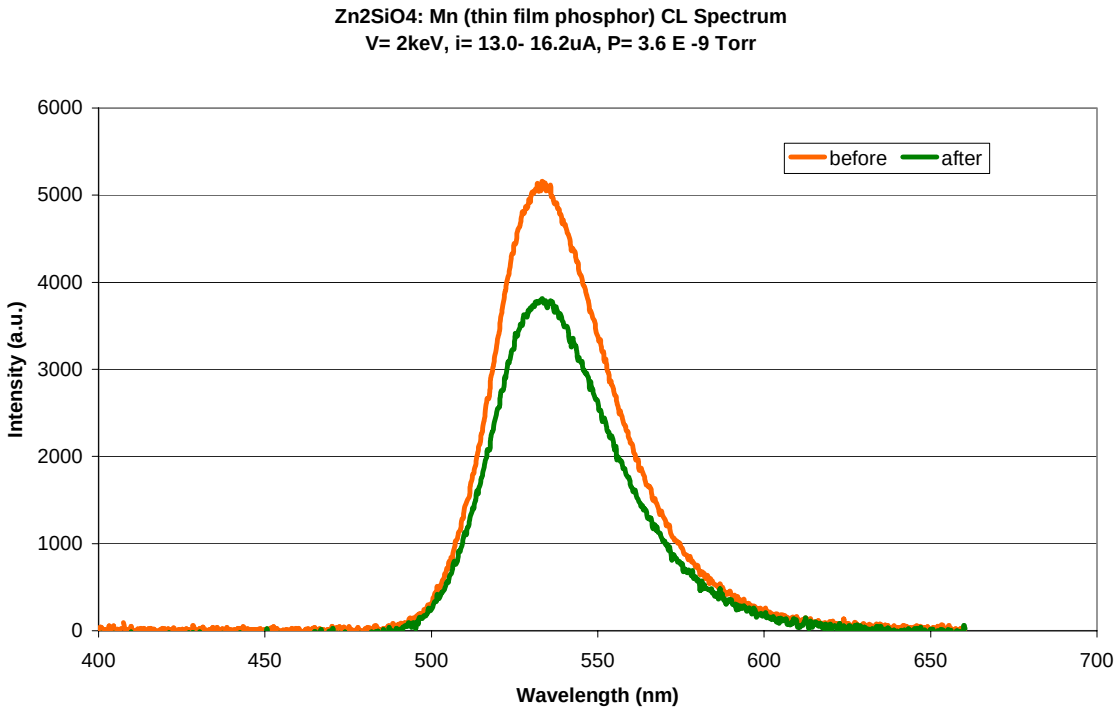

Figure 5-6. Cathodoluminescent spectrum of thin film phosphor before and after degradation at high excitation current density.

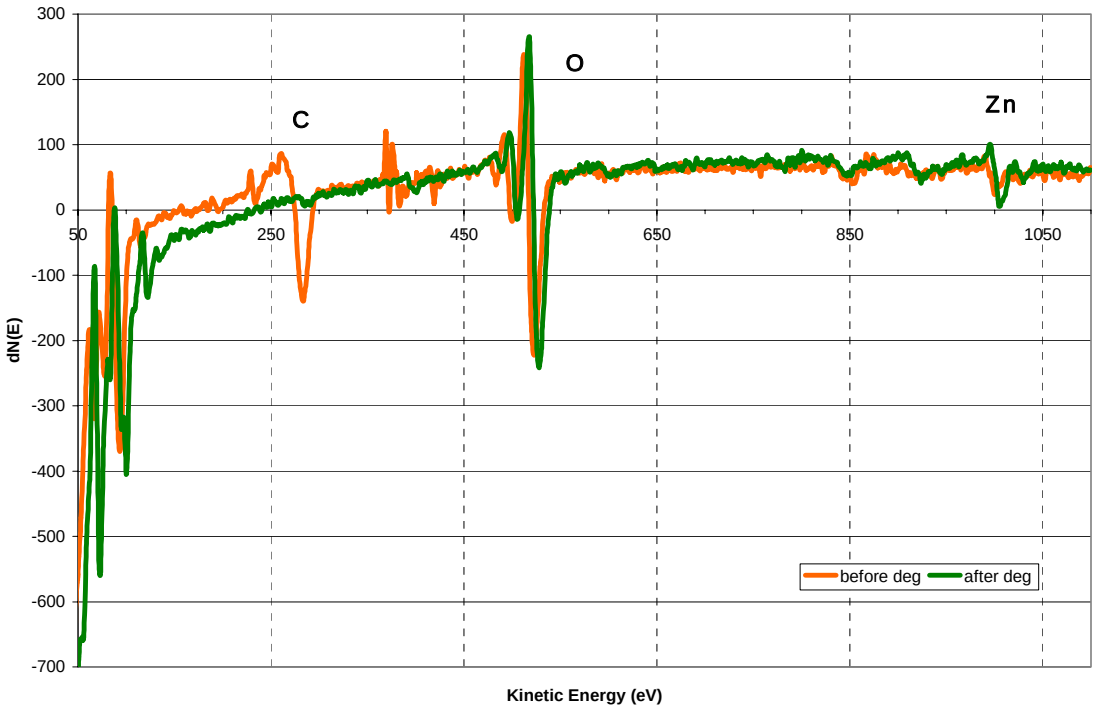

Figure 5.7. Auger spectrum before and after degradation on thin film, i= 13.0 μA.

5.3.1.2 Cathodoluminescence recovery

The same phosphor was examined to determine if the loss in cathodoluminescence could be recovered over time. For this experiment, the phosphors were exposed continuously to an electron beam for 10 minutes (E= 2000 eV) and then the beam was turned off. For the first 30 minutes after beam exposure, the phosphor was exposed to the electron beam for ~5 seconds every minute to measure the CL response from the phosphor. At the end of 30 minutes, a CL measurement was taken followed immediately by an Auger survey over the next 1.5 minutes. Another CL scan was taken upon completion of the Auger survey. This experiment was completed at low and high current densities and the results are discussed below.

As reported, thin film Zn_2SiO_4: Mn degraded to 80% of its original intensity within 10 minutes of continuous beam exposure at low beam current = 3.0 μA (J= 95 μA/ cm^2). The CL spectra for the degraded phosphor are compared for several time intervals in Figure 5.8 to determine if the phosphor could recover to its original intensity without continuous beam exposure. The maximum recovery was to 89% of the original intensity after 30 minutes of intermittent exposure to the electron beam. Auger scans were taken from 200- 300 eV during the 10 minutes of continuous beam exposure and the C signal shifted with time as indicated in Figure 5.9. The surface charging indicated by the shift in C kinetic energy with time and the presence of charging features within the Auger spectra can be correlated with the decrease and non- recovery of cathodoluminescent intensity.

A similar response from the phosphor was observed as the current density was increased to 414 μA/ cm^2 (i=13 μA). The phosphor degraded to 92% of its original

intensity during the 10 minutes of continuous beam exposure. The maximum recovery was to 95% of original intensity after intermittent beam exposure for 30 minutes as shown in Figure 5.10. Figure 5.11 shows the AES spectra which were collected during and after beam exposure. Charging is present after beam exposure and continues to be evident even after 60 minutes of limited beam exposure.

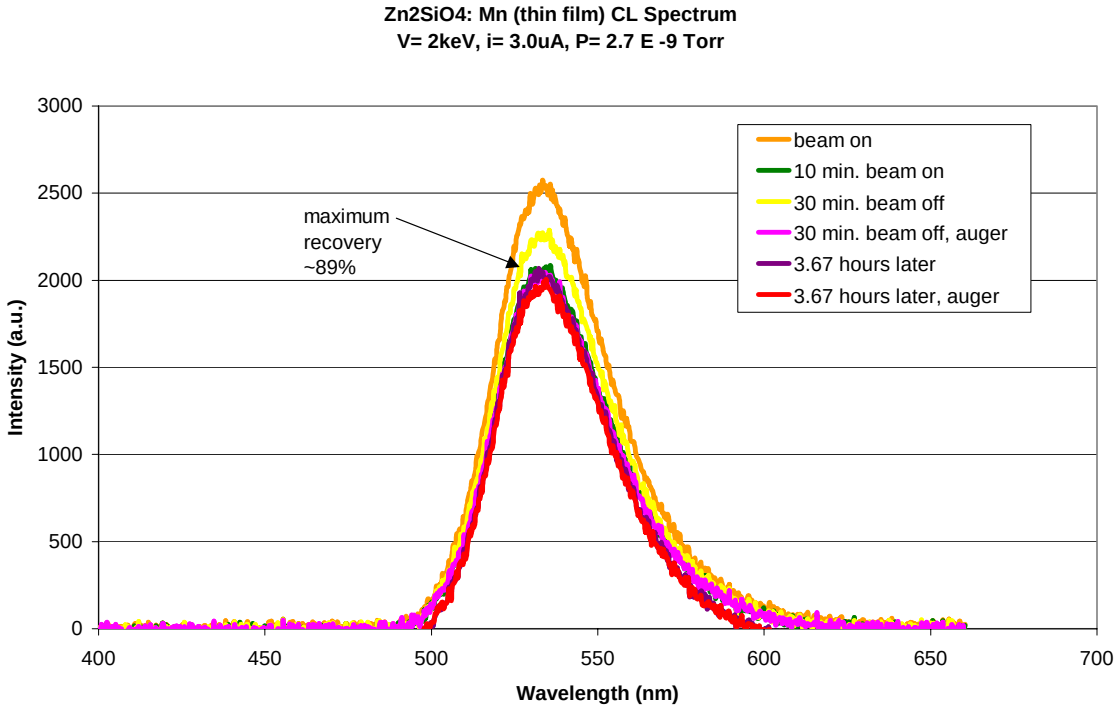

Figure 5-8. CL spectra of thin film Zn_2SiO_4:Mn at V= 2keV, i= 3.0 μA for 10 minutes of continuous beam exposure and recovery over 3.67 hours indicating permanent degradation of phosphor.

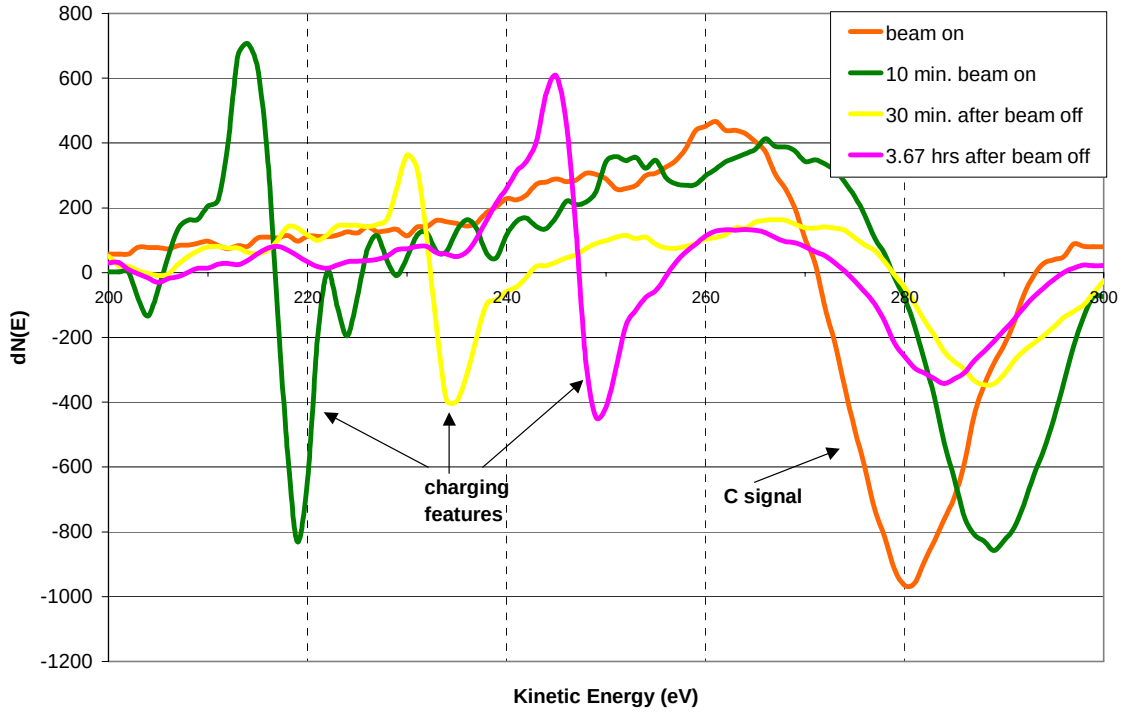

Figure 5-9. AES spectra from Zn_2SiO_4: Mn thin film phosphor during and after beam exposure (i= 3.0 μA).

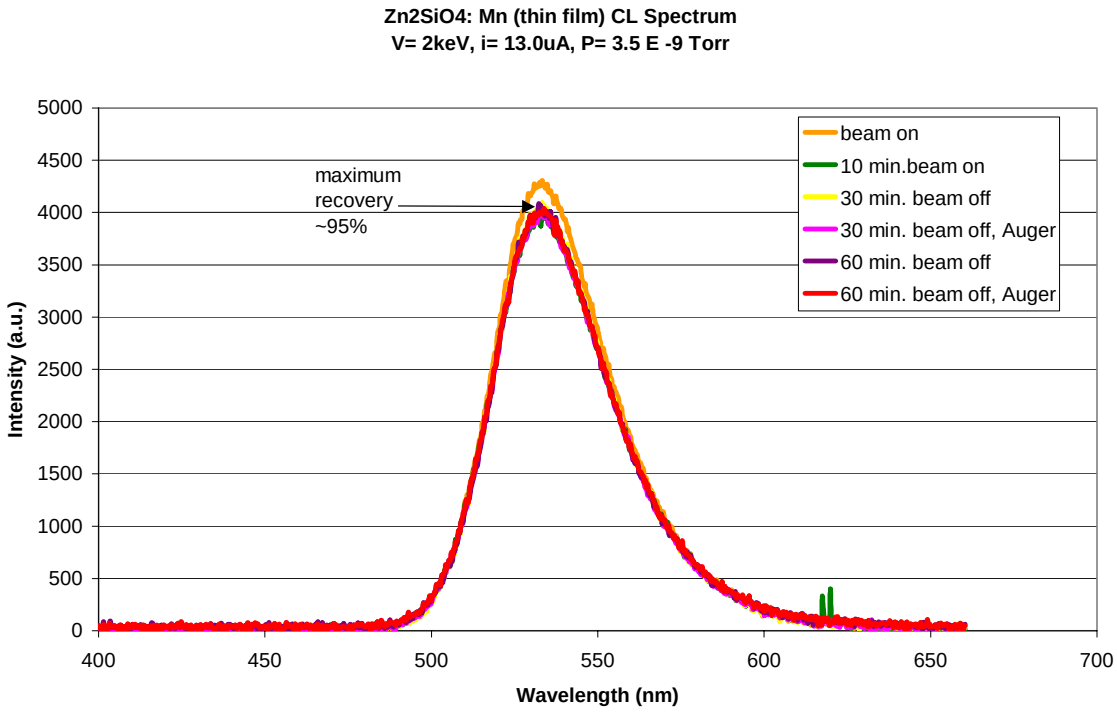

Figure 5-10. CL spectra of thin film Zn_2SiO_4:Mn at V= 2keV, i= 13.0 μA for 10 minutes of continuous beam exposure and recovery over 60 minutes indicating permanent degradation of phosphor.

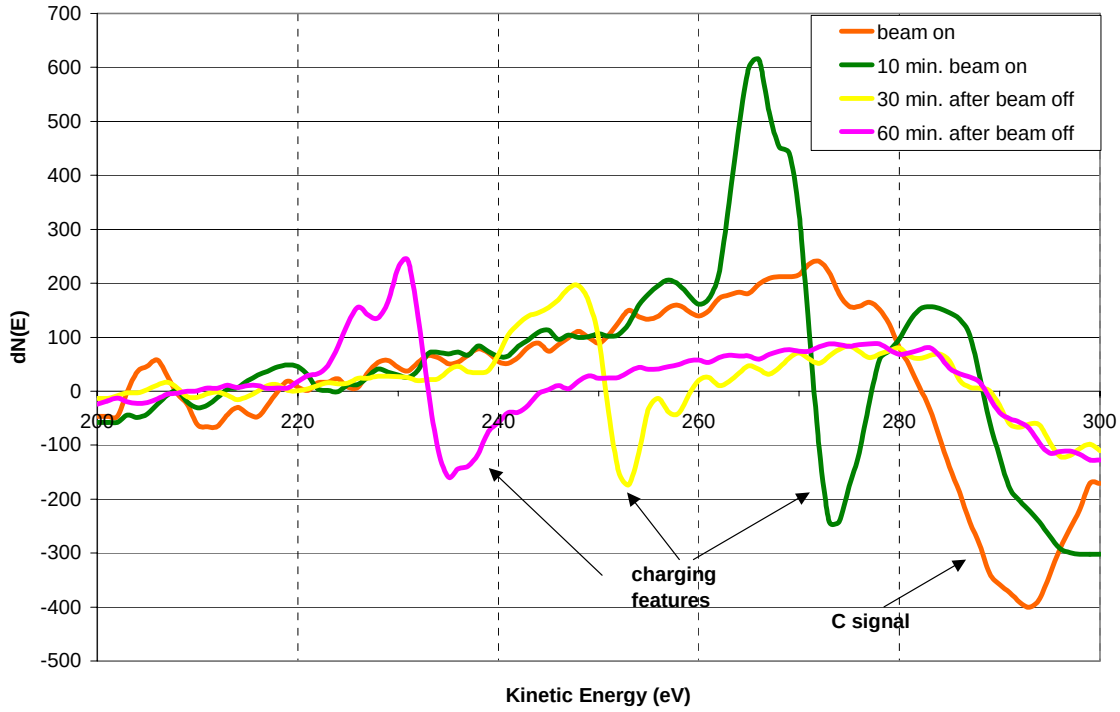

Figure 5-11. AES spectra from Zn_2SiO_4: Mn thin film phosphor during and after beam exposure (i= 13.0 μA).

5.3.2 Powder Zn_2SiO_4: Mn Phosphor

5.3.2.1 24 hour CL degradation

The cathodoluminescent degradation was also observed for Zn_2SiO_4: Mn powder phosphors. Conditions similar to those for the thin film experiments were chosen for the experiments for the powder phosphor. The CL degradation trend for a beam voltage= 2000 eV and a low beam current, i= 3.5 ± 0.5 μA, is given in Figure 5.12. The current density was measured as 111 ± 15.0 μA/ cm^2. The cathodoluminescence decreased by 56% during beam exposure. The biggest decrease in cathodoluminescent intensity occurred during the first twenty minutes of beam exposure, as seen in Figure 5.13. The phosphor degraded to 70% of its original intensity in less than 20 minutes. The CL

spectra from before and after degradation are shown in Figure 5.14. Again, the electron beam exposure does not affect the shape or position of the CL emission spectra.

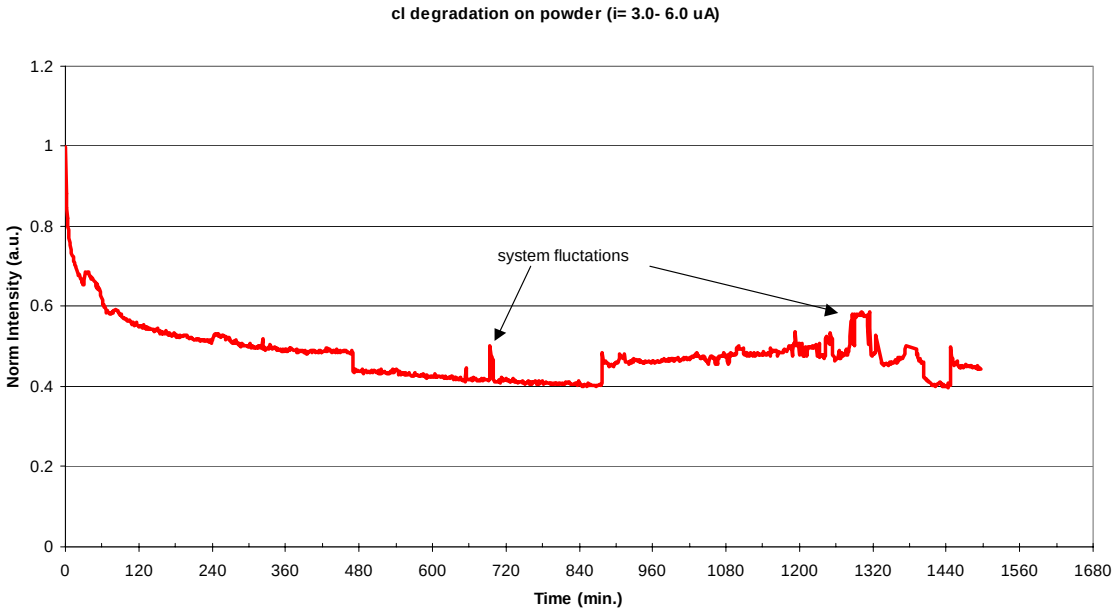

Figure 5-12. Cathodoluminescent degradation of powder phosphor at V= 2 keV, i= 3.0 μA.

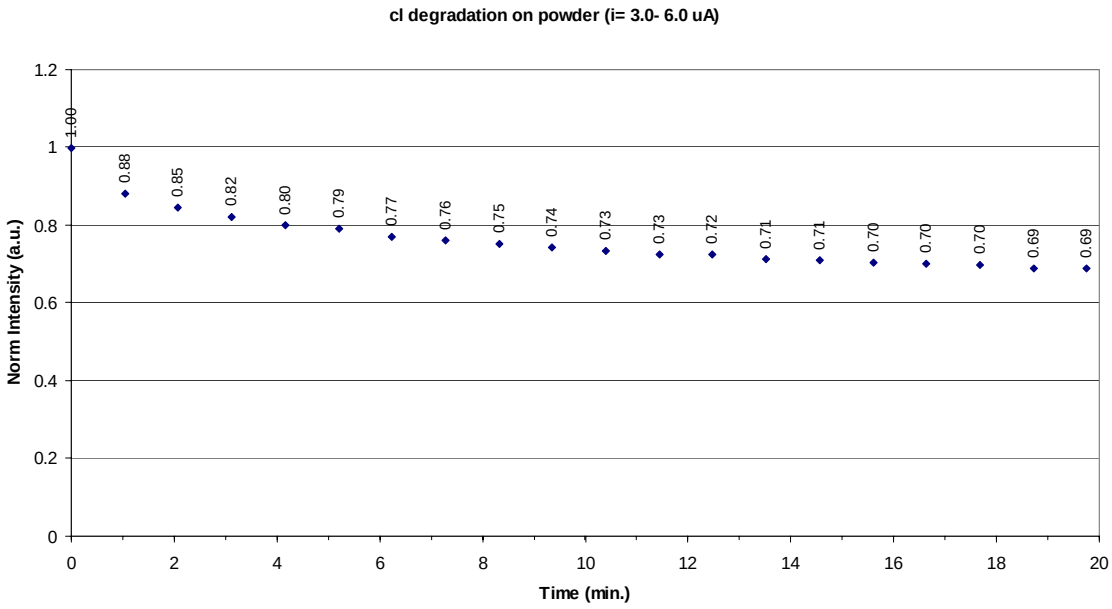

Figure 5-13. Degradation within the first 20 minutes for the powder phosphor at i= 3.0-6.0 μA.

Auger spectra of the powder phosphor before and after degradation are shown in Figure 5.15. The carbon signal is present before and after degradation and has shifted due to charging. Nevertheless, the intensity of the C signal has decreased indicating some removal of adventitious carbon from the phosphor surface. All of the carbon is not removed during beam exposure due to the packing of particles with 3 dimensional surfaces exposed to the electron beam. The zinc signal is low, but detectable before and after degradation. The oxygen signal is slightly stronger after degradation, presumably because of C removal from the phosphor. There are also Auger signals from iron before and after degradation. This signal comes from the stainless steel sample holder during electron beam exposure to the phosphor.

The powders were also observed under an increased beam current, i= 15.0 ± 1.9 μA. The decrease in CL intensity with time is shown in Figure 5.16, at a high current

density corresponding to a current density of 477 ± 60.5 μA/ cm^2. In this experiment, the cathodoluminescent intensity decreased to 24 % of its original intensity in 24 hours. The greatest decrease took place in the first 60 minutes of degradation during which the phosphor brightness decreased to 40% of its original intensity. By 3 hours of continuous beam exposure, the phosphor has already degraded to 35 % of its original intensity. The before and after spectra are shown in Figure 5.17 where no changes in the spectral distribution or peak shape for the phosphor are noted. AES data were collected from this phosphor during electron beam exposure. The changes in surface composition before and after degradation are shown by the Auger electron spectra in Figure 5.18. The spectra also give an indication of the charging the sample experiences based on the artifacts indicated in the spectra.

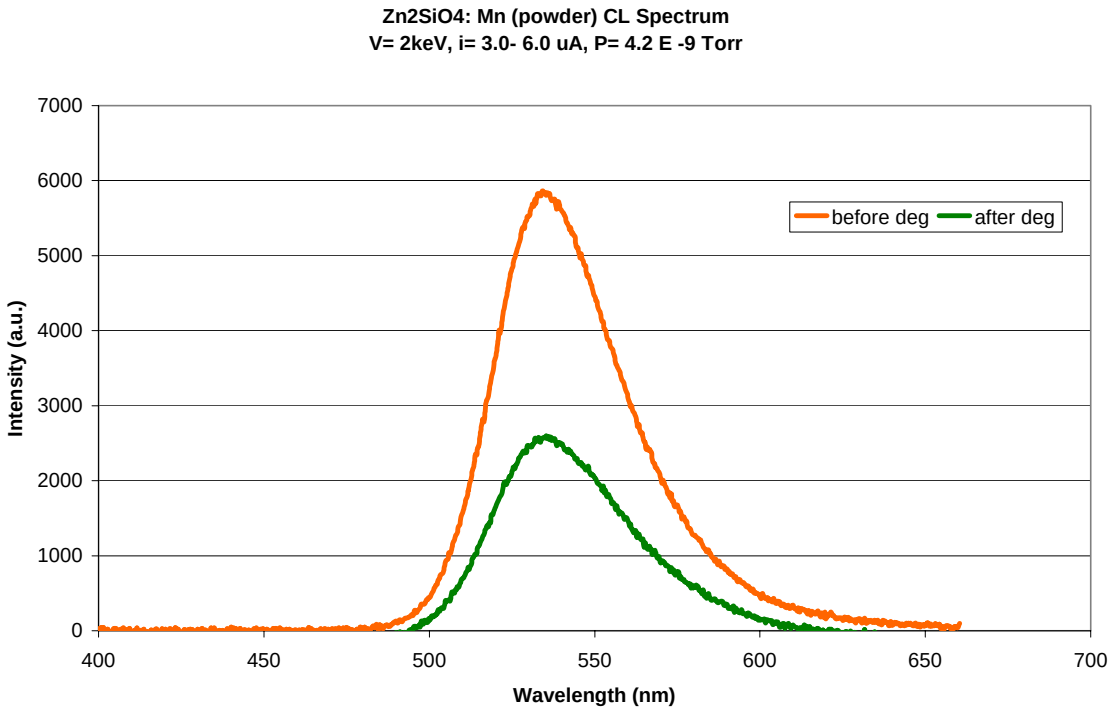

Figure 5-14. Cathodoluminescent spectrum of powder phosphor before and after 24 hours of degradation at low excitation current density.

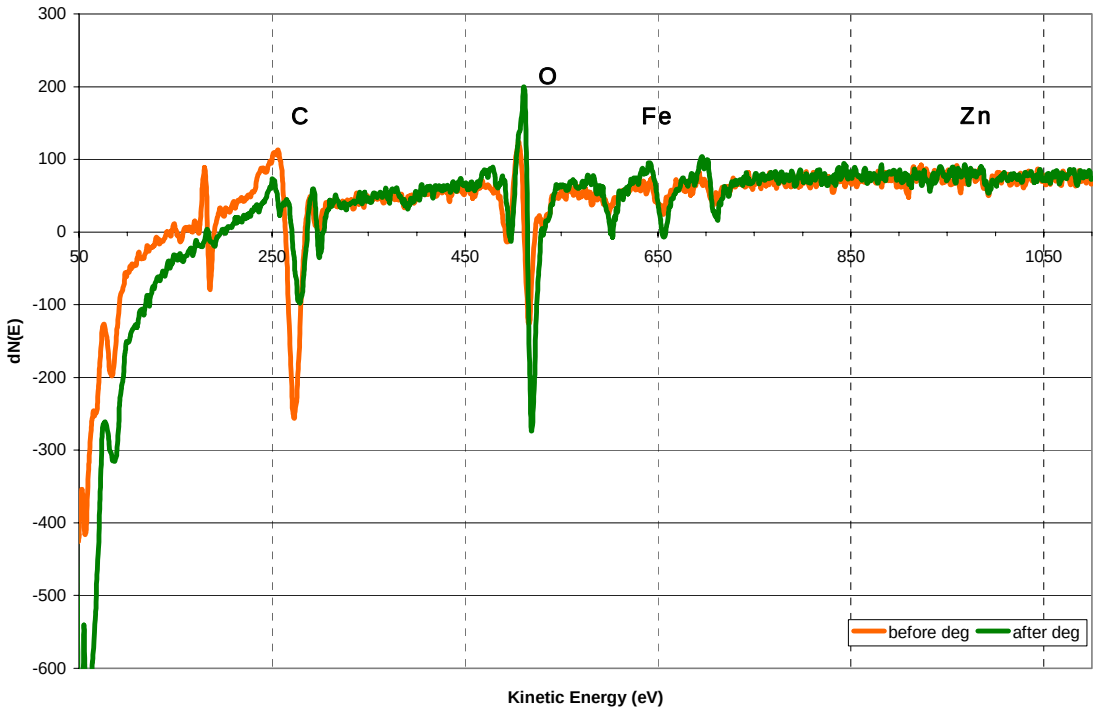

Figure 5-15 Auger spectrum before and after 24 hours degradation on powder phosphor, i= 3.0 μA.

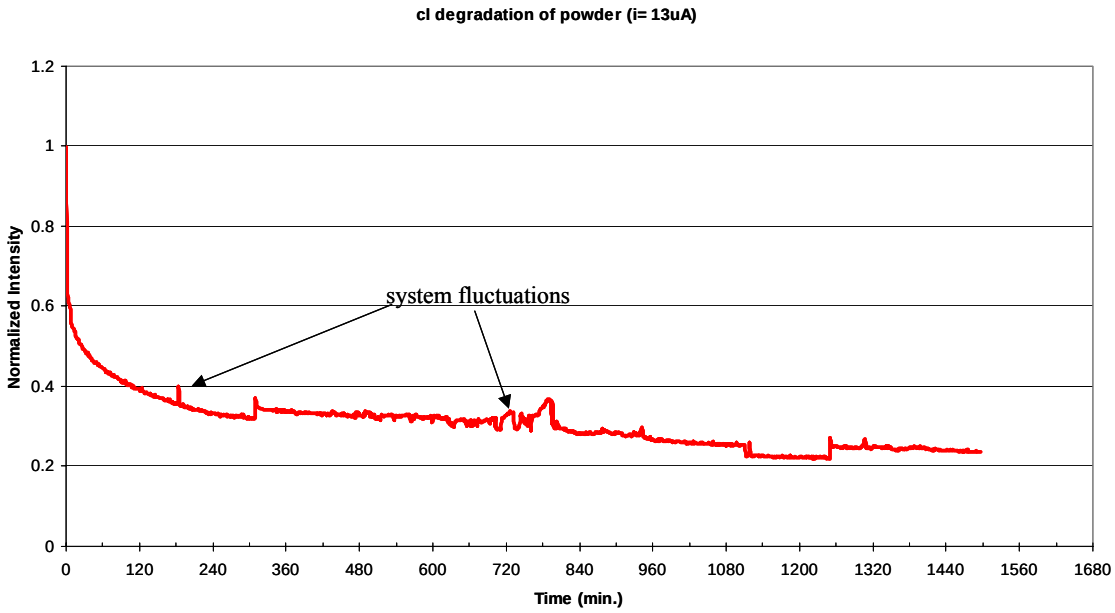

Figure 5-16. Cathodoluminescent degradation of powder phosphor at V= 2 keV, i= 13μA.

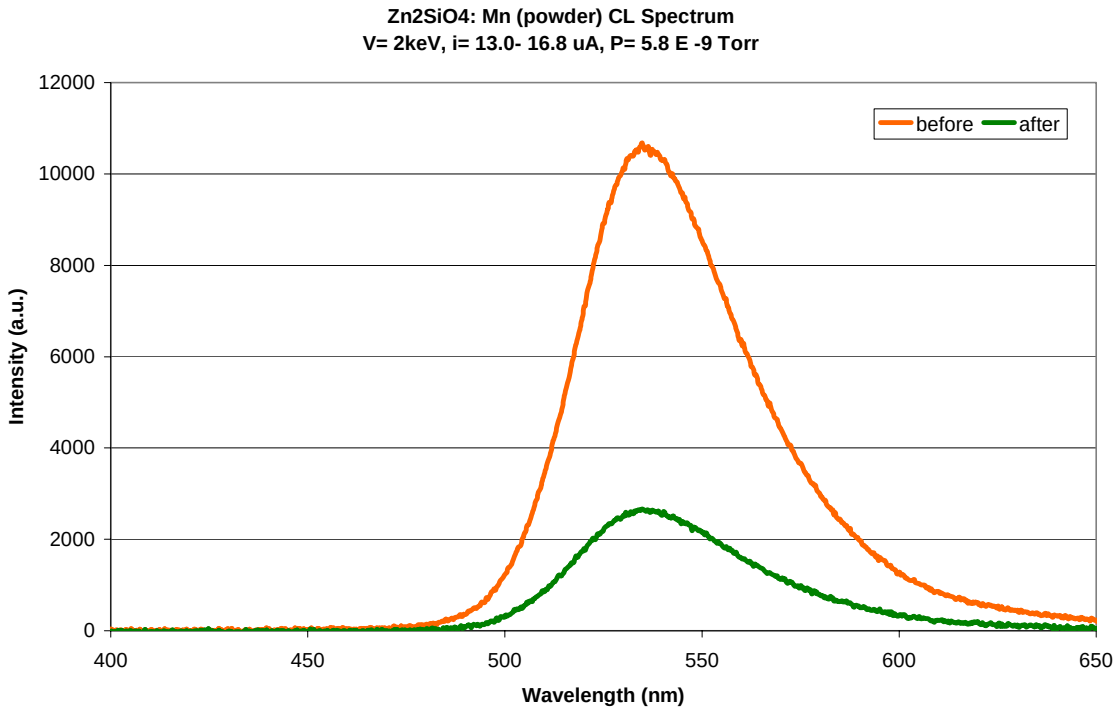

Figure 5-17. Cathodoluminescent spectrum of powder phosphor before and after degradation at high excitation current density.

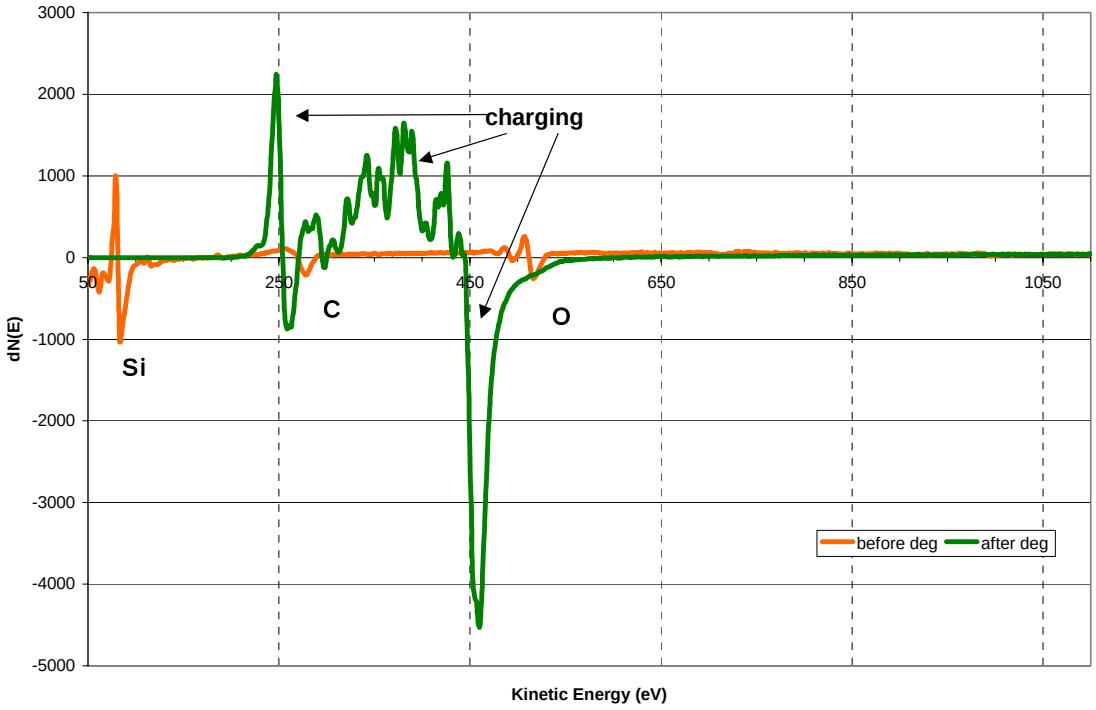

Figure 5-18. Auger spectrum before and after degradation on powder phosphor, i= 13.0 μA.

5.3.2.2 Cathodoluminescence recovery

The experiment described in section 5.3.1.2. measuring any recovery of cathodoluminescence with the primary beam off was also performed for the powder phosphors. The phosphor was exposed to the electron beam for 10 minutes and the recovery of the phosphor was monitored over the next 30 minutes with limited (5 seconds) intermittent beam exposures. The powder phosphor was examined at low and high current density.

The Zn_2SiO_4: Mn phosphor powder degraded to 74% of its initial intensity for low current density = 115 μA/ cm^2 (i= 3.6 μA) after 10 minutes of continuous electron beam exposure. The CL emission spectra for several time intervals are shown in Figure 5.19.

The CL intensity increased from the degraded CL intensity after 5 sec. intermittent exposure to the electron beam in 1minute intervals for a span of 30 minutes. The maximum recovery during intermittent beam exposure over 30 minutes was from 74% to 85% of initial intensity. The CL was evaluated 15 hours later for further CL recovery. After 15 hours of no beam exposure, the phosphor only recovered to the CL intensity measured after 30 min. of intermittent exposure to the beam. AES spectra were collected during observation of the cathodoluminescence and are shown in Figure 5.20. The shift in the carbon Auger signal over time indicates that the phosphor is charging, which can be correlated with the loss in cathodoluminescent intensity.

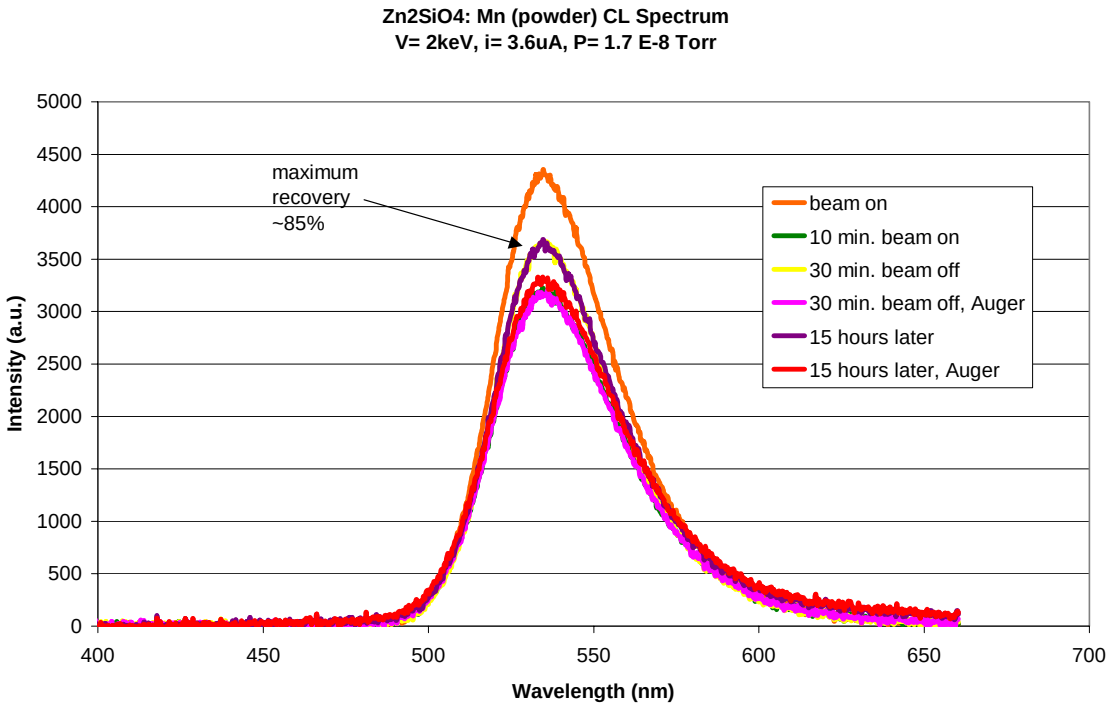

Figure 5-19 CL spectra of powder Zn_2SiO_4:Mn at V= 2keV, i= 3.0 μA for 10 minutes of continuous beam exposure and recovery over 15 hours indicating permanent degradation of phosphor.

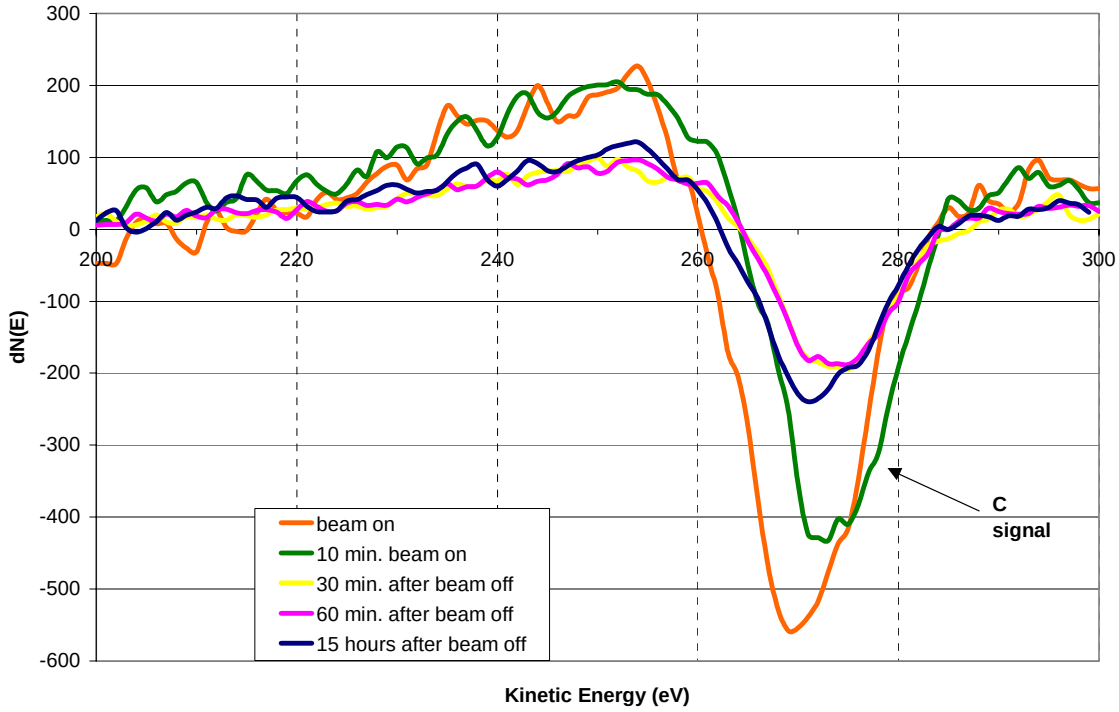

Figure 5-20. AES spectra from Zn_2SiO_4: Mn powder phosphor during and after beam exposure (i= 3.0 μA).

The powder phosphor was also examined for CL recovery at a higher current density of 414 μA/ cm^2 (i= 13 μA). The Zn_2SiO_4: Mn degraded to 34% of its initial intensity within 10 minutes of beam exposure. The maximum recovery from degradation was to 70% of the initial intensity after 30 minutes of intermittent exposure to the electron beam, as shown in Figure 5.21. The CL intensity was monitored for 12 hours after the 10 minute degradation experiment to determine if further recovery of the CL was possible, however no further recovery of intensity was detected. The loss of CL can be correlated to the Auger spectra shown in Figure 5.22. The shift in the Auger energy signal for carbon indicates that the surface is charging, even after 12 hours of limited electron beam exposure.

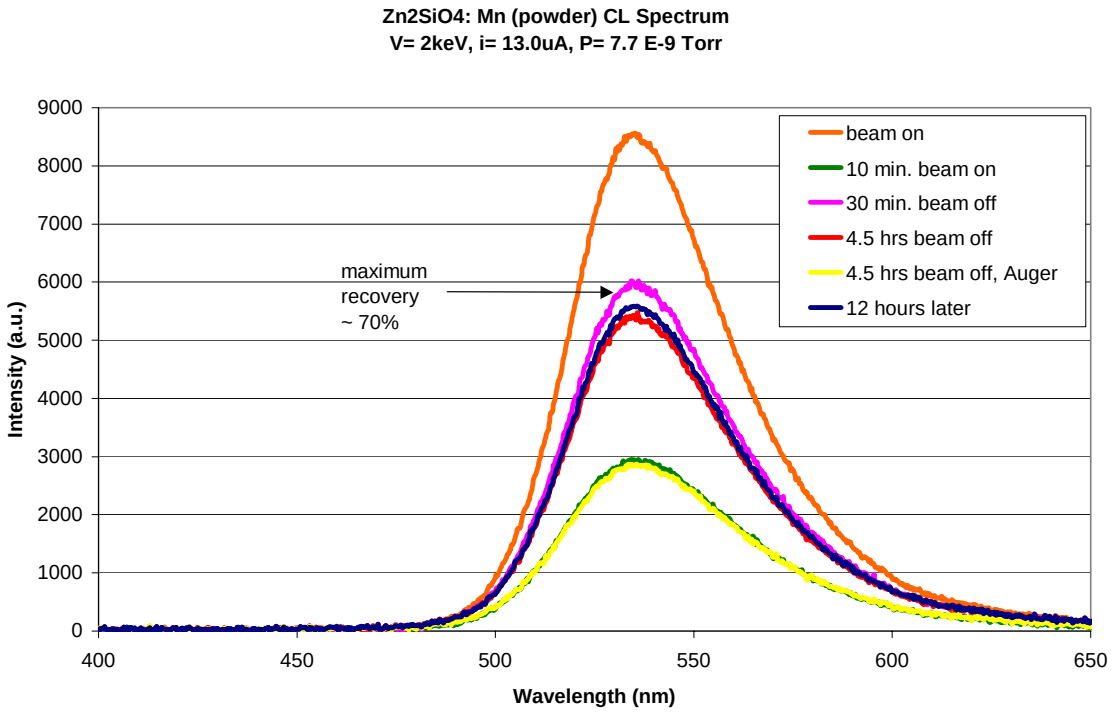

Figure 5-21. CL spectra of powder Zn_2SiO_4:Mn at V= 2keV, i= 13.0 μA for 10 minutes of continuous beam exposure and recovery over 12 hours indicating permanent degradation of phosphor.

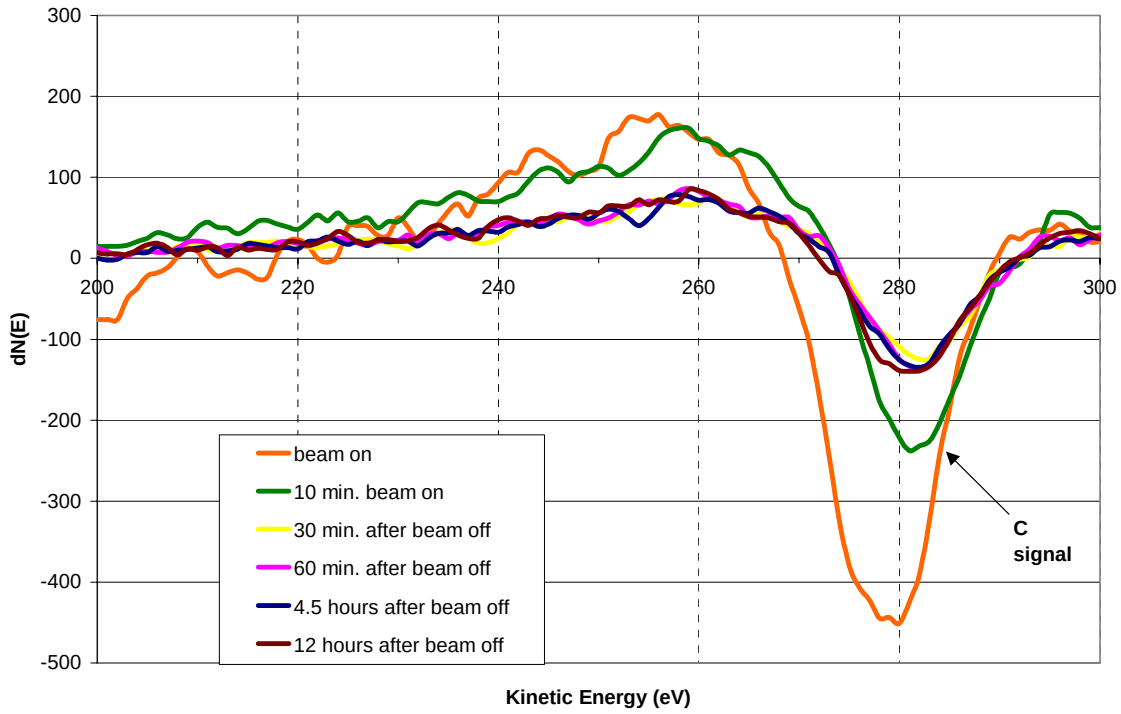

Figure 5-22. AES spectra from Zn_2SiO_4: Mn powder phosphor during and after beam exposure (i= 13.0 μA).

5.4 Discussion

5.4.1 Thin Film Zn_2SiO_4: Mn phosphor Degradation

The thin film phosphor degraded to 86% of its original intensity under low current excitation density, J= 95 μA/ cm^2. This decrease in cathodoluminescence occurred within the first ten minutes of beam exposure, where the CL intensity has already reached 86% of the initial intensity. The fast decrease in cathodoluminescence results from the phosphor charging on the surface as well the development of an internal electric field, as will be discussed further.

Charging of the phosphor was evident for both low and high current densities. Charging was observed based on non- Auger features at lower energies (≈ 200 eV) in the

secondary electron spectra and from a shift in Auger electron peaks. The decrease in cathodoluminescence is correlated to the charging observed during these times.

The degradation that resulted during early beam exposure was examined further to determine if recovery of the CL was possible and to investigate the mechanism which leads to the rapid CL loss. A shorter degradation experiment was completed with continuous beam exposure for 10 minutes. After exposure to the electron beam (V= 2keV, i= 3μA), thin film Zn_2SiO_4: Mn degraded to 80% of its initial intensity. At the end 10 minutes of beam exposure, a shift in the C Auger peak due to charging is also noted. The CL improved and recovered to 89% of its original intensity after 30 min. of intermittent beam exposure for ~5 sec. every minute. It is also reasonable to assume that an internal electric field has been generated. Bang et al. has shown that an electric field generated within seconds can quench cathodoluminescence in La_2O_2S and ZnS phosphors. The induced internal electric field results from charge separation at the surface [74]. A negative space charge present near the end of the range of electron beam penetration and a positive charge near the insulator surface would induce an electric field effect in insulators as suggested by Cazaux [75] and in phosphors as postulated by Bang [76]. The data also suggests that the induced internal electric field leads polarization of the surface. However, it has been shown that the phosphor crystals may retain their polarization after the electric field is removed until it is depolarized by high energy radiation such as high energy electrons [77]. The intermittent beam exposure depolarizes the phosphor where now an increase in luminescence is observed after 30 minutes of intermittent beam exposure. The intermittent exposure helped to increase the CL by depolarizing the phosphor.

Conversely, the CL quickly decreased to the final degraded intensity (80%) during the time (1.25 min.) required to complete an Auger survey of the surface which can be correlated with charging, as indicated by a shift of the C Auger signal to higher energies. No further recovery of cathodoluminescence was observed for the phosphor over 3.6 hours of observation. Nevertheless, charging of the phosphor was still evident, which is considered to contribute to the degradation. Surface charging occurs when there is net charge accumulation on the surface. The accumulation is dependent upon the ability of the electron beam current to flow through the phosphor to an electrical ground. The amount of current travel is reduced for wide band gap phosphors, such as Zn_2SiO_4. The shift of the Auger signal to higher energies indicates a net negative surface charge is present relative to ground. Charging has been shown to degrade the cathodoluminescence in ZnS, $SrGa_2S_4$, ZnO, and Y_2O_3 phosphors [78]. The charging reduces cathodoluminescence by enhancing non- radiative effects at the surface due to recombination between electrons and holes. An increase in non- radiative effects decreases the radiant efficiency of a phosphor, which is observed as decreased luminescence and efficiency of a phosphor.

The magnitude of degradation for the cathodoluminescence brightness increased as the excitation density was also increased. The phosphor degraded to 74% of its original intensity when the current density was increased to 461 $\mu A/ cm^2$ over 24 hours. There was no shift or change in the spectral distribution for the CL emission spectrum for the thin films at either current density after exposure to the electron beam during this time period.

A shorter degradation study was also completed on this phosphor. With an increased current, i= 13 μA, the phosphor degraded to 92% of its original intensity, with maximum recovery to 95% of original intensity. The maximum recovery occurred within the same time, 30 minutes, as the phosphor degraded at the lower current density. In this case, charging was evident as well and is considered as the cause for the loss in CL intensity.

At high and low current densities, the AES spectra indicated that the carbon peak was decreased by electron beam exposure. At the end of the degradation experiments, an increase in the oxygen and zinc signal was observed. This is correlated with the removal of carbon from the surface. No other changes in the surface chemistry were observed through the Auger analysis. Electron stimulated surface chemical reactions (ESSCR) does not contribute to the degradation of Zn_2SiO_4: Mn during electron beam exposure.

5.4.2 Powder Zn_2SiO_4: Mn phosphor Degradation

The powder phosphor also degraded less at the lower current excitation density. The phosphor decreased to 44% of its original CL intensity at a beam current density, J ~ 111.4 μA/ cm^2. The biggest decrease occurred within 20 minutes to about 70% of its initial intensity. The degradation of the Zn_2SiO_4: Mn phosphor is dependent upon the excitation density. The magnitude of CL degradation increased to 24% of initial intensity when the beam current density was increased to ~ 477.4 μA/ cm^2. The CL emission spectra indicated no shift or change in the spectral distribution for the for the powder phosphors at either current density after exposure to the electron beam for 24 hours.

Recovery and the rapid loss of the cathodoluminescence was investigated for the powder phosphors. The CL intensity for the Zn_2SiO_4: Mn powder was reduced to 74% of

its initial intensity within 10 minutes of electron beam (V= 2keV) exposure at low current, i= 3.6 μA. The maximum recovery was to 85% of initial intensity, which was obtained after 30 minutes of intermittent electron beam exposure. Again, it is postulated that intermittent electron beam exposure improves the CL by depolarization of the phosphor, allowing radiative photon emission to occur. As shown for the thin film phosphors, the emission was reduced to its 10 minute degraded CL intensity level after only 1.25 minutes of electron beam exposure. The Auger spectra indicate that charging is still present in the phosphor. After 15 hours of very limited exposure to the electron beam, the CL recovers to same intensity level as seen after 30 minutes of intermittent beam exposure. A reduction in the charging is also evident from a positive shift of the C Auger signal towards the initial C Auger signal. The CL intensity also degraded to 34% of its initial intensity after 10 minutes of continuous beam exposure at high current density.

As the current level was increased to 13 μA, the phosphor increased its level of degradation to 34% of its initial CL intensity with 10 minutes of continuous beam exposure. The maximum CL recovery to 70% of its initial intensity again occurred after 30 minutes of intermittent beam exposure. In this case, the CL intensity recovered (68% of initial intensity) with minimum beam exposure within 4.5 hours and remained at that level 12 hours after the initial beam exposure. This change can be expected after examining the Auger spectra, where there are no shifts in the Auger signal at 4.5 and 12 hours.

An increase in charging is expected as the excitation density increases. The Auger data correlates to this expected behavior. The degradation of the CL intensity is the result

of charging, as with the thin film phosphors. As the charging increases and becomes more evident, the phosphor experiences a higher magnitude of degradation. The phosphors were permanently degraded and were limited in their recovery. Charging was observed for the phosphor through the Auger spectra and was correlated with the degradation of cathodoluminescence.

The powder and thin film phosphors experienced the highest degradation at the higher excitation current density for the same experimental conditions. The degradation was more severe for the powder phosphor. The lower level of degradation for the thin film phosphor may be attributed to the ability of the thin film to possess an uninterrupted electrical path to ground due to its continuous nature, thus reducing the surface charge leading to degradation.

CHAPTER 6
CONCLUSIONS

6.1 Cathodoluminescence of Zn_2GeO_4: Mn Thin Films

Zn_2GeO_4: Mn was successfully pulsed laser deposited onto MgO, Si, and YSZ substrates and the cathodoluminescent and photoluminescent properties of the film were characterized. The characteristic green emission peak for the Zn_2GeO_4: Mn phosphor film was observed at 540nm for films deposited at $T \geq 650$ °C. The intensity of the cathodoluminescence varied with the deposition temperature, being high from films deposited at 650- 700 °C for MgO and Si substrate samples, and being highest for films deposited at 750 °C for YSZ substrate samples. The film deposited at 750 °C onto YSZ had a strongly preferred (110) texture and the largest Zn/GE atomic ratio of 0.89. All other films that resulted in the characteristic green CL emission at 540 nm were more randomly polycrystalline. The numerical value of the ratio of Zn/Ge ratio was discussed and concluded to have large errors, but to accurately represent trends in the change in concentrations of Zn and Ge with deposition parameters. Higher ratios were shown to be consistent with improvement in crystallinity and CL intensity.

A shift to red emission at 650 nm was noted for all films grown at 600 °C. This shift in emission is attributed to change in the valence state of the activator from Mn^{2+} to Mn^{4+}. A distinct difference was noted in the PL excitation spectra, indicating that different excited states are responsible for green and red emission. The change in valence state was suggested to result from a change in the substitution site for the Mn ion. The

Mn^{2+} ion substitutes for the Zn^{2+} in Zn_2GeO_4: Mn, resulting in green emission. However, when the Mn^{4+} ion substitutes for the Ge^{4+} ion, the emission is red-shifted to 650 nm.

6.2 Development of Zn_2SiO_4: Mn Thin Films

Thin film Zn_2SiO_4: Mn phosphors were successfully grown by pulsed laser deposition, sputter deposition, and combustion chemical vapor deposition. The films were made on silicon for PLD and quartz substrates for sputter and CCVD. There was no luminescence from the as- deposited films, even with an elevated film growth temperature for those made by PLD and sputter deposition. The film did have the characteristic green emission and spectral properties after a rapid thermal anneal to 1100 ºC in N_2 atmosphere, indicating that an elevated temperature is necessary to improve the crystallinity of the phosphors. The as- deposited CCVD films were polycrystalline. The films were characterized in terms of structural properties and luminescent quality.

The composition of the films is critical for developing the good luminescent phosphors. The luminescence of the phosphors increased as the zinc to silicon ratio increased. As the crystallinity and thickness of the films increase, an increase in the phosphors CL intensity was also observed.

6.3 Degradation of Zn_2SiO_4: Mn Phosphors

The degradation behavior was characterized for thin film and powder Zn_2SiO_4: Mn phosphors. An electron beam voltage of 2 keV was used for all the experiments in this section. The thin film phosphor degraded to 86% of its original intensity under low current excitation density (~95 $\mu A/ cm^2$). The decrease in cathodoluminescence occurred within the first ten minutes of beam exposure. The magnitude of degradation for the cathodoluminescence brightness increased as the excitation density was also increased (~460 $\mu A/ cm^2$). The phosphor degraded to 74% of its original intensity under high

current excitation density. In both cases, the AES spectra indicated that carbon was removed during the film surface during electron beam exposure. At the end of the degradation experiments, an increase in the oxygen and zinc signal could be observed. This is the result of the carbon removal from the surface. No detectable changes in the surface composition that may have been stimulated by electron beam exposure were observed through the Auger analysis. The decrease in luminescence is attributed to the development of an internal electric field and surface charging observed during degradation.

The powder phosphor also degraded less at the lower current excitation density. The phosphor initially decreased to 74 % of its original CL intensity at a beam current, i= 3.0 μA. The degradation of the Zn_2SiO_4: Mn phosphor is dependent upon the excitation density. The magnitude of degradation increases to 24% of its original intensity as the beam current density also increases to 13 μA. An increase in charging is expected as the excitation density increases. The Auger data correlates to this expected behavior. The degradation of the CL intensity can be related to the development of an internal electric field and charging, as with the thin film phosphors. As the charging increases and becomes more evident in the data, the phosphor experiences a higher magnitude of degradation.

The powder and thin film phosphors experienced the highest degradation at the higher excitation density. The degradation was more severe for the powder phosphor. The lower degradation for the thin film phosphor may be attributed to the ability of the thin film to continuous electrical path to ground. The electron beam did not affect the

chemistry of the phosphor surfaces and no changes in the composition of the phosphors were noted for all conditions.

The Zn_2SiO_4: Mn phosphor has been shown to maintain chemical stability during electron beam exposure. This attribute satisfies one of the critical components for application in low voltage field emission display devices. Continued work towards improvement in the brightness of this phosphor would help to make this phosphor a feasible candidate for use in FED technology.

LIST OF REFERENCES

1 Sony Learning Center: Choosing a Screen Type, http://www.sonystyle.com (Sony Electronics e-Solutions Company LLC, 2004).

2 M. Leskela, Journal of Alloys and Compounds **275- 277**, 702- 08 (1998).

3 Lyuji Ozawa, *Cathodoluminescence: Theory and Applications*. (VCH Publishers, New York, 1990).

4 Mary Bellis, The History of the Cathode Ray Tube, http://inventors.about.com/library/inventors/blcathoderaytube.htm (2004).

5 Yoshimasa A. Ono, *Electroluminescent Displays*. (World Scientific Publishing Co. Pte. Ltd., New Jersey, 1995).

6 Chemistry Learning Center, http://www.chem.uiuc.edu/clcwebsite/cathode.html (UIUC Chemistry Department, 2004).

7 G. Blasse and B. C. Grabmaier, *Luminescent Materials*. (Springer- Verlag, New York, 1994).

8 The Coming Resolution, http://www.pbs.org/opb/crashcourse/resolution (PBS Online, 1998).

9 RGB Color Info, http://www.rgbworld.com/color.html (RGB World, 1999).

10 How Television Works, http://entertainment.howstuffworks.com/tv.htm/printable (Howstuffworks, 2004).

11 G. Hopple and C. Curtin, Information Display (4&5), 34- 37 (2000).

12 L. E. Shea, The Electrochemical Society Interface (Summer), 24- 27 (1998).

13 K. Y. Sasaki and J. B. Talbot, Advanced Materials **11** (2), 91- 105 (1999).

14 L. Ozawa, in *Asia Display '98* (Seoul, Korea, 1998).

15 William F. Smith, *Principles of Materials Science and Engineering*, 2nd ed. (McGraw-Hill, Inc., New York, 1990).

16 Rolf E. Hummel, *Electronic Properties of Materials*, 3rd ed. (Springer- Verlag, Inc., New York, 2001).

17 P. H. Holloway, T. A. Trottier, B. Abrams, C. Kondoleon, S. L. Jones, J. S. Sebastian, and W. J. Thomes, J. Vac. Sci. Technol. B **17** (2), 758- 64 (1999).

18 P. H. Holloway, T. A. Trottier, J. Sebastian, S. Jones, X.- M. Zhang, J.- S. Bang, B. Abrams, W. J. Thomes, and T.- J. Kim, Journal of Applied Physics **88** (1), 483- 88 (2000).

19 H. C. Swart, J. S. Sebastian, T. A. Trottier, S. L. Jones, and P. H. Holloway, J. Vac. Sci. Technol. A **14** (3), 1697- 703 (1996).

20 S. Itoh, T. Kimizuka, and T. Tonegawa, Journal of the Electrochemical Society **136** (6), 1819- 23 (1989).

21 S. Itoh, H. Toki, F. Kataoka, Y. Sato, and K. Tamura, Journal of the SID (Supplement-1), 187- 92 (2000).

22 J. P. Bender, J. F. Wager, J. Kissick, B. L. Clark, and D. A. Keszler, Journal of Luminescence **99** (311- 324) (2002).

23 V. Bondar, L. Axelrud, V. Davydov, Yu. Dubov, S. Popovich, J. Wager, J. Bender, and S. S. Sun, presented at the 6th International Conference on the Science and Technology of Display Phosphors, San Diego, CA, 2000.

24 Phosphor Technology Center of Excellence, *Low voltage phosphor data sheets*. (Georgia Institute of Technology, Atlanta, 1996).

25 M. Garcia- Hipolito, O. Alvarez- Fregoso, E. Martinez, C. Falcony, and M. A. Aguilar- Frutis, Optical Materials **20**, 113- 18 (2002).

26 Y. C. Kang and H. D. Park, Applied Physics A: Materials Science and Processing **77**, 529- 32 (2003).

27 T. S. Copeland, B. I. Lee, J. Qi, and A. K. Elrod, Journal of Luminescence **97**, 168- 73 (2002).

28 V. B. Bhatkar, S. K. Omanwar, and S. V. Moharil, phys. stat. sol. (a) **191** (1), 272- 76 (2002).

29 T. H. Cho and H. J. Chang, Ceramics International **29**, 611- 18 (2003).

30 X. W. Sun and H. S. Kwok, Applied Physics A: Materials Science and Processing **69** (Suppl.), S39- S43 (1999).

31 Z. Ji, S. Yongliang, and Y. Zhizhen, Journal of Crystal Growth **255**, 353- 56 (2003).

32 R. Selomulya, S. Ski, K. Pita, C. H. Kam, Q. Y. Zhang, and S. Buddhudu, Materials Science & Engineering B **B100**, 136- 41 (2003).

33 V. Bondar, M. Vasyliv, Ya. Vasyltziv, M. Grytsiv, and Yu. Dubov, presented at the 4th International Conference on the Science and Technology of Display Phosphors & 9th International Workshop on Inorganic and Organic Electroluminescence, Bend, Oregon, 1998.

34 Sean Liam Jones, PhD., University of Florida, Gainesville, 1997.

35 John S. Lewis and Paul H. Holloway, Journal of the Electrochemical Society **147** (8), 3148 50 (2000).

36 Tao Feng, Ph.D., University of Florida, Gainesville, 2001.

37 John South Lewis III, Ph.D., University of Florida, Gainesville, 2000.

38 V. D. Bondar, Yu G. Dubov, and M. R. Pamasiuk, presented at the 12th International Workshop on Inorganic and Organic Electroluminescence & 2004 International Conference on the Science and Technology of Emissive Displays and Lighting, Toronto, Canada, 2004.

39 G. Stuyven, P. De Visschere, K. Neyts, and A. Kitai, Journal of Applied Physics **93** (8), 4622- 27 (2003).

40 C. Baker, J. Heikenfeld, and A. J. Steckl, IEEE Journal of Selected Topics in Quantum Electronics **8** (6), 1420- 26 (2002).

41 D. A. Trivedi, N. M. Kalkhoran, W. D. Halverson, G. D. Vakerlis, and C. A. Del Gado, SID 97 Digest, 619- 22 (1997).

42 S. Suh, D. M. Hoffman, L. M. Atagi, and D. C. Smith, Chemical Vapor Deposition **7** (2), 81- 84 (2001).

43 X. Ouyang, A. H. Kitai, and T. Xiao, J. Appl. Phys. **79** (6), 3229- 34 (1996).

44 V. Bondar, M. Vasyliv, M. Grytsiv, Y. Dbov, S. Popovich, L. Akselrud, V. Davydov, and I. Kucharsky.

45 Douglas B. Chrisey and Graham K. Hubler, *Pulsed Laser Deposition of Thin Films*. (John Wiley & Sons, Inc., New York, 1994).

46 C. C. Chang, X. D. Wu, R. Ramesh, X. X. Xi, T. S. Ravi, T. Venkatesan, D. M. Hwang, R. E. Muenchausen, S. Foltyn, and N. S. Nogar, Appl. Phys. Lett. **57** (17), 1814- 16 (1990).

47 X. D. Wu, R. E. Muenchausen, S. Foltyn, R. C. Estler, R. C. Dye, C. Flamme, N. S. Nogar, A. R. Garcia, J. Martin, and J. Tesmer, Appl. Phys. Lett. **56** (15), 1481- 83 (1990).

48 J. Narayan, N. Biunno, R. Singh, O. W. Holland, and O. Auciello, Appl. Phys. Lett. **51** (22), 1845- 47 (1987).

49 G. Koren, A. Gupta, R. J. Baseman, M. I. Lutwyche, and R. B. Laibowitz, Appl. Phys. Lett. **55** (23), 2450- 52 (1989).

50 Angus Rockett, *Sputter Deposition of Thin Films*. (American Vacuum Society, 2002).

51 R. K. Waits, J. Vac. Sci. Technol. **15** (2), 179- 87 (1978).

52 John L. Vossen and Werner Kern, *Thin Film Processes II*. (Academic Press, Inc., New York, 1991).

53 Milton Ohring, *The Materials Science of Thin Films*. (Academic Press, New York, 1992).

54 Yves Pauleau, *Chemical Physics of Thin Film Deposition Processes for Micro- and Nano- Technologies*. (Kluwer Academic Publishers, Norwell, MA, 2002).

55 J. A. Thornton, J. Vac. Sci. Technol. **15** (2), 171- 77 (1978).

56 Aicha A. R. Elshabini- Riad and III Fred D. Barlow, *Thin Film Technology Handbook*. (McGraw-Hill Companies, Inc., New York, 1997).

57 M. R. Davidson, B. Pathangey, P.. H. Holloway, P. D. Rack, S.- S. Sun, and C. N. King, Journal of Electronic Materials **26** (11), 1355- 60 (1997).

58 Light Tour: Electromagnetic Spectrum, http://cse.ssl.berkeley.edu (Regents of the University of California, 1996).

59 J. S. Sebastian, H. C. Swart, T. A. Trottier, S. L. Jones, and P. H. Holloway, J. Vac. Sci. Technol. A **15** (4), 2349- 53 (1997).

60 H. C. Swart, T. A. Trottier, J. S. Sebastian, S. L. Jones, and P. H. Holloway, Journal of Applied Physics **83** (9), 4578- 83 (1998).

61 J. M. Fitz- Gerald, T. A. Trottier, R. K. Singh, and P. H. Holloway, Appl. Phys. Lett. **72** (15), 1838- 39 (1998).

62 O. M. Ntwaeaborwa, K. T. Hillie, and H. C. Swart, phys. stat. sol. (c) (2004).

63 Y. E. Lee, D. P. Norton, and J. D. Budai, Appl. Phys. Lett. **74** (21), 3155- 57 (1999).

64 Y.E. Lee, D. P. Norton, J.D. Budai, P.D. Rack, J.Peterson, and M.Potter, in *MRS Electron Emissive Materials, Vacuum Microelectronics, and Flat Panel Display* (MRS, San Francisco, 2000).

65 C. Richard Brundle, Charles A. Evans Jr., and Shaun Wilson, *Encyclopedia of Materials Characterization*. (Butterworth Heinemann, Boston, 1992).

66 B. G. Yacobi and D. B. Holt, *Cathodoluminescence Microscopy of Inorganic Solids*. (Plenum Press, New York, 1990).

67 C.F.Yu and P.Lin, J. Appl. Phys. **79** (9), 7191- 97 (1996).

68 D. T. Palumbo and Jr. J. J. Brown, J. Electrochem. Soc.: SOLID STATE SCIENCE **117** (9), 1184- 88 (1970).

69 D. R. Lide, *CRC Handbook of Chemistry & Physics*, 78th ed. (CRC Press, Boca Raton, FL, 1997).

70 Z. T. Kang, Y. Liu, B. K. Wagner, R. Gilstrap, M. Liu, and C. J. Summers, presented at the 12th International Workshop on Inorganic and Organic Electroluminescence & 2004 International Conference on the Science and Technology of Emissive Displays and Lighting, Toronto, Canada, 2004.

71 A. T. Hunt, W. B. Carter, and J. K. Cochran, Appl. Phys. Lett. **63** (2), 266- 68 (1993).

72 John B. Hudson, *Surface Science: An Introduction*. (John Wiley & Sons, Inc., New York, 1992).

73 Billie Lynn Abrams, University of Florida, Gainesville, 2001.

74 J. Bang, B. Abrams, and Paul H. Holloway, J. Appl. Phys. **91** (11), 7091- 100 (2003).

75 J. Cazaux, J. Appl. Phys. **85** (2), 1137- 47 (1999).

76 Jungsik Bang, Ph.D., University of Florida, Gainesville, 2004.

77 L. Ozawa, Appl. Phys. Lett. **43** (11), 1073- 74 (1983).

78 C. H. Seager, W. L. Warren, and D. R. Tallant, J. Appl. Phys. **81** (12), 7994- 8001 (1997).

BIOGRAPHICAL SKETCH

Lizandra Clarissa Williams was born in Morgan City, Louisiana. She completed her high school studies at the Louisiana School for Math, Science, and the Arts with a concentration in Math Science and Humanities. Upon graduation, she went to Florida A & M University and obtained a B.S. magna cum laude degree in mechanical engineering. After working for a year for 3M in Minnesota, she began her graduate studies in Materials Science and Engineering at the University of Florida. She obtained her M.S. in 2002 and her Ph.D. in 2004.